Influence of atmospheric stability on wind farm control

Bei der Fakultät für Mathematik und Naturwissenschaften
der Carl von Ossietzky Universität Oldenburg
zur Erlangung des Grades und Titels eines

Doktors der Naturwissenschaften (Dr. rer. nat.)

angenommene Dissertation

von Lukas Vollmer

geboren am 30.04.1986 in Dortmund

Abstract

The coordinated control of individual turbines of a wind farm is currently discussed as one option to reduce the costs of wind energy. The idea behind wind farm control is to improve power yield and lifetime of a wind farm by controlling the turbines' wakes. One promising concept is wake steering by an intentional yaw misalignment of the turbines. This thesis analyses the influence of changing states of atmospheric stability on the potential and applicability of wake steering in numerical experiments with Large-Eddy-Simulations.

A comparison of the wake of a single wind turbine in three different stability regimes demonstrates that measurements of atmospheric stability or related quantities like wind veer, shear and turbulence intensity are important input parameters to estimate the wake development downstream of a wind turbine. Also, the analysis of wakes from turbines operating in yaw reveals that the assumption of an axis-symmetric wake breaks easily not only when wake steering is applied, but also in presence of wind veer. Thus, parametric models that rely on the assumption of axis-symmetry will make erroneous predictions.

When applied in a small wind farm of two turbines, wake steering increases the wind farm's energy yield in a neutral and a stable atmospheric boundary layer. In a convective boundary layer the control does not increase the energy yield in the test scenarios. This can be related to the high level of turbulence on large length scales, that poses a problem to the controller, and leads to a strong meandering of the wake downstream of the turbine. A disadvantage of wake steering is the frequent use of the yaw actuator to correct the yaw alignment of the controlled turbines. An alternative controller for wake steering, which reduces yaw correction in a certain wind sector, proves to also increase the power yield in comparison to conventional control.

To improve the capability of Large-Eddy-Simulations as test environment for wind farm control, a methodology is analyzed that incorporates forcing from numerical weather models into the simulations. The methodology is tested against measurements both at an offshore and an onshore wind farm site. The analysis points out that the methodology can simulate a measured diurnal cycle of wind conditions driven by solar irradiance. On the other hand, frequencies in the range of mesoscale fluctuations can not be resolved. Thus, the methodology might be only beneficial for simulating selected scenarios that are encountered at real wind farms. When combined with wake simulations, however, it can provide valuable additional informations to measurements about the wind field and help in interpreting the results from field campaigns.

The main conclusion of the thesis is that wind farm control by means of wake steering is a promising concept to increase the power production of a wind farm by several percentages for certain well-known inflow wind conditions. Part of the necessary information needs to be at least the turbulence intensity of the wind, as wake steering proved to be rather detrimental to

the energy yield in highly turbulent convective atmospheric boundary layers. Considering the current trend in wind energy of increasing data acquisition and monitoring, the capabilities to measure the relevant quantities that are identified in this thesis will likely be part of the standard in the near future.

Zusammenfassung

Eine koordinierte Anlagenregelung kann eine Möglichkeit darstellen den Ertrag und die Lebensdauer von Windparks zu erhöhen. Die Idee einer solchen Regelung ist es, die negativen Effekte von Nachläufen auf die genannten Faktoren zur verringern. Als vielversprechende Methode hat sich in Experimenten die Nachlaufablenkung durch absichtliche Anlagenfehlstellung gegenüber der Windrichtung etabliert. In dieser Doktorarbeit wird die Abhängigkeit des Potentials und der Anwendbarkeit dieser Methode von der atmosphärischen Stabilität untersucht. Als Testumgebung werden Large-Eddy-Simulationen von Windenergieanlagen in der atmosphärischen Grenzschicht verwendet.

Der Vergleich von Turbinennachläufen in drei unterschiedlichen Stabilitätsumgebungen zeigt, dass die Turbulenzintensität und die Drehung und Scherung des Windes mit der Höhe zu berücksichtigen sind, wenn die Entwicklung des Nachlaufs stromabwärts verstanden werden will. Darüber hinaus wird veranschaulicht, dass Turbinen in Fehlstellung stark asymmetrische Nachläufe erzeugen, die nicht mit derzeit verwendeten Ingenieursmodellen beschrieben werden können.

Die Anwendung einer Regelung zur Nachlaufablenkung in einem Windpark aus zwei Anlagen erhöht den Ertrag in stabilen und neutralen atmosphärischen Grenzschichten, jedoch nicht in einer konvektiven Grenzschicht. Der Grund dafür ist die dominante Fluktuation des Windes auf größeren Längenskalen, die problematisch für den Regler ist und zudem ein starkes Mäandrieren des Nachlaufs verursacht. Ein grundsätzlicher Nachteil der Regelung ist eine erhöhte Beanspruchung des Azimutantriebs zur Korrektur der Anlagenausrichtung. Als Alternative wird eine Regelung mit konstanter Ausrichtung der stromaufwärts stehenden Anlage in einem bestimmtem Windrichtungssektor getestet. Diese Regelung reduziert die Nutzung des Azimutantriebs und führt trotzdem noch zu einem Mehrertrag im Vergleich zu einer konventionellen Regelung.

Um die Anwendbarkeit von Large-Eddy-Simulationen als Testumgebung für Windparkregelung zu validieren und zu verbessern wird eine Methode untersucht, die Daten aus numerischen Wettermodellen berücksichtigt. Im Vergleich zu Messungen an einem Offshore- und an einem Onshore-Windpark zeigt sich, dass die Methode gut geeignet ist einen durch Sonneneinstrahlung erzeugten Tagesgang der atmosphärischen Grenzschicht zu reproduzieren, mesoskalige Fluktuationen des Windes können dagegen nicht abgebildet werden. Dies schränkt eine Anwendung bei Szenarien, in denen der Wind durch diese Fluktuationen geprägt ist, ein. Kombiniert mit Nachlaufsimulationen ermöglicht die Methode Messungen in Windparks zu ergänzen um wertvolle Mehrinformationen zu generieren.

Das Fazit der Arbeit ist, dass Nachlaufablenkung, eingesetzt bei bestimmten Windbedingungen, den Ertrag eines kleinen Windparks um einige Prozent erhöhen kann. Zur Charakterisierung der Windbedingungen ist mindestens die Turbulenzintensität zu berücksichtigen um

die Anwendung der Regelung in einer hochturbulenten konvektiven Grenzschicht zu vermeiden. Die laufende Forschung und der Trend in Richtung Digitalisierung lässt vermuten, dass eine ausreichende messtechnische Ausstattung von Windenergieanlagen in naher Zukunft Standard sein wird.

Contents

List of Figures

List of Tables

List of Abbreviations

ABL	Atmospheric boundary layer
ADM	Actuator disc model
ADM-R	Actuator disk model with rotation
AEP	Annual energy production
AGL	Above ground level
ALM	Actuator line model
AP	Available mean specific power in the wind
BSH	Bundesamt für Seeschifffahrt und Hydrographie
CBL	Convective atmospheric boundary layer
CFD	Computational fluid dynamics
COSMO	Consortium for small-scale modeling
CWEX	Crop/Wind-energy Experiment
D	Rotor diameter
DEWI	Deutsches Windenergie Institut
DWD	Deutscher Wetter Dienst
FINO	Forschungsplattformen in Nord- und Ostsee
GFS	Global Forecast System
LES	Large Eddy Simulation
lidar	Light detection and ranging device
L	Obukhov length
LES	Large Eddy Simulation
LST	Local Standard Time
MYNN	Mellor-Yamada-Nakanishi-Niino ABL scheme
(N)NBL	(Near) neutral atmospheric boundary layer
NCAR	National Center of Atmospheric Research of the US
NEWA	New European Wind Atlas
NREL	National Renewable Energy Laboratory of the US
PALM	Parallelized Large-Eddy Simulation Model
RANS	Reynolds-averaged Navier-Stokes equation
REWS	Rotor equivalent wind speed
REWD	Rotor equivalent wind direction
Ri	Richardson number
RMSE	Root mean square error
SBL	Stable atmospheric boundary layer
SGS	Sub-grid-scale
TI, I	Turbulence intensity
TKE	Turbulent kinetic energy

UTC	Coordinated Universal Time
VAD	Velocity azimuth display
WD	Wind direction
WS	Wind speed
WC	Windcube lidar (Leosphere)
WRF	Weather Research and Forecasting model

Chapter 1

Introduction

1.1 Reducing the costs of wind energy

The exploitation of fossil resources has released a huge amount of carbon dioxide (CO_2), that was previously stored under the earth surface, into the atmosphere and the ocean, causing an increase of the observed relative amount of CO_2 in the atmosphere by almost 50 %, relative to pre-industrialization measurements. As historical data from ice cores reveal a strong correlation between earth temperature and CO_2 concentration in the atmosphere (Lorius et al., 1990), leading experts were gathered in the Advisory Group on Greenhouse Gases of the Intergovernmental Panel on Climate Change in the late 1980s to make predictions about the development of the global temperature and the implications on the earth's ecosystem. They found that an increase of the surface temperature by more than $2°C$ would represent a large risk to the health of many of the earth's ecosystems and the stability of the climate system overall (Rijsberman and Swart, 1990). To prevent this scenario, multiple governments began to invest into programs to eventually replace the fossil energy sector with renewable alternatives like wind and solar energy.

Supported by a stable price environment by the governments, the world-wide installed capacity of wind energy power plants has grown in the last twenty years from 6 GW to more than 500 GW (Global Wind Energy Council, 2018). Meanwhile, individual wind turbines have developed from producing less than 1 MW with rotor diameters of approx. 50 m to more than 10 MW with rotors larger than 160 m. The steady technological development and the economics of scale have lead to a large decrease in the costs of wind energy, so that onshore wind energy is regarded to be already one of the cheapest sources of electric energy (Kost et al., 2018). One factor that is still pushing the price is the shortage of windy sites in regions that are densely populated and have a large need for energy.

While the main share of turbines are still operating onshore, the installation of offshore wind farms is steadily increasing. In 2002, the first large offshore wind farm, the 160 MW wind farm HornsRev was commissioned in Denmark. Aside of political reasons to move wind energy from the land to the ocean, offshore wind farms are supposed to benefit from the stronger and less turbulent wind over the sea. Offshore wind energy faced early growing pains, which however did not stop the further investment, as evidenced by 3,589 turbines with a capacity of 12.6 GW, that were feeding offshore wind energy into the European grid in 2016 (Wind Europe, 2017). While offshore wind energy still remains a costly alternative to

onshore wind energy, leading experts (Wiser et al., 2016) are projecting a decline of the costs by a wide margin in the next decades. As two important driving factors to lower costs of an offshore wind farm project, they state a better prediction of the annual energy production (AEP) to reduce financial risks and the extension of the lifetime of the wind farm.

When the first offshore wind farms were built, the wind conditions at turbine relevant heights were largely unknown. Even the first Danish offshore wind farms did not allow to provide realistic estimations as they were built too close to the coast. To study the potential of wind farms to be built far offshore in their territory, the German government sponsored the erection of the three meteorological FINO masts with minimum distances from the coast of 40 km, at different locations in the North and Baltic Sea. These measurements allowed giving first reliable estimations of the wind conditions for wind farms operating far from the coast (Türk, 2008).

Aside from predicting wind and weather conditions, the prediction of wind turbine wake losses and wake-induced fatigue loads plays a vital role in the estimation of AEP and turbine lifetime. Wind turbine wakes are areas of lower mean kinetic energy and higher turbulent kinetic energy downstream of wind turbines. They are created by the extraction of momentum by the turbine from the flow. Wakes lead to a lower efficiency of a wind farm (Barthelmie and Jensen, 2010) and the higher turbulent kinetic energy inside the wind farm reduces the lifetime of the turbine components (Frandsen and Thøgersen, 1999).

1.2 Boundary layer meteorology and its relevance for wind farm operation

The influence of different meteorological conditions on wind farms can be studied in farms equipped with meteorological met masts. Wind farms are operating in the atmospheric boundary layer (ABL), the lowest part of the atmosphere. The height of the ABL is variable and can range from less than 100 m to several kilometers. The wind conditions in the ABL are influenced by both, the large-scale geostrophic wind in the free atmosphere above and the properties of the earth's surface below. The ABL is a highly turbulent environment with the turbulence generated by shear stress and enhanced or reduced by buoyancy.

One meteorological characteristic that has been studied extensively in recent wind energy research is the thermal stability of the ABL. Atmospheric stability is driven by buoyancy, which is mainly created by the difference in near-surface temperature and potential air temperature. In principle, a downward potential heat flux, caused by a surface colder than the air above, leads to a stably stratified ABL (SBL). An SBL is characterized by a shallow boundary layer with increasing potential temperature with height, a large vertical shear (the change of wind speed with height) and veer (the turning of the wind vector with height) and by a low level of turbulence. A warmer surface than the air above, on the other hand, provides a source of energy that leads to a highly turbulent convective ABL (CBL), that is well mixed and has little vertical shear. A CBL can reach heights of more than one kilometer. A neutrally stable

ABL (NBL) exists, when surface and potential air temperature are in relative equilibrium, and the potential temperature inside the ABL is constant with height. This is mostly the case in strong winds, when shear-produced turbulence dominates the buoyancy effects.

The most important influence of atmospheric stability for wind farm operation is, that the extrapolation of the logarithmic wind profile from near-surface measurements needs to be corrected with the difference in wind shear to derive the wind speed at rotor-relevant heights (Gryning et al., 2007). With the cubic dependency of wind power on wind speed, already little deviations in wind speed estimation create large differences in the energy yield of a wind turbine. A neutrally stratified atmosphere is still mostly assumed during the planning of wind farms as the wind profile can be quite well described by analytical equations and as stability measurements are rarely part of the assessment of the site where the wind farm is going to be built. While this assumption might still produce good results for a long-term assessment due to potentially compensating errors, it increases the uncertainty of the short-term prediction of the wind resource as atmospheric stability is constantly changing.

The change of atmospheric stability can be mostly related to the variation of the near-surface temperature. At land, the variation of near-surface temperature is driven by solar insolation that heats the ground during the day. Thus, atmospheric stability has a daily cycle in clear sky conditions with a quickly established daytime CBL and a slowly building nocturnal SBL. Offshore, the near-surface temperature changes only little during the day, due to the high heat capacity of the ocean. On the other hand, offshore wind farms are mostly built close to the coast, where the state of the ABL can be influenced by advection of air from land to sea. The observed cycle of atmospheric stability at offshore wind farms thus heavily depends on the distance to the coast and the prevailing wind directions (Dörenkämper, 2015).

Multiple recent studies have addressed the atmospheric stability conditions at wind farms (Fig. 1.1). Dörenkämper (2015) classified the measured stability conditions at the three FINO metmasts and found a dominance of stable ABLs in the North Sea and a low occurrence of neutral conditions overall. Studies at several Danish wind farms observed similar distributions (Motta et al., 2005; Hansen et al., 2012), while Archer et al. (2016) assessed predominant convective conditions at the site of the first US offshore wind farm at the US east coast. Wharton and Lundquist (2012) and Rajewski et al. (2013) analyzed among others atmospheric stability at onshore wind farms and also found a high occurrence of non-neutral conditions. These studies offer only a small sample size and a quantitative comparison is difficult as all authors use different measurement devices and thresholds to define the stability classes. However, these studies point out a dominance of non-neutral atmospheric stability conditions at the measurement sites, which makes a correction of the wind profile or measurements at hub height a critical part of the site assessment.

Barthelmie and Jensen (2010); Hansen et al. (2012) and Dörenkämper (2015) have analyzed the influence of different meteorological parameters on the array efficiency of offshore wind farms. A hierarchy of the parameters is made in Barthelmie et al. (2013). The hub height wind speed is identified as the most important parameter, which can be related to the wind speed dependent thrust of wind turbines. The distance between the turbines is identified as second most important parameter, as the wakes recover with increasing distance from
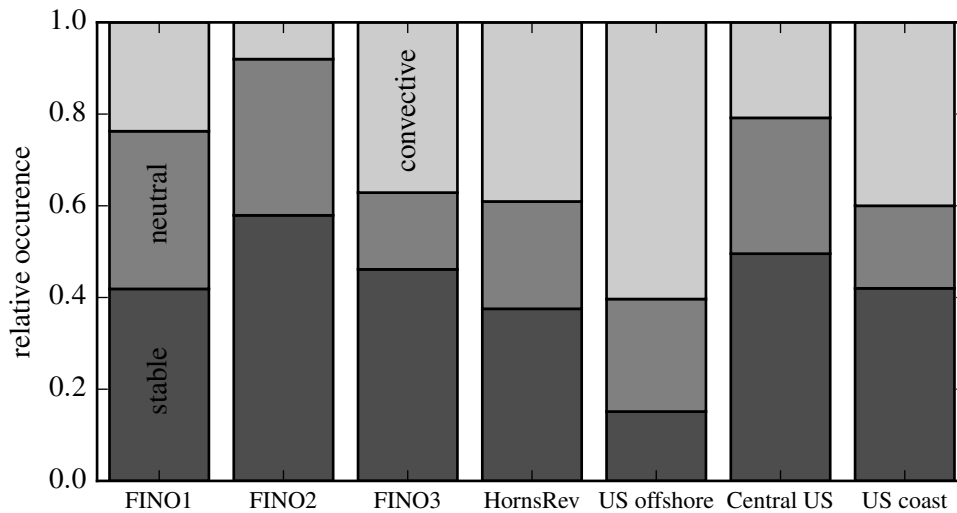
Figure 1.1: Examples of stability distributions at different wind farm sites. FINO data taken from Dörenkämper (2015), HornsRev from Hansen et al. (2012), US offshore from Archer et al. (2016), Central US from Vanderwende and Lundquist (2012) and US coast (onshore) from Wharton and Lundquist (2012). [Note that different methods were used to classify the stability regions]

the turbine due to the mixing with the ambient wind. As the other two important parameters Barthelmie et al. (2013) identify turbulence intensity (TI) and atmospheric stability. Figure 1.2 shows the dependency of wind farm efficiency on TI with data from Barthelmie and Jensen (2010) and Dörenkämper (2015). The illustration reveals that the efficiency decreases by several percentages below a certain threshold of about a 10% level of TI. The relation between atmospheric stability and wind farm efficiency is actually harder to demonstrate with the available measurements. However, Barthelmie et al. (2013) claim that while the relation between TI and wind farm efficiency is better recognizable from measurements, the reduced TI has to be related to the suppression of turbulence in a stable ABL.

The main reason for the difficulties to find a significant dependency of wind farm efficiency on atmospheric stability is that a good measurement of atmospheric stability requires a considerable additional effort and expertise compared to standard measurements at wind farms. The measurement requires either heat and momentum flux measurements or well calibrated and precise temperature sensors at different heights. Furthermore, the height at which atmospheric stability needs to be measured to be representative for the wind and turbulence conditions at the heights of the rotor is still under discussion. Archer et al. (2016) list the variety of measurements and classifications for atmospheric stability used in wind farm studies. The wide spread of approaches makes a direct comparison of these studies challenging.
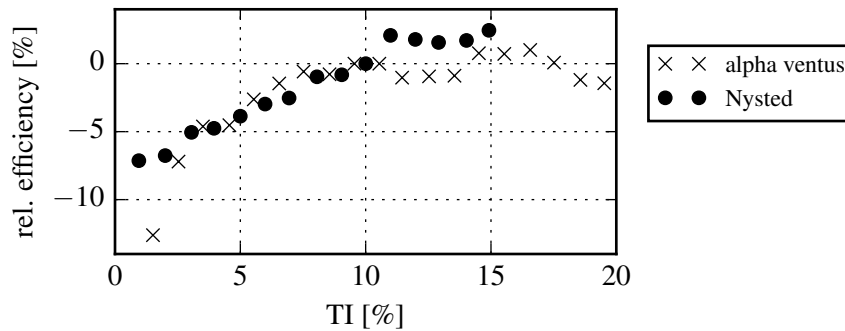
Figure 1.2: Relative dependency of wind farm efficiency on ambient TI. The baseline is the efficiency at 10 % TI. Data from Dörenkämper (2015) for the northern 6 turbines of the wind farm *alpha ventus* and from Barthelmie and Jensen (2010) for the wind farm Nysted.

1.3 Wake models and wind farm experiments

Numerical wind farm models play a large role for the planning and assessment of wind farms. These models estimate the energy yield and the wakes of the turbines in wind farms. Depending on the complexity of the wake model they are able to provide estimations of wind farm efficiency and fatigue loads of the turbines. The concept of wind turbine wake models has been already present since Jensen (1983), and in the last two decades large wind farms have provided valuable validation data.

Engineering wake models developed for wind farm planning and operation range from empirical models (Jensen, 1983; Frandsen et al., 2006) to simplified computational fluid dynamic (CFD) models (Ainslie, 1988; Larsen, 1988). The wind turbines in these models are modelled as actuator discs and momentum balance theory is used to get an initial wake profile downstream of the turbines. For the downstream development of the wake, these so-called engineering models rely on a small set of parameters, that describe the influence of turbine thrust and turbulence on the wake and that need to be carefully calibrated.

While engineering models allow for a calculation of an estimation of wind farm AEP in only few minutes, computational more expensive models have been utilized to conduct numerical wind farm experiments. Models based on the Reynolds-averaged Navier Stokes equations (RANS) allow for a calculation of flow in large wind farms with reasonable computational effort. For example, van der Laan et al. (2015) calculated the interaction of the large Danish wind farms Rodsand II and Nysted for multiple wind directions. However, RANS simulations only simulate an average state of the flow and still have to rely on empirical parameters to be able to consider the high anisotropy of wake turbulence (Sanderse et al., 2011).

In contrast to RANS, Large-Eddy-Simulations (LES) are able to resolve a wide range of turbulent length scales. LES only parameterize the turbulent scales below the grid lengths of the model mesh, which should be chosen fine enough, so that the non-resolved turbulence

is mostly isotropic. With a mesh in the order of a few meters, LES are clearly superior to RANS in the replication of measured wakes (Réthoré, 2009). LES have become a popular tool to study the turbulent flow inside of wind farms (Churchfield et al., 2010; Meyers and Meneveau, 2010; Steinfeld et al., 2010; Porté-Agel et al., 2011), as with LES, not only information about the mean wake influences on wind farm power performance can be gained, but also on the fluctuations that are important for the turbines' lifetimes.

Different kinds of models to represent the turbines of a wind farm have been deployed in LES and RANS depending on the purpose of the research. In the actuator line method (ALM; Sørensen and Shen, 2002) the blades are represented by a line of points on which the body forces of the airfoils are calculated for every time step. This method actually resolves near-wake features as tip and hub vortices, but requires a small time step and is thus quite slow and computationally expensive. Faster methods to represent the turbines in CFD are based on the actuator disc concept. In the simplest actuator disc method (ADM), the thrust of the turbine is uniformly distributed over the rotor and depends on wind speed and thrust coefficient (Mikkelsen, 2003). A more advanced method is to distribute the thrust along the radial axis by using the body forces from the airfoils (Wu and Porté-Agel, 2011). This so-called actuator disc with rotation method (ADM-R) delivers close results to ALM simulations as the rotation of the wake is reproduced. Far downstream of the turbine, where the initial wake rotation becomes negligible, all three actuator methods deliver nearly the same results (Wu and Porté-Agel, 2011; Witha et al., 2014b).

An alternative for wake research to numerical experiments are wind tunnel experiments (Aubrun et al., 2013; Bottasso et al., 2014; Hancock and Zhang, 2015; Schottler et al., 2017). Depending on the focus of the research, different types of wind tunnels and wind turbine models have been and are currently used for wind energy research, ranging from large atmospheric wind tunnels (Hancock and Zhang, 2015; Weitemeyer et al., 2013) that aim at reproducing realistic atmospheric turbulence conditions to engineering wind tunnels that allow for a quick modification of the turbines' control or positioning (Bottasso et al., 2014). Even though the differences in Reynolds-number have to be considered when transferring wind tunnel results to full-scale turbines, these experiments have provided further benchmarks for CFD models.

Wind tunnel and CFD provide the possibility to conduct experiments in reproducible and well-known boundary conditions, thus allow to gain knowledge about the origins of the phenomena that are observed at full-scale wind turbines and farms. These tools are frequently used because experiments on full-scale turbines are much more difficult to conduct. Besides the dependency on wind and weather conditions, one reason is, that wind turbines and wind farms are usually not equipped with adequate measurement devices for scientific experiments of wake interaction. The other reason is that wind turbines are quite expensive test objects and that the owners have to be convinced to invest in field research at their operating wind farms.

LES experiments have been conducted to analyze the influence of atmospheric stability on wind farm performance. Dörenkämper (2015) showed that the wake recovers more slowly downstream of a wind turbine in a stably stratified ABL due to the lower ambient turbulence, but also that turbulence levels at rotor height become less dependent from ambient

stratification downstream from the second turbine in a row, as the wake induced turbulence predominates. To explain the lower power of turbines further downstream, Abkar and Porté-Agel (2013) relate the lower efficiency of wind farms in a stable ABL to the stronger stratification above the wind farm, that diminishes the vertical transport of momentum. A different approach is to relate the increase of efficiency with decreasing stability to the increased meandering of the wake in neutral and unstable conditions (Keck et al., 2014). Regarding the lifetime of the turbines, Churchfield et al. (2012) and Keck et al. (2014) find different structural loads for wind turbines operating in wakes between neutral and convective ABLs. In stable stratification, Lu and Porté-Agel (2011) and Bromm et al. (2017) report high asymmetric rotor loads, especially when operating in the wake of an upwind turbine. These examples demonstrate, that the analysis and discussion of the influence of atmospheric stability on wind farm performance are still ongoing and that more experiments are necessary.

1.4 Wind farm control

Based on recently conducted wind tunnel experiments and numerical studies, the concept of aerodynamic wind farm control is attracting high attention. In wind farm control research, approaches are being investigated that try to actively alter the flow patterns inside wind farms. The aim of these concepts is to either increase the wind farm efficiency or the lifetime of the wind farms' turbines by a reduction of the wake effects. A reduction of wake effects would also make it more economical to place the turbines of a wind farm closer together. This aspect becomes especially interesting for onshore wind energy in densely populated areas like Central Europe.

First research on wind park control in wind tunnels showed that the wake flow downstream of a turbine can be altered by a control that differs from the optimal control of the isolated turbines (Corten and Schaak, 2003; Medici and Dahlberg, 2003). In principle two different approaches have become accepted as promising options to alter the wake flow: induction control and wake steering (Fig. 1.3). Both approaches lead to a lower power at the upwind turbine, with the idea to enable a larger increase of power at the downwind turbines. The first approach relies mostly on the non-linear relation of wind speed, power and thrust of the wind turbine. By reducing the induction at the upwind turbine, not only the power but also the thrust and thus the wake deficit decreases, leading to higher wind speeds at the downwind turbine. While Corten and Schaak (2003) use the control to improve wind farm efficiency in wind tunnel experiments, Annoni et al. (2016) did not find an improvement in LES. They relate their results to the recovery rate of the wake downstream of the wind turbine in a turbulent environment, that decreases with a decreased induction of the turbine.

The second approach, wake steering, uses a deliberate misalignment of the wind turbine to the wind direction to induce a cross-stream momentum that alters the wake trajectory. The magnitude of the wake deflection is assumed to be dependent on the misalignment (the relative turbine yaw angle) and the thrust applied by the wind turbine (Jimenez et al., 2010).

(a) standard control   (b) induction control   (c) wake steering
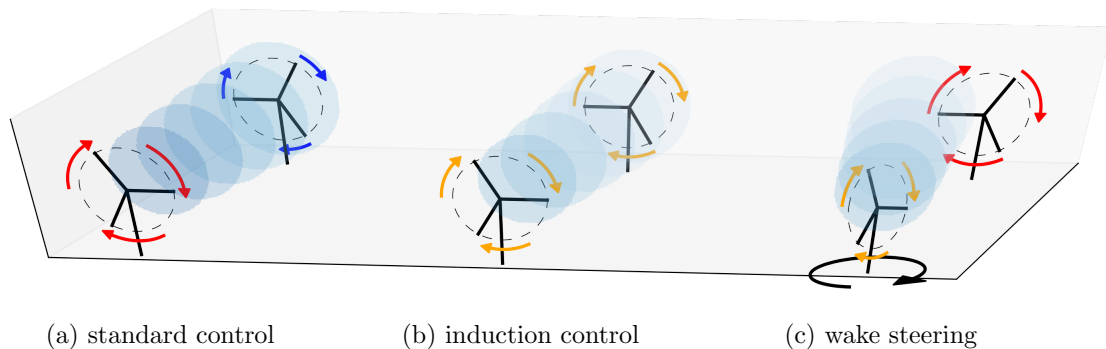
Figure 1.3: Examples for wind farm control. **(a)** Standard control: all turbines are operated to individually extract maximum energy. The downwind turbine has less available kinetic energy in the wind due to the upwind turbine's wake. **(b)** Induction control: the upwind turbine reduces the energy extraction to make more mean kinetic energy available to the downstream turbine. **(c)** Wake steering: the upwind turbine operates in yaw. Besides extracting less energy, the turbine also induces a cross-stream momentum that leads to a different trajectory of the wake.

Medici and Dahlberg (2003) in the wind tunnel, and Fleming et al. (2015) in LES, were able to find yaw angles of the upwind turbine that increase the energy yield of a two-turbine configuration.

A parametrization of wake steering by yaw was developed from LES with an ADM by Jimenez et al. (2010) with the goal to develop wind farm control models that use the effect for optimizing the energy yield. Principally, an optimization of the control of all turbines of a wind farm is possible with these models. Gebraad et al. (2017), e.g., use an analytic wake model to calculate a maximum annual energy production (AEP) improvement of 3.7% by wake steering in an example wind farm. To develop wind farm control further towards application, current model development focuses on including simplified dynamics of the flow while still being fast enough for controller design purposes (Gebraad et al., 2016b; Boersma et al., 2018).

The engineering models that are currently used for wind farm control are only tuned with a very limited set of LES cases in neutral atmospheric stability. Because the effect of wind farm control is only at a few percentages at most, however, the accuracy of the model predictions for other stability conditions than neutral is crucial. For increasing the credibility of these models it needs to be proven that the effects observed in the few cases can be translated to other wind and stability conditions, or it has to be determined how these models need to be modified otherwise.

With the increased attention for the wind farm control topic, recent measurement campaigns were designed with the focus to validate wake steering on real wind turbines (Bromm et al., 2018; Fleming et al., 2017b). To create a picture of the wake in free field as complete as possible, light detection and ranging (lidar) measurements are used for a quick remote

sensing of the wind at multiple heights and distances. The campaigns are designed to collect field data for the validation of the model predictions of wake deflection. However, to isolate the effect of yawing on the wake trajectory, other potential influencing factors of the wind conditions on the wakes have to be identified and quantified.

Another strategy for validating wind farm control is to actually apply it in a wind farm and to measure the power difference between baseline control and wind farm control. The main issue of this approach is the long measurement period that is necessary to reach a statistical convergence of the energy yield with an uncertainty that lies within the few percentages that can potentially be gained by the control. Even when the wind farm is operated in baseline control, multiple months of measurements are usually necessary to derive significant mean relations between wind speeds and wake losses for the narrow wind direction sectors in which wind farm control is potentially beneficial. When atmospheric stability or turbulence intensity are used as additional categories to specify the relationship, the required period of measurements increases further (see e.g. Barthelmie et al., 2013). A control evaluation would require to use two different controls at least once in wind conditions that would normally lead to exactly the same energy yield of the wind farm. For a successful validation it is thus crucial to have the appropriate measurement setup to identify these identical wind conditions for the wind farm.

1.5 Objectives and structure of the thesis

The main goal of this thesis is to analyze the influences of changing atmospheric stability conditions on the wind farm control approach of wake steering and to suggest how to modify control strategies based on the findings. It is supposed to provide a previously missing link between the meteorology-based research in the wind energy community and the engineering-based research. The main methodology that is used throughout this thesis is the simulation of the interaction of atmospheric flow with wind turbines by means of LES with the Parallelized Large-Eddy Simulation Model (PALM; Maronga et al., 2015) and the ADM-R turbine parametrization. Two different approaches are used for the analysis. In the first approach wake steering is applied in three different LES wind fields that are example representations of three distinct stability states of the ABL. From these simulations the factors that influence the wake characteristics and the energy yield of the wind farm are identified. In the second approach, a methodology is tested to set up LES with profiles from numerical weather models to replicate the wind conditions that were actually measured in a measurement campaign. These simulations are used to directly interpret field measurements of wakes.

Three main research questions can be defined for this work:

- How does the variation of wind conditions by atmospheric stability influence the steered wake?

- What are the power benefits of wake steering in a small wind farm and how does the control need to be modified when atmospheric stability changes?

- How accurate are the wind conditions and wakes measured at wind farms replicated by LES driven with data from numerical weather models and what are the benefits of this methodology for studying wind farm flow?

The thesis consists of two already published peer-reviewed paper contributions, one peer-reviewed conference proceedings contribution, a fourth previously unpublished chapter and a conclusion of the thesis' findings. The contents of the chapters are summarized shortly in the following.

In Chapter 2, Vollmer et al., 2016, *Estimating the wake deflection of a wind turbine in yaw in different atmospheric stabilities: An LES study*, the wake flow behind a single wind turbine in LES of example ABLs of stable, neutral and unstable stratification is compared. To study wake steering, the turbine is operated at different yaw angles to the incoming wind. Various methods to define the wake center for the evaluation of the trajectory are compared with a discussion of the implications on the design of measurement campaigns and the parametrization in wake models. Furthermore, the averaging period to define a mean wake profile and trajectory is altered to consider different possible reaction times for a wind farm controller. The results are discussed with respect to the application of wake steering in a wind farm.

In Chapter 3, Vollmer et al. 2017, *Transient LES of an offshore wind turbine*, a method is proposed to include changing synoptic weather conditions in an LES to be able to reproduce realistically changing wind and weather conditions at a wind farm site during one single simulation. The results of the methodology are compared with met mast measurements at FINO 1. The transient LES is used to simulate the wake flow of a wind turbine of *alpha ventus* at different times during a day for which lidar measurements of the same turbine's wake were available. Simulation results and lidar measurements are compared to validate the wake simulation approach. The discussion focuses on the sources for the deviations and the possible application of the model chain approach for studying wind farms in the ABL.

In Chapter 4, Vollmer et al. 2017, *A wind turbine wake in changing atmospheric conditions: LES and lidar measurements*, the previously introduced model chain method is used to simulate a strong diurnal cycle of atmospheric stability, based on a measured case at an onshore wind farm in Iowa, USA. The diurnal cycle includes even stronger periods of stable and convective stability conditions than the cases studied in Ch. 2. Due to the steady development of the boundary layer turbulence, an observation of the continuous change of wake behavior is possible. The previously introduced methods to define the wake center are applied on the flow results with the focus on the implications on wind farm control.

In Chapter 5, *Wind farm control applied in different atmospheric stabilities*, LES is used as an experimental environment to test wake steering in a two-turbine wind farm. From the simulations of Ch. 2, a simple wake model is developed, that is used for open-loop model-based yaw control of the upwind turbine. A comparison between the application in the three different stability regimes is made. The critical situations for the controller are identified and the controller is modified to improve the performance for these situations. The findings of

the chapter are discussed with a focus on the applicability in real wind farms.

The results of the thesis are summarized in the last chapter, with an overview over parallel and related developments and an outlook and suggestions for the research and application of wind farm control.

Chapter 2

Estimating the wake deflection downstream of a wind turbine in different atmospheric stabilities: an LES study [1]

Abstract   An intentional yaw misalignment of wind turbines is currently discussed as one possibility to increase the overall energy yield of wind farms. The idea behind this control is to decrease wake losses of downstream turbines by altering the wake trajectory of the controlled upwind turbines. For an application of such an operational control, precise knowledge about the inflow wind conditions, the magnitude of wake deflection by a yawed turbine and the propagation of the wake is crucial. The dependency of the wake deflection on the ambient wind conditions as well as the uncertainty of its trajectory are not sufficiently covered in current wind farm control models. In this study we analyze multiple sources that contribute to the uncertainty of the estimation of the wake deflection downstream of yawed wind turbines in different ambient wind conditions. We find that the wake shapes and the magnitude of deflection differ in the three evaluated atmospheric boundary layers of neutral, stable and unstable thermal stability. Uncertainty in the wake deflection estimation increases for smaller temporal averaging intervals. We also consider the choice of the method to define the wake center as a source of uncertainty as it modifies the result. The variance of the wake deflection estimation increases with decreasing atmospheric stability. Control of the wake position in a highly convective environment is therefore not recommended.

2.1 Introduction

The performance of a wind farm does not only depend on the ability of its wind turbines to convert available kinetic energy into electric energy but is also largely influenced by the fluctuation of the atmospheric winds and the wakes created by the turbines. Wind turbine wakes are areas of lower wind speed and enhanced turbulence that result from the extraction of kinetic energy from the flow by the turbine and can have a significant impact on the wind conditions up to 10–15 rotor diameters downstream. To minimize the losses due to wind turbine wakes, the wind rose measured at a location is usually taken into account during the design process of the wind farm layout. However, in most locations, in particular in mid-latitudes with alternating low- and high-pressure systems, the unsteady wind direction creates a high occurrence of situations for which wake losses remain large.

Multiple studies, e.g., Barthelmie and Jensen (2010); Hansen et al. (2012), have shown that the wake losses in wind farms depend on the turbulence intensity of the ambient wind, with decreasing efficiency of the wind farm for low turbulence. Sources of turbulence in the atmospheric boundary layer are mechanical shear and buoyancy. The latter depends mainly on the thermal stratification and can also be a sink of turbulence. In a stably stratified atmospheric boundary layer (SBL) turbulence is suppressed by the stable thermal stratification that decelerates the vertical movement of air masses while in a convective atmospheric boundary layer (CBL) the source of energy at the bottom of the atmosphere enhances the turbulent motion. Studies of atmospheric stability have shown that convective and stable conditions occur at least as often as neutral conditions (NBL) at onshore (Vanderwende and Lundquist, 2012; Wharton and Lundquist, 2012) and offshore (Barthelmie and Jensen, 2010; Hansen et al., 2012; Dörenkämper et al., 2014) wind farms and that wind farms are least efficient in stable conditions (Barthelmie and Jensen, 2010; Hansen et al., 2012; Dörenkämper et al., 2014).

The observation of a change of wind farm performance with different atmospheric stability has been supported by wind tunnel experiments and numerical studies. It has been either related to a generally different level of turbulence (Hancock and Zhang, 2015) or to the presence of large-scale fluctuations that enhance the so-called meandering of the wakes in less stable situations (Machefaux et al., 2015a; Larsen et al., 2015; Keck et al., 2014; España et al., 2011). Emeis (2010) and Abkar and Porté-Agel (2013) argue that the thermal stratification above the wind farm becomes important for large wind farms as the vertical momentum transport becomes the only kinetic energy source to refill the wake deficit. Apart from the energy yield, the structural loads on turbines in the wake also differ with atmospheric stability as they are influenced by up- and downdrafts and large coherent structures in a CBL (Churchfield et al., 2012) and by sharp velocity gradients in an SBL (Bromm et al., 2017).

With increasing capacity of wind turbines the value of every additional percentage of energy that can be harvested from the wind becomes larger. As a consequence the interest to increase the power output for unfavorable wake situations is growing. Recent studies focus on the control of upwind turbines to minimize wake losses of downwind turbines by either

reducing the induction (Corten and Schaak, 2003) or by an intentional yaw angle of the turbine to the wind direction (Medici and Dahlberg, 2003; Jimenez et al., 2010; Fleming et al., 2014). The first approach aims on less extraction of energy from the wind by the upwind turbine and therefore more remaining energy that can be extracted by downwind turbines. The second approach relies on an induction of a cross stream momentum by the upwind turbine to change the trajectory of the wake with the goal to deflect it away from the downwind turbine. While in both approaches the upwind turbine experiences a loss in power and possibly an increase in structural loads, the additional gain at the downwind turbine is assumed to exceed this loss, thus leading to a surplus of total power output of the wind farm. Based on this assumption, simple models for a joint control of wind turbines to increase power output during operation for a fixed layout have been proposed (Annoni et al., 2016; Gebraad et al., 2016b). Fleming et al. (2016) even suggest including power yield optimization by wind farm control in the design process of new wind farm layouts.

Crucial for wind farm control models is a proper description of the wake trajectory as a wrong description would almost certainly lead to a reduction of energy yield of the wind farm due to the lower energy yield of the upwind turbines. However, magnitudes of the wake deflection differ already in the parameterizations of Jimenez et al. (2010) and Gebraad et al. (2016b). Possible reasons for the differences include the use of different turbine models, the method to extract the wake trajectory from the measured wind field and the ambient wind conditions. Apart from the differences in the description of the mean wake trajectory, an aspect that is not considered yet in current wind farm control models is the stochastic nature of the wake trajectory. Keck et al. (2014) show not only that the movement of the wake becomes more and more stochastic for small averaging intervals, but also that these motions are linked to atmospheric stability. Considering that the potential to improve wind farm efficiency through wind farm control appears to be dependent on atmospheric stability, little knowledge exists on how the control would need to adapt to changes of the wind conditions as influenced by atmospheric stability.

In this study we analyze multiple sources that contribute to the uncertainty of the estimation of the wake deflection downstream of yawed wind turbines in different ambient wind conditions. The ambient wind conditions are created by Large Eddy Simulations (LES) of atmospheric boundary layers of neutral, stable and unstable stability. The simulations are run with the same mean wind speed and wind direction but changing the stability produces differences in the shear and turbulence of the wind. The wind turbine wakes are created by enhanced actuator disc models with rotation (Dörenkämper et al., 2015b). We use the data from these simulations not only to analyze if the stability changes the magnitude of the wake deflection but also to compare different fitting routines to extract the wake center. In addition to these aspects, that we already consider as contributors to the uncertainty of the wake deflection estimation, we also look at the influence of different temporal averaging intervals on our results.
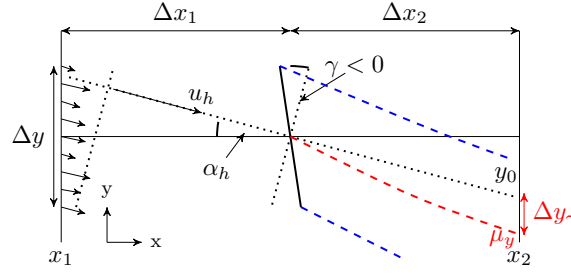
Figure 2.1: Conceptual image of the method to calculate the wake deflection $\Delta y_\gamma(x_2)$ by using the inflow wind direction $\alpha_h(x_1)$ of the wind speed $u_h(x_1)$ at hub height and the position of the wake center $\mu_y(x_2)$. Here, the x axis is the mean wind direction. The yaw angle γ is defined relative to α_h, with $\gamma > 0$ for a clockwise turning of the rotor. Inflow wind speed and direction are averaged along Δy.

2.2 Methods

2.2.1 Estimating the wake deflection

We assume that the wake position μ_y at a certain distance downstream of a wind turbine can be predicted when the hub height wind direction α_h and the wake deflection Δy_γ are known.

$$\mu_y = y_0(\alpha_h) + \Delta y_\gamma, \tag{2.1}$$

where y_0 is the displacement of the wake in a fixed coordinate system by the change of wind direction (Fig. 2.1).

The advantage of LES is that the wake position and the wind direction can be assessed directly from the flow field to estimate the unknown deflection of the wake by the yawed turbine. For a fixed thrust coefficient, turbine site, wind speed and wind direction, the wake deflection is assumed to be a function of the yaw angle γ and the atmospheric stability, e.g., given by the Monin-Obhukov length L.

$$\Delta y_\gamma = \Delta y_\gamma(\gamma, L) \tag{2.2}$$

The relationship of Δy_γ on the yaw angle and the atmospheric stability is estimated from multiple LES with different γ and L.

$$< \Delta y_\gamma > |_{\gamma,L} = < \mu_y(f_i) > - < y_0(\alpha_h) > \tag{2.3}$$

Here we consider that the estimate of μ_y depends on the algorithm f_i used to estimate the wake center position from the simulated flow field. To calculate the temporal variation of the wake deflection we divide the time series into shorter intervals Δt and calculate the variance of this individual estimates about the mean.

2.2.2 Estimating the wake displacement by the change of wind direction

We consider the wind conditions at $x_1 = 2.5$ rotor diameters (D) upstream as reference inflow conditions to a wind turbine. This distance is chosen as the wind field closer to the turbine might be modified by the induction of the rotor (IEC-61400-12-1, 2005). More precisely our inflow information is hub height wind speed u_h and wind direction α_h averaged at x_1 on a line extending $\Delta y = 2\,\mathrm{D}$ perpendicular to the expected mean wind direction (Fig. 2.1). We choose cross stream averaged variables instead of a point measurement as we consider them more representative for the wind conditions for the wind turbine rotor.

To estimate the wake displacement y_0 we assume an advection of the wake with the ambient wind. If the wind direction coincides with the x axis ($\alpha_h = 0$), the wind flows along the x axis and interacts with the wind turbine to form a wake structure that is advected downstream, supposedly centered around $y_0 = 0$. For wind directions $\alpha_h \neq 0$ the x axis and wind direction differ and the center μ_γ of the wake is expected to be shifted by $y_0 = \Delta x_2 \tan \alpha_h$ along the y axis (Fig. 2.1). As we only consider deviations of the wind direction from the x axis of less than $10°$, the change of x_2 with α_h is neglected.

This simple consideration already allows for a first estimation of how the uncertainty from the calculation of the wind direction can propagate into the error of the wake deflection estimation. For an error of the wind direction estimation of $\sigma_{\alpha_h} = \pm 5°(10°)$ the wake center displacement y_0 at $x_2 = 6\,\mathrm{D}$ downstream would have an uncertainty of $\sigma_{y_0} \approx \pm 0.5\,\mathrm{D}(1.0\,\mathrm{D})$.

2.2.3 Estimation of the wake center

Three different methods to estimate the wake center position are compared in this study to assess the bias introduced to μ_y by the choice of the method f_i. As a first approach the position of the wake is calculated by fitting the mean wake deficit at hub height to a Gaussian-like function.

$$f_h(y) = u_a \exp\left(-\frac{(y - \mu_y)^2}{2\sigma_y^2}\right) \tag{2.4}$$

The center μ_y of the Gaussian is considered as the horizontal wake center, the amplitude u_a as the wake deficit and σ_y as a measure of the width of the wake.

As we also have information about the vertical structure of the wake, a two dimentional Gaussian-like fit as proposed by Trujillo et al. (2011) is used as alternative fitting routine.

$$f_{2\,\mathrm{D}}(y) = u_a \exp\left[-\frac{1}{2(1 - r^2)}\left(\frac{(y - \mu_y)^2}{\sigma_y^2}\right.\right.$$
$$\left.\left. - \frac{2\rho(y - \mu_y)(z - \mu_z)}{\sigma_y^2 \sigma_z^2} + \frac{(z - \mu_z)^2}{\sigma_z^2}\right)\right] \tag{2.5}$$

with μ_z the equivalent to μ_y on the vertical axis and $r^2 < 1$ a correlation factor. For a perfect circular shape of the wake $r = 0$, whereas for an elliptic wake shape $r \neq 0$. Both

functions are fitted to the data through a least-squares approach.

We introduce a third method to determine the wake position based on the available mean specific power in the wind (AP). As the main interest of wind farm control is the increase of the power output of downstream turbines, we consider the position along the y axis of a hypothetical turbine placed at x_2 that feels the lowest AP as the center point of the wake. For this purpose the cube of the mean flow in wind direction is averaged on circular planes of diameter D centered around hub height z_h. The AP is normalized by the air density, as density variations are not considered.

$$f_{AP}(y) = 1/2 \int_{y1}^{y2} \int_{z1}^{z2} u^3(y', z') dz' dy',$$
$$(y' - y)^2 + (z' - z_h)^2 \leq (D/2)^2 \tag{2.6}$$

The wake center μ_y is the value of y that minimizes Eq. (2.6).

2.2.4 Temporal averaging interval

To study the uncertainty of the wake deflection by the used temporal averaging interval, we divide time series of inflow at x_1 and wake flow at x_2 in multiple time intervals Δt. We chose time intervals of respectively $\Delta t = 10$, 3 and 1 min as we consider them realistic for wind farm control.

For small Δt the wind conditions at x_1 and x_2 become more and more uncorrelated, thus the advection time of the turbulent structures between these points is considered for each averaging interval. Turbulent structures in the wind field are expected to be transported by the mean wind following Taylor's hypothesis of frozen turbulence. To describe the time τ it takes for a structure to be advected from the position x_1 to the position x_2 we use the following approximation:

$$\tau = (\Delta x_1 + \Delta x_2)/u_h \tag{2.7}$$

with Δx_1 and Δx_2 being the distances from x_1 and x_2 to the wind turbine, respectively. In presence of a turbulent structure of lower velocity like a wind turbine wake, the advection velocity downstream of the turbine along Δx_2 is not well studied. Following Larsen et al. (2008) we assume that the wake is moved like a passive tracer by the ambient wind field. Thus the advection velocity downstream of the turbine remains the same as upstream.

Combining the methods presented in previous subsections we find multiple estimates of the wake deflection Δy_γ by calculating the wind direction α_h and the wake center μ_y for different averaging intervals Δt, with the time series at x_2 shifted by τ, and for different methods f_i to identify the wake center from the wake flow.

2.2.5 LES model

The simulations presented in here are conducted with the LES model PALM (Maronga et al., 2015). PALM is an open source LES code that was developed for atmospheric and oceanic flows and is optimized for massively parallel computer architectures. It uses central differences to discretize the non-hydrostatic incompressible Boussinesq approximation of the Navier-Stokes equations on a uniformly spaced Cartesian grid. PALM allows for a variety of schemes to solve the discretized equations.

The following schemes are used in this study: advection terms are solved by a fifth-order Wicker-Skamarock scheme, for the time integration a third-order Runge-Kutta scheme is applied. For cyclic horizontal boundary conditions a FFT solver of the Poisson equation is used to ensure incompressibility, while for non-cyclic horizontal boundary conditions an iterative multi-grid scheme is utilized. A modified Smagorinsky sub-grid scale parametrization by Deardorff (1980) is used to model the impact of turbulence of scales smaller than the model grid length on the resolved turbulence. Roughness lengths for momentum and heat are prescribed to calculate momentum and heat fluxes at the lowest grid level following Monin-Obukhov similarity theory.

The simulations in PALM are initialized with a laminar flow field. Random perturbations of the flow during the start of the simulation initiate the development of turbulence. The statistics of the steady turbulence that develops after some spin-up time depend on the initial conditions provided for the fluid, e.g., the temperature profile, and the boundary conditions during the simulation, e.g., surface heat fluxes. For more information about the general capabilities of the model the reader is referred to Maronga et al. (2015).

2.2.6 Wind turbine model

The effect of the wind turbine on the flow is parameterized by means of an enhanced actuator disk model with rotation (ADM-R) as in Witha et al. (2014a); Dörenkämper et al. (2015b). The rotor disk is divided into rotor annulus segments with changing blade properties along the radial axis. The blade segments positions are fixed in time but each owns an azimuthal velocity due to the clockwise rotation of the rotor. Local velocities at the segment positions are used in combination with the local lift and drag coefficients of the blade to calculate lift and drag forces. The forces are scaled for a three bladed turbine and are afterwards projected onto the grid of the LES by a smearing function with a Gaussian kernel as described in Dörenkämper et al. (2015b). In internal sensitivity studies we found that a value of twice the grid size is a good choice for the regularization parameter as also concluded by Troldborg et al. (2014). The rotor can be rotated around the y axis and the z axis enabling a free choice of yaw and tilt configuration. The influence of tower and nacelle on the flow is represented by constant drag coefficients.

The blade properties as well as the hub height of $z_h = 90\,\mathrm{m}$ and the rotor diameter of $D = 126\,\mathrm{m}$ originate from the NREL 5MW research turbine (Jonkman et al., 2009). A
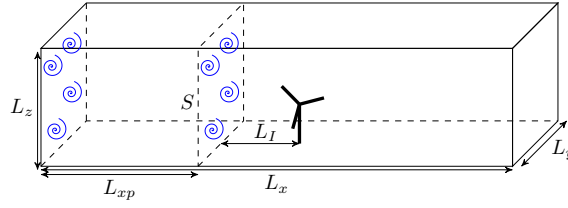
Figure 2.2: Domain of the main simulations. L_{xp} is the length of the prerun domain. The turbulence at the recycling surface S is used as input at the inflow again. L_I is the distance from the recycling surface to the wind turbine.

variable-speed generator-torque controller is implemented in the same way as described in Jonkman et al. (2009). Note that no vertical tilt is applied to the rotor to exclude the wake displacement that might result from a mean vertical momentum of the wake.

2.2.7 Precursor simulations

Precursor simulations of the atmospheric boundary layer for the representation of three different atmospheric stabilities, stable, neutral and convective, are conducted with the goal of creating different shear and turbulence characteristics but with the same mean wind speed and direction at hub height. All domains have a horizontal and vertical grid resolution of $\Delta = 5\,\text{m}$ up until the initial height of the boundary layer in each simulation. Above this height the vertical grid size increases by $6\,\%$ per vertical grid cell. The roughness length is kept constant in all simulations at $z_0 = 0.1\,\text{m}$, representing a low onshore roughness representative for low crops and few larger objects. The Coriolis parameter corresponds to $54°\,\text{N}$. Cyclic lateral boundary conditions are used and the simulations are initialized with a vertically constant geostrophic wind. Due to Coriolis forces, bottom friction and stratification, height-dependent wind speed and wind direction profiles evolve after several hours of spin-up

Table 2.1: Setup of the three simulations and results by the end of the prerun. Domain dimensions (see Fig. 2.2) are given in multiples of rotor diameter D. The number of turbines in the main simulation is n_T. Results consist of wind speed u_h and turbulence intensity TI_h at hub height, wind shear coefficient α_s and veer $\delta\alpha$, both evaluated between lower and upper rotor tip, Monin-Obukhov-Length L, and boundary layer height z_i.

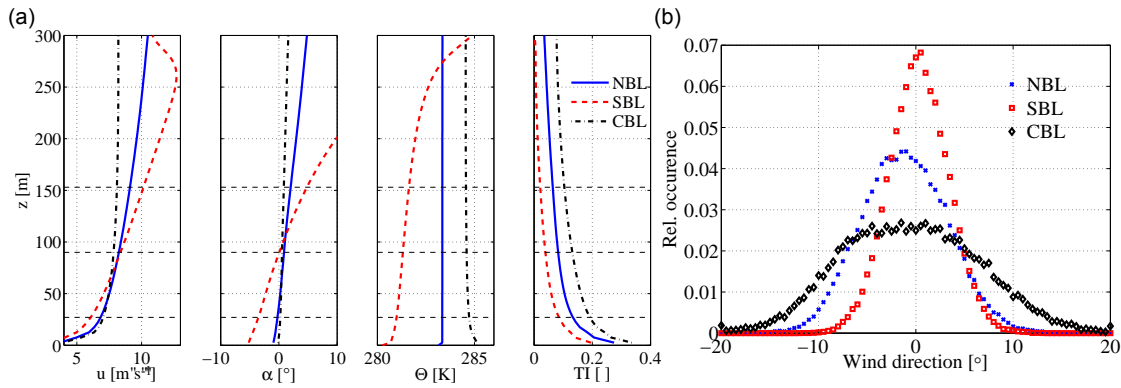|	Setup						Results					
	L_x	L_{xp}	L_y	L_I	L_z	n_T	u_h	TI_h	α_s	$\delta\alpha$	L	z_i
	[D]	[D]	[D]	[D]	[D]	[ms^{-1}]	[%]	[]	[°]	[m]	[m]	
SBL	30.5	11.4	7.6	3.0	4.5	1	8.4	4.0	0.30	8.2	170	300
NBL	61.0	23.7	20.3	6.0	13.6	1	8.3	8.3	0.17	2.2	∞	550
CBL	132.0	81.3	50.8	8.0/20.0	11.6	8	7.8	13.3	0.08	0.6	-180	650

Figure 2.3: Flow statistics during the last hour of the precursor simulations. **(a)** Horizontally averaged vertical profiles of wind speed, flow direction, potential temperature and turbulence intensity. Horizontal lines denote the height of the blade tips and the hub. **(b)** Distribution of the 1 Hz wind direction from point measurements at hub height.

time.

For the generation of a SBL, a constant cooling of the lowest grid cells is prescribed. The initial temperature profile of the potential temperature Θ and the rate of bottom cooling ($d\Theta/dt = 1\,K/4\,h$) are set as in Beare and Macvean (2004). A CBL is established by prescribing a constant kinematic sensible heat flux of $60\,W\,m^{-2}$ at the bottom boundary. The bottom heat flux is fixed to zero for the NBL. The initial potential temperature profiles of the NBL and CBL are constant up to 500 m height with a strong inversion of $d\Theta/dz = 8\,K/100\,m$ between 500 and 600 m and a stable stratification of $d\Theta/dz = 1\,K/100\,m$ up to the upper model boundary.

The results of the precursor simulations are shown in Figs. 2.3, 2.4 and Table 2.1. The simulations differ in their horizontal and vertical extent (see Table 2.1), a consequence of the different heights of the mixing layers and the different sizes of the largest eddies that need to be explicitly resolved. These simulations are afterwards used as initial wind fields for the main simulations described in Sect. 2.8 that include the impact of the wind turbine on the flow by the ADM-R parametrization. As intended, the domain averaged profiles have similar mean wind speed and direction at hub height but differ in vertical shear of the wind speed, wind veer and turbulence intensity (Fig. 2.3). The SBL is characterized by a strong vertical shear of wind speed and wind direction over the height of the rotor. Shear coefficient $\alpha_s = 0.30$ and Monin-Obhukov length $L = 170\,m$ correspond to a stable to highly stable stability class following Wharton and Lundquist (2012). The wind direction changes by 8° from the lower rotor tip to the upper rotor tip. Below the top of the SBL at around $z_i = 300\,m$, the wind speed has a super-geostrophic maximum, an event called low level jet, that has been documented in measurements onshore as well as offshore (Smedman et al., 1996; Emeis, 2014; Dörenkämper et al., 2015a).

The NBL and the CBL exhibit only low vertical dependency of the wind vector above
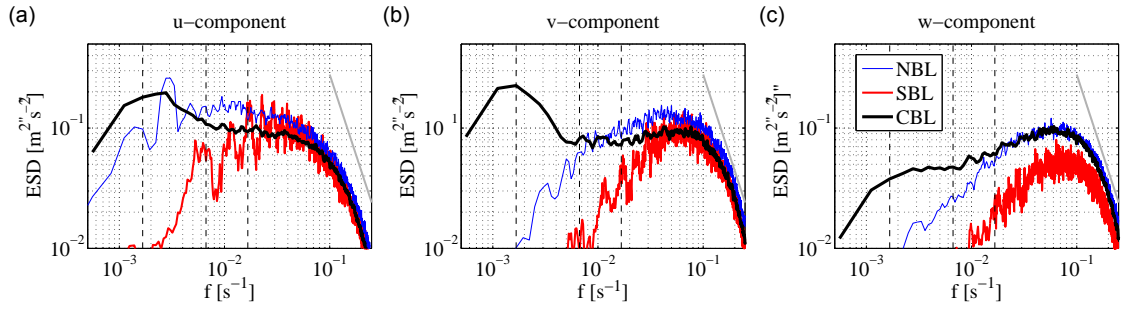
Figure 2.4: Energy spectral density of the three different wind components at hub height during the last hour of the precursor simulations. The gray line denotes the slope of the Kolmogorov cascade. Vertical lines are at $T = 10\,\text{min}$, $3\,\text{min}$ and $1\,\text{min}$.

the lower rotor tip. Responsible for the low vertical wind speed gradient is the increased amount of turbulent kinetic energy that leads to a stronger mixing. The spectra of the three velocity components at hub height shown in Fig. 2.4 reveal that not only the total amount of turbulent kinetic energy is larger in the neutral and convective case, but the most energetic motion also occurs on larger scales.

The CBL represents a rather moderate convective boundary layer with $L = -180\,\text{m}$ and a ratio between the boundary layer height z_i and L of $z_i/L = -3.6$. Characteristic for such moderate convective boundary layers in flat terrain are large roll-vortices, whose axes of rotation are approximately aligned with the mean wind direction and that have a vertical extension up to the top of the boundary layer (Etling and Brown, 1993; Gryschka et al., 2008). The presence of these vortices can be seen in the highly energetic low frequently motion of the v- and w-components and the large variance of the wind direction.

The meteorological conditions of the CBL and SBL simulation cases are regularly occurring at wind farm sites (Hansen et al., 2012; Vanderwende and Lundquist, 2012; Wharton and Lundquist, 2012). Numerical simulations comparable to the CBL and NBL case are studied in Churchfield et al. (2012), while Mirocha et al. (2015) simulate even stronger stable and convective conditions, which are motivated by measured events.

2.2.8 Setup of the wind turbine wake simulations

For the main simulations a turbulence recycling method (Maronga et al., 2015) is used at the upstream domain boundary instead of a cyclic boundary (Fig. 2.2). This allows for studying a single turbine along the x axis instead of an infinitively long row of turbines. Undisturbed outflow at the right boundary is ensured by a radiation boundary condition. For the use of the turbulent recycling method the model domain from the precursor simulations is extended along the x axis and the recycling surface is positioned at the domain length L_{xp} of the precursor run. Test simulations showed a minimum of $L_y^{\min} \approx 8\,\text{D}$ to prevent blockage of the flow by the turbine and a minimum distance between recycling surface and turbine of
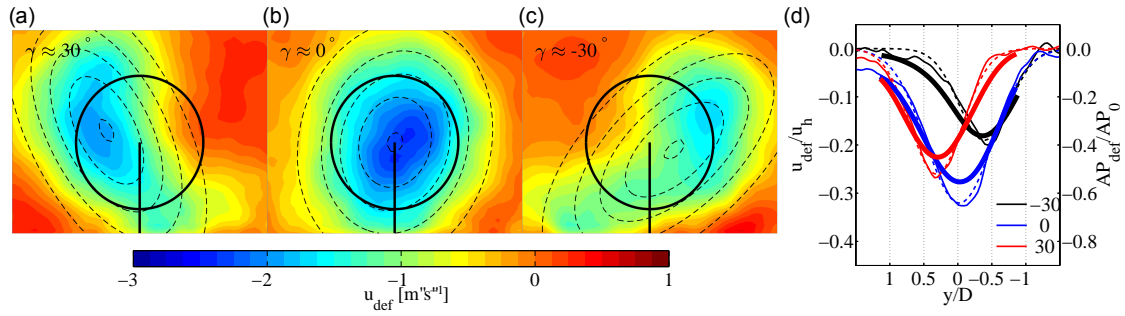
Figure 2.5: **(a–c)** Mean wake deficit 6 D downstream of a wind turbine in the NBL. The turbine is yawed by **(a)** 30°, **(b)** 0° and **(c)** −30°. Straight contours denote the position of the upstream turbine. Dashed contours are the isolines of constant f_{2D}. **(d)** Cross sections of normalized u_{def} at hub height (thin) and results of f_{AP} (bold) and f_h (dashed).
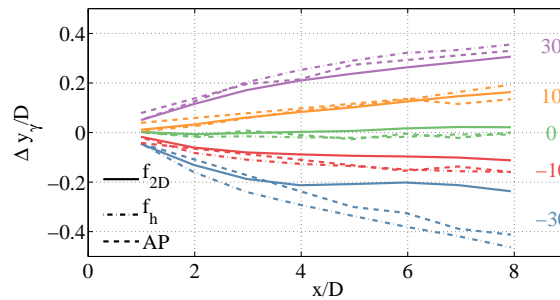
Figure 2.6: Wake deflection trajectories in the NBL from different fits to the data. Numbers on the right denote the turbine yaw angle for the different trajectories.

$L_l^{min} \approx 3\,D$ to prevent an influence of the induction zone on the turbulence at the recycling surface.

The main simulations of the NBL and SBL are conducted for single turbines with a different yaw angle to the x axis. For each change in yaw angle a separate simulation of 25 min length is conducted from which the first 5 min, during which the wake still develops, are discarded from the analysis. Yaw angles ranging from −30 to 30° in steps of 10° are chosen. Positive yaw angles are defined as a clockwise turning of the rotor when seen from above and the wind coming from the left-hand side.

In the CBL the domain width L_y is more than 6 times larger than the minimum size of L_y^{min}. We use this to include all different turbine yaw angle configurations in one simulation consisting of two staggered rows of four turbines each, separated by more than L_y^{min} in y and 12 D in x direction. The distances are chosen large enough that a mutual interaction of the turbines can be excluded. Each of the turbines had a different yaw angle to the x axis and the simulation was run for 65 min from which the first 5 min were discarded. The longer simulation time of the CBL is motivated by the larger turbulence length scales of the flow that cause longer necessary averaging intervals to get information about mean properties.
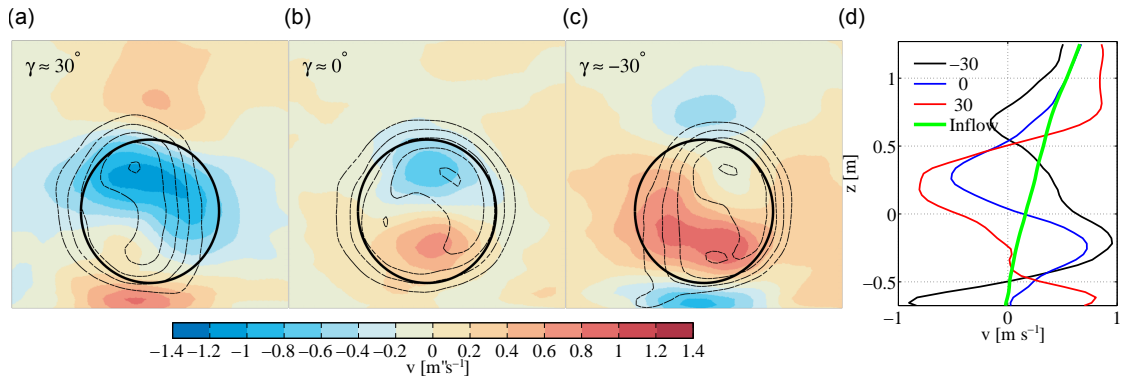
Figure 2.7: **(a–c)** Residual cross stream component of the flow at $x_2 = 2\,$D downstream of the wind turbine for the same simulations as in Fig. 2.5. Positive (negative) values stand for a flow to the right (left). Dashed contours denote the position of the wake deficit. **(d)** Vertical profile of the total v component at y_0 and x_2, and the average inflow profile.
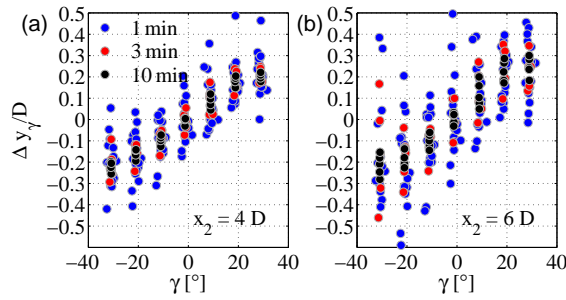
Figure 2.8: Scatter plot of the horizontal wake deflection in the NBL from the $f_{2\,\mathrm{D}}$-fit over yaw angle γ at different downstream positions x_2 and for different averaging intervals.

Note that due to the cyclic lateral boundary conditions, the turbines in all simulations are part of an infinite row along y separated by more than L_y^{min}.

2.3 Results

In this section we compare the results of the main simulations with presence of wind turbines. The vertical planes of the LES flow that are shown on the following pages represent the view of an upstream observer looking downstream. If not explicitly noted otherwise, the zero coordinate of the x axis coincides with the x position of the rotor center and the zero coordinate of the y axis with y_0, i.e., the zero coordinate of y corrected by the measured inflow wind direction α_{h}. The y axis is positive to the left-hand side of the upstream observer.

2.3.1 Neutral atmospheric boundary layer

We start the analysis with the NBL, as this case is the most studied case in wind energy applications. Figures 2.5a–c show vertical planes of the wake deficit u_{def}, averaged over the whole simulation time, for three different yaw angles γ at $x_2 = 6\,\mathrm{D}$. The velocity u_{def} is defined as the difference between the inflow velocity profile of $u(y, z)$ measured as inflow at x_1 and averaged along $\Delta y = 2\,\mathrm{D}$ and the velocity field $u(y, z)$ at x_2 downstream of the wind turbines (Fig. 2.1). The isolines of the 2-D fitting method $f_{2\,\mathrm{D}}$ are denoted by dashed contours. The wake deflection Δy_γ that results from this routine is visible as the innermost ring. Cross sections of Fig. 2.5a–c at hub height are shown together with the results of f_{h} and f_{AP} in Fig. 2.5d. The wake centers are the positions along y for which the functions take the smallest values.

As apparent in Fig. 2.5 the wake deficit is lower for the two cases of turbines with a large yaw angle, a consequence of the loss of energy yield and induction, if a wind turbine is yawed out of the wind direction. For a positive (negative) yaw angle the wake deficit is deflected to the left (right) when looking from upstream. Figure 2.6 shows the mean deflection Δy_γ of the wake center for multiple distances downstream of the rotor using the three different approaches f_i. The Gaussian-like fit at hub height f_{h} returns the largest deflection of the wake. The smallest deflection is found when the wake is approximated by the 2 D normal fit $f_{2\,\mathrm{D}}$ while the wake position of minimal f_{AP} lies mostly between the two curves.

The reason for the different output of the three methods is the deviation of the wake from a perfect symmetric shape as evident in Fig. 2.5. The crescent shapes of the wakes indicate that the lateral displacement is largest at the height around the rotor center while it is lower around the upper and the lower rotor tip, which explains the largest magnitude of wake deflection for f_{h}.

A look at the cross stream component of the flow reveals the origin of the crescent shape of the wakes of a yawed turbine. Figure 2.7 shows the residual cross stream component of the flow in the near wake. The residual component is the difference between the inflow profile and the downstream wind field. For $\gamma = 0°$, the dominant feature of the cross stream flow is the counterclockwise rotation of the wake that is induced by the clockwise rotation of the rotor. For $\gamma \neq 0°$, the rotation is superimposed by the induction of cross stream momentum caused by the yawed turbine. Figure 2.7a, c show that this cross stream momentum is either opposing the rotor rotation below or above the hub, which, together with the influence of wind veer, leads to the asymmetries further downstream as evident in Fig. 2.5a, c.

As apparent in Fig. 2.7 the induced cross stream momentum also triggers a counter momentum above and below the rotor area. The opposing cross stream velocities appear to be responsible for the varying magnitude of lateral displacement at different heights and the crescent shape of the wake further downstream. The counter momentum is stronger below the rotor area, which is likely to be related to the presence of the bottom just 27 m below the blade tip.

To assess the influence of the temporal averaging interval on the standard deviation of the wake deflection, Δy_γ is calculated for different time intervals. Advection of frozen ambient

turbulence between x_1 and x_2 is considered by shifting the second time interval by τ (Eq. 2.7). To have more than two estimates for the 10 min interval, the intervals are overlapping to a large degree resulting in seven individual estimates per yaw configuration. Figure 2.8 shows the spread of the estimates of $f_{2\,D}$ at two different positions x_2. We find that the standard deviation of the wake deflection appears to be independent of the yaw angle but depends on the temporal averaging interval. The used fitting method has little influence on the standard deviation of the mean wake deflection in the NBL (Table 2.2).

2.3.2 Stable atmospheric boundary layer

As shown earlier in Fig. 2.3, the simulated SBL is characterized by lower TI and a stronger vertical shear of wind speed and direction than the NBL. For the simulated wind turbine wake in the SBL, the strong wind veer leads to a strong slanted shape of the wake deficit, even if the rotor plane is perpendicular to the wind direction at hub height (Fig. 2.9b). Below the rotor center, the wake is shifted towards the left-hand side and above towards the right-hand side. Thus, the extend of the wake cross section at hub height (Fig. 2.9d) is less representative for the whole wake extension than in the NBL simulation (Fig. 2.5). The amplitude at $x_2 = 6\,D$ of the wake deficit u_{def} is larger than in the NBL. The larger amplitude can be related to the lower ambient turbulent kinetic energy and to the lower fluctuation of the inflow wind direction.

The wakes for $\gamma \neq 0°$ show a similar crescent shape to the wakes in the NBL. The differences between the deficit position at hub height and around the upper and lower rotor tips are even larger, a consequence of the addition of induced momentum by the yawed turbine and ambient wind veer. In the case of a yaw angle of $\gamma \approx -30°$ the lower part of the wake detaches from the rest of the structure. In contrast to the fit $f_{2\,D}$ of the wake at $\gamma \approx 30°$ this detached part is neglected by the optimal fit.

The trajectories of the wake deflection shown in Fig. 2.10 have a distinct bias to the right of the rotor. This appears in all trajectories but is strongest in the $f_{2\,D}$ trajectory where basically no deflection to the left is found. The wake deflection to the right may be related

Table 2.2: Standard deviation of the wake deflection at $x_2 = 6\,D$ for different Δt[min]. Values are averages over all seven yaw configurations. Note that the 10 min standard deviation might be biased as the intervals are not strictly independent.

	std(f_{h}) $[10^{-1}D]$			std($f_{2\,D}$) $[10^{-1}D]$			std(f_{AP}) $[10^{-1}D]$		
Δt	10	3	1	10	3	1	10	3	1
SBL	0.1	0.3	0.5	0.1	0.3	0.5	0.1	0.3	0.5
NBL	0.4	1.2	2.2	0.4	1.3	2.2	0.3	0.7	1.6
CBL	1.4	2.4	2.8	1.3	2.4	3.0	2.0	2.2	2.3

Figure 2.9: Same as in Fig. 2.5 but for the SBL simulation.
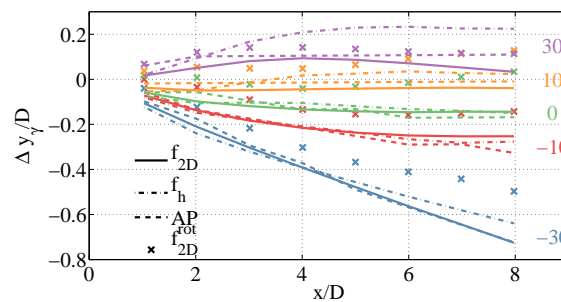
Figure 2.10: Same as in Fig. 2.6 but for the SBL simulation. Crosses mark the wake trajectories for simulations with opposite sense of rotation of the rotor.

to two different mechanisms. Firstly, it can be related to advection of lower momentum from below the rotor to one side and advection of high momentum from above the rotor to the other side of the wake by its rotation. The second effect that could be responsible for the deflection of the wake to the right is the stronger veer of the wind in the upper rotor half, where the mean flow is towards the right, compared to the lower rotor half, where the mean flow is slightly towards the left. Trajectories of simulations with a reversed rotation of the rotor show that the sense of rotation is not exclusively responsible for the bias to the right as this would lead to a mirroring of the trajectories about the wind direction for opposite rotor rotations (Fig. 2.10). As apparent in Fig. 2.9, the wake center is located a little higher than hub height, therefore the ambient wind direction at wake center height could also lead to a slight advection towards the right. Thus both effects seem to be responsible for the difference between the wake deflection in the SBL and the NBL.

The uncertainty of the estimate of the wake deflection is much smaller in the SBL than in the NBL for all time intervals (Fig. 2.11). Compared to the NBL, the variance of the wind direction (Fig. 2.3b) is lower and the energy of the cross stream motion (Fig. 2.4) is already low on the minute scale. Thus, a 1 min averaging window filters most of the cross stream fluctuation that might be responsible for the uncertainty of the prediction of the flow field between x_1 and x_2 and therefore the uncertainty of the wake deflection.
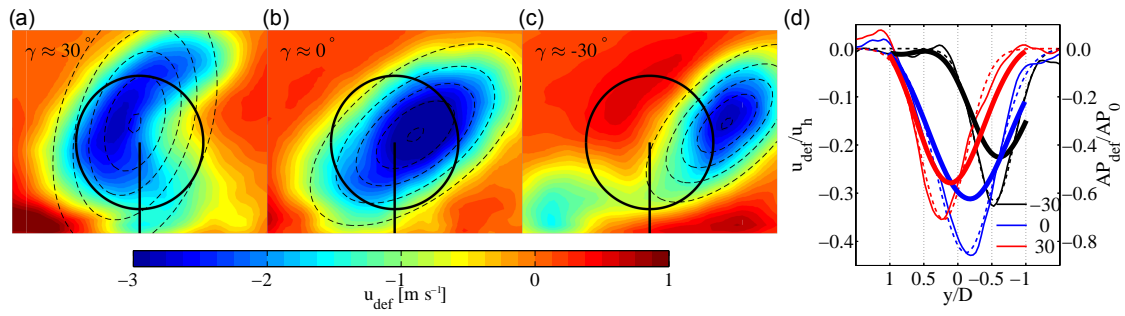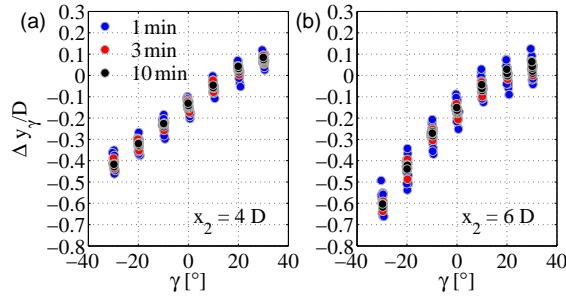
Figure 2.11: Same as in Fig. 2.8 but for the SBL simulation.
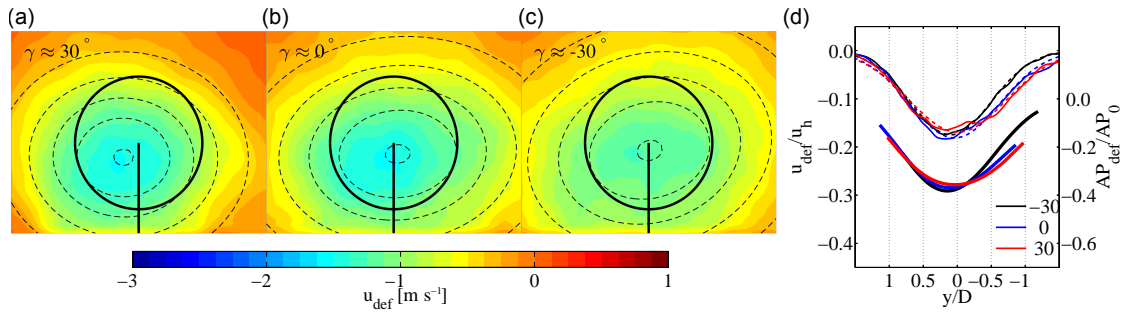
Figure 2.12: Same as in Fig. 2.5 but for the CBL simulation and for a time series of 60 min.

2.3.3 Convective atmospheric boundary layer

The deflected wakes in the CBL show a completely different behavior than in the previous presented boundary layer simulations. Figure 2.12 shows the yz transects as in Figs. 2.5 and 2.9 but for the CBL. The results are averaged over 1 hour of simulation time instead over 20 min like in the other simulations. The large deficit width in Fig. 2.12 is mainly a consequence of the large variance of wind direction (Fig. 2.3b) during the averaging time interval, that leads to a strong fluctuation of the wake position (Larsen et al., 2015; Machefaux et al., 2015a). A consequence is a much weaker mean deficit than in the NBL and SBL simulations.

As Fig. 2.12 shows, the wake deflection to the left (right) for a positive (negative) yaw angle is not found in the results of the CBL simulation. This does not only hold for the long time average but also for shorter time intervals Δt as apparent in Fig. 2.13. The uncertainty of the estimated wake deflection is less dependent on the averaging interval than in the other simulation (Table 2.2).

Following the considerations made in Sect. 2.3 about the uncertainty of the wake deflection due to the uncertainty of the wind direction, an approximate error of $\pm 2.5°$ of the 3 min wind direction α_h can be derived from the spread of the 3 min results (Table 2.2).

A large spread of yaw angles of the turbines to the wind is encountered during the simulation (Fig. 2.13). The reason for the spread are the wide streaks of the convection rolls that create strong cross stream components (Fig. 2.14), a feature that distinguishes the
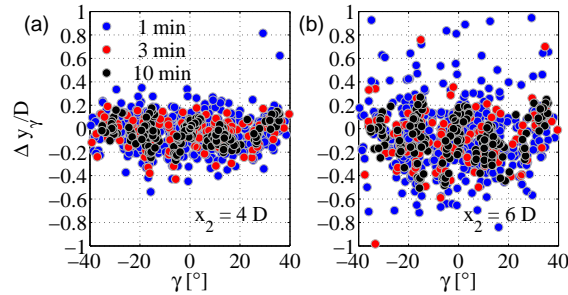
Figure 2.13: Same as in Fig. 2.8 but for the CBL simulation and for a time series of 60 min.

CBL from the other simulated cases. Due to this feature, the local inflow wind direction usually differs from the domain-averaged wind direction, shown in Fig. 2.3, to which the turbines are originally yawed. These streaks explain the spread of identified wind directions but can not explain the high variance of the wake deflection for the same yaw and inflow angle. Moreover, the averaged wind speed and direction measured in front of the turbine appears to be insufficient to characterize the flow further downstream.

To test the similarity of the free stream flow at different streamwise locations we calculate the root mean square error (RMSE) of two time series in undisturbed flow with and without considering the time shift τ (Fig. 2.15). Wind speed and wind direction are averaged at hub height along a cross stream distance as described in Sect. 2.3. A shift of the downstream time series by τ has the largest effect on the similarity of the wind conditions in the CBL, where especially the variance of the wind direction is large. On the other hand that means that a bad estimation of τ introduces the largest error to the estimation of y_0 in the CBL.

2.4 Discussion of the wake deflection estimation

Three different sources of uncertainty of the wake deflection estimation are evaluated in this study. First we show that the incoming wind shear and veer has to be well known by comparing the results from the neutral and stable thermal stability situation. The influence of shear and veer is not considered yet by studies of potential improvement of the wind farm efficiency with wind farm control like Annoni et al. (2016) and Gebraad et al. (2016b). Table 2.3 shows the coefficients derived from the two simulations for the analytical description proposed in Jimenez et al. (2010) and Gebraad et al. (2016b) compared to their results. Gebraad et al. (2016b) show that the energy yield of a small wind farm can be well predicted by a simplified parametric model, which is fitted to simulated atmospheric conditions of neutral stability, and that the energy yield of a small wind farm can be improved by more than 10 % for certain scenarios. Assuming the same parameters for the stable wind field from our study would lead to a miscalculation of the wake position which corresponds to a yaw induced deflection by a yaw angle of about 10°. Thus, the described parametrization of the model would likely propose an unfavorable control for stable situations. A proper description of the
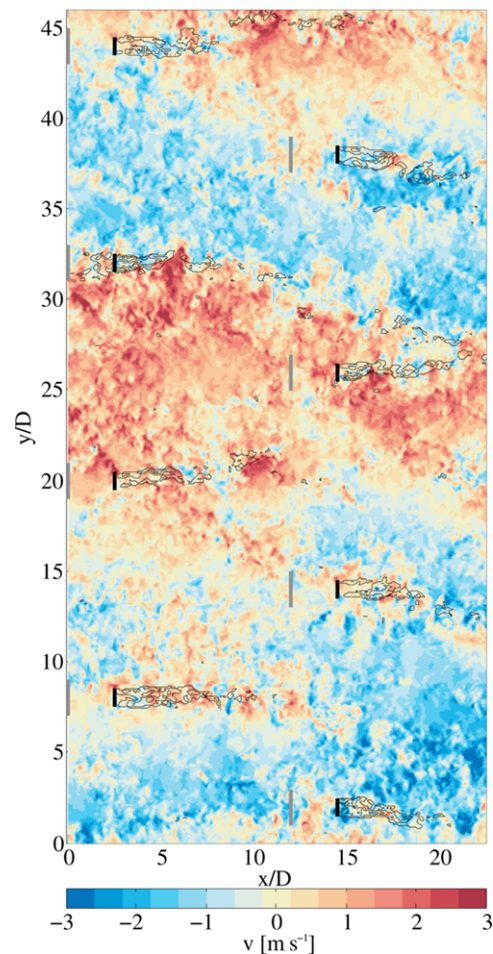
Figure 2.14: Example of the instantaneous v component at hub height in the CBL. Turbine wakes are denoted by black contours. Black lines denote the rotor positions, gray lines denote the position of the inflow measurement for each turbine.

wake trajectory in stable situations is important as the interest to apply wind farm control in stable atmospheric stability should be higher than in more turbulent conditions due to the increased wake losses. With the high occurrence of stable situations onshore (Vanderwende and Lundquist, 2012; Wharton and Lundquist, 2012) as well as offshore (Barthelmie and Jensen, 2010; Dörenkämper et al., 2014) the difference in the wake trajectory might be even worth considering in the design process of a wind farm.

As a second source of uncertainty we consider the choice of the method to derive the wake position. These methods are most often dependent on the measurement device thus we do not expect that it will be possible to establish a universally applicable method in the near future. For future studies aiming to study the deflection of the wake we emphasize that the choice of wake fitting routine for the measured wind field has significant influence on the results in particular when the turbine yaw angle is large.
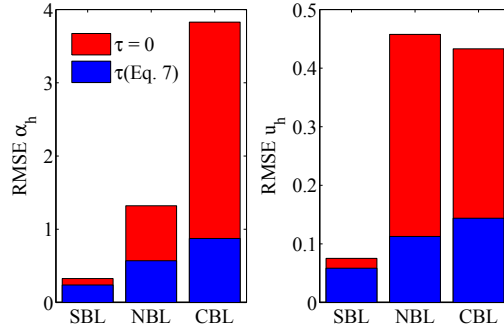
Figure 2.15: RMSE of the time series of 3 min averaged a_h and u_h at two different positions in the model domain separated by $\Delta x = 8\,\mathrm{D}$, with a advection time shift of the downstream time series of τ (Eq. 2.7) and without time shift ($\tau = 0$).

The third source of uncertainty that is considered in this study is the influence of the time averaging interval to find the wake deflection. The underlying question behind this analysis is: at what timescales makes wind farm control sense and what needs to be taken into account at the different timescales. In the NBL and SBL cases the estimation of the wake deflection on a 10 min scale shows only little variance. However, here we benefit from the steady wind field in the LES where we do not expect a change of wind direction over this time interval. In practice, meso-scale wind fluctuations might cause a change of the wind direction on this time scale. For smaller time intervals than 10 min the variance of the wake deflection increases, thus a prediction of the wake position by measuring the inflow becomes more uncertain.

The CBL analysis differs from the two other cases as we find no correlation between yaw angle of the turbine and wake deflection on any of the tested time averaging intervals. This makes a prediction of the wake position more uncertain and makes an interference by yaw control unreasonable. Apparently, the stochastic fluctuation of the wake caused by the large fluctuations of the cross stream component are superimposing the trajectory change of the

Table 2.3: Best fit parameters to the wake deflection output of the different methods using Gebraad et al. (2016b), Eq. (12). Comparison with the results of the aforementioned study and with Jimenez et al. (2010). The parameter k_d defines the recovery of the wake trajectory to the mean wind direction, and a_d and b_d the displacement due to the interaction of wind shear and rotation of the wake.

	f_h		$f_{2\,D}$		f_{AP}	
	k_d	a_d, b_d	k_d	a_d, b_d	k_d	a_d, b_d
SBL	0.14	−7.7, −1.4	0.23	−8.1, −2.1	0.19	−6.0, −2.4
NBL	0.16	−3.1, 0.4	0.25	−2.8, 0.9	0.18	−2.4, 0.3
Jim.	0.06	−	−	−	−	−
Geb.	0.15	−4.5, −1.3	−	−	−	−

wake caused by the induction of the turbine to a degree that the latter signal is not detectable any more. The larger fluctuation of the wake trajectory in convective conditions has been shown before in measurements and simulations (Keck et al., 2014; Mirocha et al., 2015) but has not been related to the applicability of wind farm control, yet.

Investigating the hypothesis of frozen turbulence in flow undisturbed by the wind turbine shows that the consideration of the time delay between the time series at two streamwise positioned measurements is especially important in the CBL. However, in flow with a wake structure of lower mean velocity than the ambient wind field, the advection velocity relevant for the lateral movement of the structure is not well-defined. Thus, the time delay between inflow measurement and wake measurement can not be estimated accurately. A better understanding of the relevant advection velocity of the wake might improve a prediction of the wake position in highly turbulent environments. Attempts to improve the description of the advection velocity are made for example in Machefaux et al. (2015b).

A source that we do not address in this study is the uncertainty of the wind direction estimate by the error of the measurement device that is used. The cross stream average of hub height flow upstream of the turbine, that we use here, is just one possibility to measure the inflow. The only way to apply this method in the field would be by using nacelle based lidar systems like proposed in Schlipf et al. (2013).

The shown simulations represent only examples of thermal stability conditions for stationary and barotropic flow. In addition to atmospheric stability other factor like baroclinicity and topography influence the wind profile. Thus, from the shown simulations we can conclude little about the influence of atmospheric stability at a specific location. For the fine-tuning of wake models it would be beneficial to study the exact effect of shear and veer on the wake position and shape in more detail.

2.5 Conclusions

In this study we contribute to the current discussion about wind farm control by considering atmospheric stability and uncertainty of the wake deflection estimation. From LES case studies of yawed wind turbines in atmospheric boundary layers of different thermal stratification we conclude that both a precise wind direction measurement and measurements of shear and turbulence of the flow are necessary to be able to accurately predict the position of the wake downstream of the turbine. These factors should be considered by any comprehensive study aiming to evaluate the costs and benefits of wind farm control concepts. As current approaches of wind farm control require a loss of power as well as often an increased structural load at upwind turbines, a wrong prediction of the wake position will most likely not lead to an improvement of wind farm performance.

We also emphasize that the wake position in a turbulent atmospheric boundary layer becomes more and more stochastic for small time intervals. Furthermore, in a highly turbulent environment, the use of yawed turbines to deflect the wake might even not be reasonable at all as we find no correlation between the wake position and the turbine yaw angle relative

to the measured inflow in a simulation of a convective situation. However, the use of wind farm control is regarded to produce the strongest improvement of wind farm performance in stable conditions because the power losses due to wakes are highest. Our study shows that an application of an intentional wake deflection in these conditions might be feasible if the trajectory is well described because the fluctuation of the wake position is low.

Acknowledgements

Chapter 3

Transient LES of an offshore wind turbine [1]

Abstract   The estimation of the cost of energy of offshore wind farms has a high uncertainty, which is partly due to the lacking accuracy of information on wind conditions and wake losses inside of the farm. Wake models that aim to reduce the uncertainty by modeling the wake interaction of turbines for various wind conditions need to be validated with measurement data before they can be considered as a reliable estimator. In this paper a methodology that enables a direct comparison of modeled with measured flow data is evaluated. To create the simulation data, a model chain including a mesoscale model, a Large Eddy Simulation (LES) model and a wind turbine model is used. Different setups are compared to assess the capability of the method to reproduce the wind conditions at the hub height of current offshore wind turbines. The 2-day-long simulation of the ambient wind conditions and the wake simulation generally show good agreements with data from a met mast and lidar measurements, respectively. Wind fluctuations due to boundary layer turbulence and synoptic-scale motions are resolved with a lower representation of mesoscale fluctuations. Advanced metrics to describe the wake shape and development are derived from simulations and measurements but a quantitative comparison proves to be difficult due to the scarcity and the low sampling rate of the available measurement data. Due to the implementation of changing synoptic wind conditions in the LES, the methodology could also be beneficial for case studies of wind farm performance or wind farm control.

---

[1]The content of this chapter is identical to the following journal article published in Wind Energy Science: © Author(s) 2017. This work is distributed under the Creative Commons Attribution 4.0 License. Reprinted, with permission, from Vollmer, L., G. Steinfeld, and M. Kühn, 2017: Transient LES of an offshore wind turbine. *Wind Energy Science*, **2**, 603–614

3.1 Introduction

Offshore wind energy still remains an expensive alternative to onshore wind energy, which has been established as one of the cheapest options to generate electricity. One of the reasons for the comparatively high costs of offshore wind energy is the scarcity of long-term atmospheric measurements at existing or planned wind farms. The resource assessment at these locations is difficult and prone to large errors (Walker et al., 2016). In addition, missing measurements during operation prohibit the thorough analysis of turbine malfunctions and unexpected underperformance.

Only a few offshore wind farms deploy permanent met masts that allow for studying the influence of atmospheric conditions on wind farm performance. The available measurements indicate that due to the generally lower level of turbulent kinetic energy offshore compared to onshore, the wakes of the wind turbines are frequently more persistent, which leads to higher wake losses at downwind turbines even over larger distances. An even lower turbulence level caused by stable atmospheric stratification leads to a further increase in wake losses (Barthelmie and Jensen, 2010; Hansen et al., 2012; Dörenkämper et al., 2014).

Several numerical models have been developed with the purpose of calculating the optimal layout of offshore wind farms under consideration of the wake losses. Simplified engineering models allow a fast calculation of multiple wind scenarios and an optimization of wind farm layouts (Sanderse et al., 2011). These steady-state models, however, have a low representation of the flow physics and rely largely on the parametrization of turbulence and on a simplified interaction of turbine and flow.

A high-fidelity solution for wind farm simulations are Large Eddy Simulations (LESs). Coupled with wind turbine models, LESs provide a detailed solution of the flow inside of a wind farm with a high representation of the relevant physics. Due to the high computational costs, LESs of offshore wind farms have been restricted to simulations of idealized atmospheric conditions or to case studies of specific situations, e.g., Churchfield et al. (2012); Dörenkämper et al. (2015b); Lu and Porté-Agel (2011). An issue of all wind farm models is the need for validation with measured data to evaluate the capability of the model to reproduce the actual wind conditions and performance of the wind farm under these conditions (Moriarty et al., 2014).

In addition to performance measurements from the data acquisition system of wind turbines, which are often kept confidential, flow measurements using the light detection and ranging methodology (lidar) have become a widespread tool for scientific research. To optimize this technique for model validation, the lidar measurement campaigns have to be designed and postprocessed to allow for a meaningful comparison with simulations. One aspect of the measurement design is the measurement of free flow conditions, which can be used as meteorological boundary conditions for the simulations.

Especially offshore the measurement or derivation of boundary conditions to set up simulations is challenging. For example, onshore LESs are often run with boundary conditions derived from near-surface measurements (e.g., heat flux measurements) and are compared to wind profiles derived from lidar devices (Mirocha et al., 2015; Machefaux et al., 2015a)

or met masts. This procedure is rarely possible at offshore sites because usually near-surface measurements and wind speed profiles are not available. Furthermore, for many models additional input is required, e.g., the height of the atmospheric boundary layer or a large-scale pressure gradient to drive the flow. These properties have to be estimated or set to default values.

In this paper we investigate a methodology to use profiles and boundary conditions derived from a mesoscale simulation for a continuous LES of an offshore wind turbine wake over several hours. The purpose is to evaluate if this model chain can be used to conduct wake simulations in a wind field with the same turbulent properties and the same profile shape as measured. Measurements from an offshore met mast are used for the evaluation. The model chain is further evaluated by a comparison of the flow distortion by a wind turbine model with the wind field extracted from lidar measurements (van Dooren et al., 2016) of a wake during the simulated time period.

Recently, long-term LESs of multiple days up to 1 year have been run with this approach to study the changes of meteorological conditions at a measurement site (Neggers et al., 2012; Schalkwijk et al., 2015; Heinze et al., 2017). In the context of wind energy, the approach had only been used in Vollmer et al. (2015), in which the measurement and simulation setup of this paper was briefly introduced. Here we extend the study in Vollmer et al. (2015) by analyzing a much larger time interval of measurements and simulations, by a sensitivity study of the method and by a quantitative comparison of wake characteristics.

3.2 Data and methodology

3.2.1 Measurement data

The case study that is analyzed in this paper is based on measurements on 20 February 2014 at the German offshore wind farm Alpha ventus. Two independent data sets were used for comparison with the model results. The simulated ambient wind conditions without turbines were compared to measurements from the met mast FINO1 located at $54°01'$ N, $6°35'$ E. Time series from cup anemometers, wind vanes and temperature probes at different heights as well as sea surface temperature from a buoy were provided by the Bundesamt für Seeschifffahrt und Hydrographie (BSH). These time series provide mean values obtained from averaging over 10 min. For the wind speed, 1 Hz measurements were made available by DEWI (UL International GmbH). The wind directions of the wind vanes at all heights were corrected using a direction-dependent bias (DEWI, personal communication). During the analyzed time period the flow measurement devices did not operate in the mast shadow or in the wake of a wind turbine and should thus provide accurate information about the undisturbed marine atmospheric boundary layer.

The lidar measurements, which were used for comparison with the simulated wakes, are part of a measurement campaign that took place from August 2013 until March 2014.

During the analyzed day, two long-range lidar devices (Windcube WLS200S) executed single elevation plan position indicator scans in the wake of turbine AV10 with one lidar positioned on FINO1 and the other one on the converter station of the wind farm (Fig. 3.1).

The line of sight velocities of the lidars were combined and averaged to get a 10 min mean horizontal vector wind field at hub height (van Dooren et al., 2016). Measurements were filtered at both ends of the range of the carrier-to-noise level to remove low backscatter data as well as reflections from objects. Time periods in which a yaw activity of more than 3° was observed were removed from the database. Averaging was done on volumes with a diameter of 20 m centered at hub height. Because both lidars scan over a relatively small range of azimuth angles (Fig. 3.1), seven (WLS2) and five (WLS3) sweeps over the scan area contribute to the calculation of the mean velocities. The view of the lidar devices to certain areas of the scan is blocked by other wind turbines; thus, a varying total of 100–350 individual line-of-sight wind speed values contribute to the average at each grid point of the final wind field. Grid points with a lower number of values were removed. The coordinate system in which the flow field is presented is oriented north by scanning the distance to the turbines of the wind farm with known geographical coordinate positions. More information on the calculation of the vector field from the line-of-sight velocities can be found in van Dooren et al. (2016).

3.2.2 Model equations

Revision 1928 of the Parallelized Large Eddy Simulation Model (PALM) (Maronga et al., 2015) was used for this study with the same numerical schemes as in Vollmer et al. (2016), using a Deardorff model for the sub-grid-scale (SGS) fluxes. The extension of the model equations to include time-dependent forcing is based on Heinze et al. (2017) with an extension to include large-scale advection of momentum. The modified equation of motion before applying any approximations is

$$
\frac{\partial u_i}{\partial t} = \underbrace{- u_j \frac{\partial u_i}{\partial x_j}}_{1} \underbrace{- \epsilon_{ijk} f_j u_k}_{2} \underbrace{- \frac{1}{\rho} \frac{\partial p}{\partial x_i}}_{3}
$$

$$
\underbrace{+ \nu_{\mathrm{m}} \left(\frac{\partial^2 u_i}{\partial x_j^2} + \frac{1}{3} \frac{\partial}{\partial x_i} \frac{\partial u_j}{\partial x_j} \right)}_{4} \underbrace{- \epsilon_{i3j} f_3 u_{g_j}|_{\mathrm{LS}}}_{5}
$$

$$
\underbrace{+ \frac{\partial u_i}{\partial t}\Big|_{\mathrm{LS}}}_{6} \underbrace{- \frac{\langle u_i \rangle - u_{i_{\mathrm{LS}}}}{\tau}}_{7}, \tag{3.1}
$$

with term 1 representing the momentum advection, term 2 the Coriolis force with the Coriolis parameter f_j, term 3 the pressure gradient and term 4 the friction terms with the kinematic viscosity of momentum ν_{m}. Terms 5–7 are the external forcing terms. For the external forcing, a large-scale velocity denoted by $|_{\mathrm{LS}}$ is defined. Term 5 defines a large-scale pressure

gradient by prescribing a horizontal geostrophic wind speed u_g. Term 6 prescribes a large-scale sink or source of momentum and term 7 is a time relaxation of the momentum towards a large-scale state (Neggers et al., 2012; Heinze et al., 2017).

The momentum relaxation has no physical justification but is used to prevent a drift of the model from the large-scale state. The term depends on the difference between the horizontal average $< u_i >$ of each velocity component and the large-scale velocity component u_{i_LS}, scaled by a relaxation time constant of τ. All large-scale properties are horizontally homogeneous to preserve the turbulent structures.

The equation for scalars $s \in (\Theta, q)$ is

$$\frac{\partial s}{\partial t} = \underbrace{- u_j \frac{\partial s}{\partial x_j}}_{1} + \underbrace{\nu_\mathrm{s} \frac{\partial^2 s}{\partial x_j^2}}_{4} + \underbrace{\frac{\partial s}{\partial t}|_\mathrm{LS}}_{6} - \underbrace{\frac{\langle s \rangle - s_\mathrm{LS}}{\tau}}_{7} + \underbrace{S_\mathrm{s}}_{8},\tag{3.2}$$

with terms 1, 4, 6 and 7 equivalent to the corresponding terms in Eq. (3.1), with ν_s being the molecular diffusivity of the scalar. Term 8 is the surface flux divergence of either specific humidity q or potential temperature Θ.

Time dependency of the external forcing is achieved by prescribing profiles of the time-variant geostrophic wind, source terms of horizontal momentum and scalar properties, and of the large-scale state of the relaxation term. The surface fluxes are calculated by making use of the Monin–Obukhov similarity theory, with the values of the surface pressure, temperature and humidity also prescribed by the time-dependent large-scale state.

3.3 Simulation of free stream flow

In this section we analyze the simulation of the ambient conditions with the large-scale forcing derived from the output of a mesoscale simulation. Different parameters are modified to analyze their influence on the results. In Sect. 3.3.1 we look at the meteorological conditions that were present on the day of the measurements. In Sect. 3.3.2 we compare profiles from the mesoscale model with the FINO1 measurements and in Sect. 3.3.3 we compare the LES model output of different setups with the mesoscale model and the FINO1 measurements.

3.3.1 Meteorological conditions

The lidar measurements were conducted on 20 February 2014. After filtering according to the criteria mentioned in Sect. 3.2.1, 15 10 min time periods remained for further analysis. The 15 time periods can be sorted into three periods, with three measurements starting at 01:00 UTC (night period), nine around 06:00 UTC (morning period) and another three starting at 21:40 UTC (evening period) (Fig. 3.2).

The wind direction at FINO1 is southwest during the night and south during the rest of
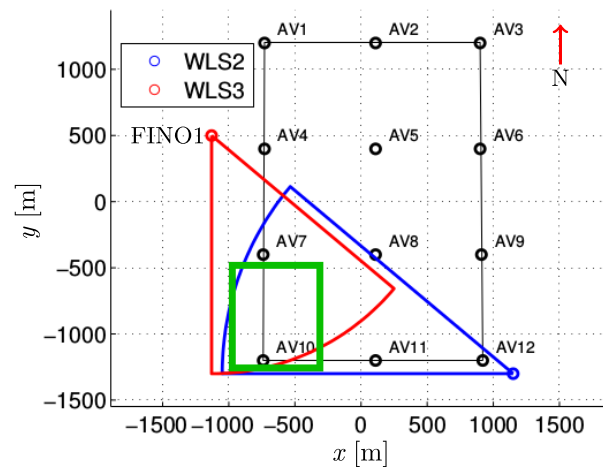
Figure 3.1: Layout of Alpha ventus and position of the two lidars that were used for the construction of the wind field. Circular segments denote the scan areas of the lidars. The green box denotes the region of the vector wind field reconstruction.

the day, with an increase in the wind speed at hub height of the Alpha ventus wind turbines (90 m) from about $8\,\mathrm{ms^{-1}}$ to about $16\,\mathrm{ms^{-1}}$. The day is a rather warm winter day, with the measured temperature at 35 m ranging from 5.5 to $8\,^\circ\mathrm{C}$. Compared to onshore, the diurnal cycle of surface temperature is very small at offshore locations because of the large heat capacity of the ocean surface. The observed drop of air temperature during the morning hours is thus most likely related to the advection of colder air from the land. The German coast is approximately 45 km to the south of Alpha ventus. The advected cold air leads to thermally slightly unstable conditions between about 02:00 and 09:00 am. During the rest of the day the stratification is slightly stable.

3.3.2 Input data from COSMO-DE

The profiles for the large-scale tendencies are calculated from the operational analysis of the COSMO-DE model (Baldauf et al., 2009) of the German Weather Service (DWD). COSMO-DE has a horizontal resolution of $2.8 \times 2.8\,\mathrm{km}$ and 50 vertical levels in total, with 20 vertical levels in the lower 3000 m of the atmospheric boundary layer. The DWD delivers hourly model data.

Following Heinze et al. (2017) three-dimensional and surface data are averaged over a horizontal averaging domain of multiple grid points. The nearest grid cell to the FINO1 coordinates is chosen as the center of the averaging domain. Because of the necessary spin-up time of the LES for the development of turbulence, 24 h of simulation time (19 February, whole day) was added. The profile of the geostrophic wind is calculated using the pressure gradient between neighboring averaging domains (Fig. 3.3). The component of the
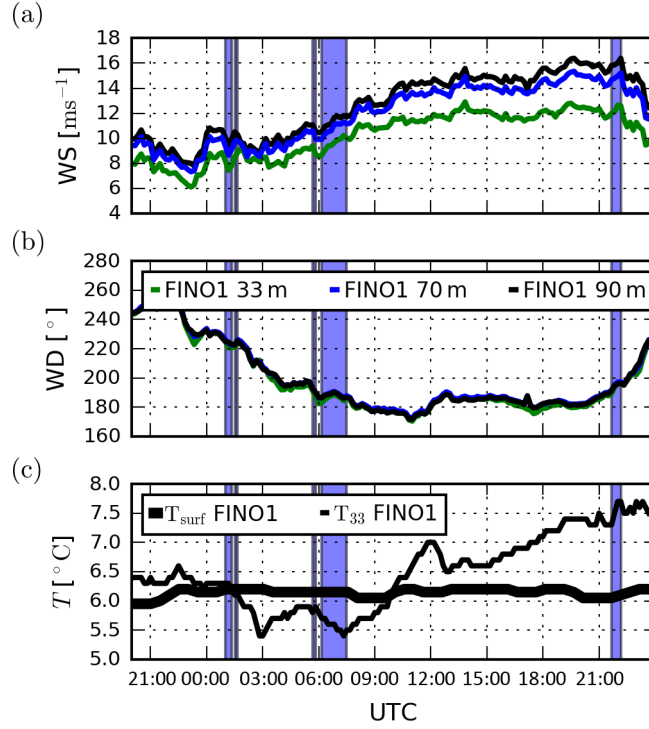
Figure 3.2: Meteorological conditions on 20 February 2014, as measured at FINO1. **(a, b)** Wind speed and wind direction at different heights. **(c)** Temperature as measured at height and the sea surface. The periods of the selected lidar measurements are shaded in blue.

geostrophic wind along the west–east axis is defined by

$$u_{\mathrm{g}_1}^{I,J}|_{\mathrm{LS}} = -(f\rho^{I,J})^{-1}\frac{P^{I,J+1} - P^{I,J-1}}{2\mathrm{d}X_2}, \tag{3.3}$$

with $P^{I,J}$ and $\rho^{I,J}$ the domain-averaged quantities of density and pressure in domain (I, J), f the Coriolis parameter, and $\mathrm{d}X_i$ the length of the averaging domain. The north–south wind component $u_{\mathrm{g}_2}^{I,J}$ is defined accordingly. The source terms $\frac{\partial u_i}{\partial t}|_{\mathrm{LS}}$, $\frac{\partial \Theta}{\partial t}|_{\mathrm{LS}}$ and $\frac{\partial q}{\partial t}|_{\mathrm{LS}}$ result from the advection into the averaging domain. The source term of the potential temperature Θ for example is defined by

$$\begin{aligned}\frac{\partial \Theta}{\partial t}|_{\mathrm{LS}} &= U_1^{I,J}\frac{\Theta^{I+1,J} - \Theta^{I-1,J}}{2\mathrm{d}X_1}. \\ &+ U_2^{I,J}\frac{\Theta^{I,J+1} - \Theta^{I,J-1}}{2\mathrm{d}X_2}.\end{aligned} \tag{3.4}$$

We analyzed the influence of the size of the averaging domain on the profiles required by the LES model by comparing three different quadratic domain sizes with grid lengths of 1/8, 1/2 and 2°. Figure 3.4 compares the measured 70 m wind speed and direction from FINO1
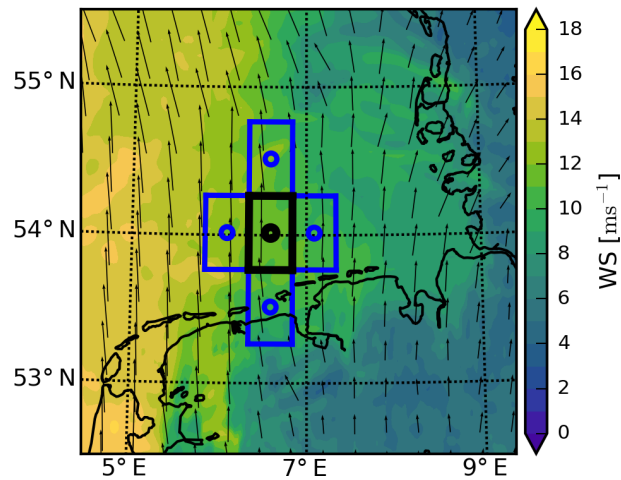
Figure 3.3: COSMO-DE wind speed and direction on 20 February 2014 at 07:00 UTC on the model level of 73.5 m. The black square marks the averaging domain surrounding FINO1 and the blue squares mark the neighboring domains that are used for the calculation of the gradients.

with the horizontal and the geostrophic wind speed and direction from the different averaging domains.

The comparison of the different averaging domains (Fig. 3.4) shows that the smaller domains contain more fluctuation, but not necessarily at the same time as the measurements. In addition, the geostrophic wind that is calculated from the pressure gradients in the model becomes noisier with decreasing averaging domain size (Fig. 3.4). Because the geostrophic wind is directly used in the equations of motion, we chose to use the middle-sized domain. It generally contains less noise than the small domain, and in contrast to the large domain, it covers just grid points over the sea, thus representing a horizontally rather homogeneous area.

Figure 3.5 shows Hovmöller diagrams of most of the large-scale forcing data we used for the LES model. As assumed from the measurements, an advection of colder temperature during the morning hours of the second day is visible in the mesoscale simulation (Fig. 3.5f). The change of wind direction with height is mostly related to the Ekman turning, which can be seen in the differences between the geostrophic and the effective wind direction (Fig. 3.5b and e, respectively).

3.3.3 Comparison with met mast data

To transfer the input profiles from the COSMO-DE time steps and height levels to the LES model, they were linearly interpolated on the vertical LES grid and on the time steps of the simulation. The LESs were initialized with the set of large-scale profiles on 19 February at 00:00 UTC and nudging was applied only after 6 h to enable a free development of turbulence
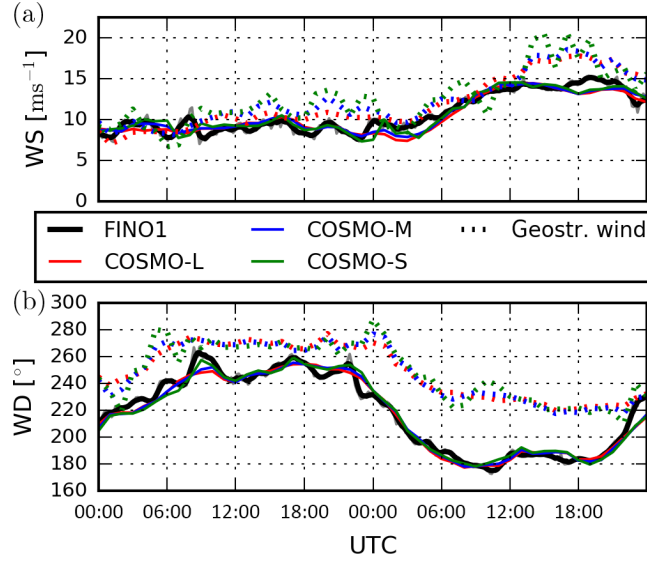
Figure 3.4: Time series for 19 and 20 February 2014 of **(a)** wind speed at 70 m. **(b)** Wind direction at 70 m. FINO1 1 h running average (black). COSMO-DE averaging domain sizes of $(1/8)^{2\circ}$ (COSMO-S), $(1/2)^2$ degrees (COSMO-M) and 2^2 degrees (COSMO-L). Dotted lines represent the calculated geostrophic wind speed and direction at the same height.

Table 3.1: Comparison of the different simulation setups and the RMSE of the difference between the time series of simulated wind direction and wind speed of simulations P_x and the time series of the COSMO-DE input (C), the FINO1 measurements (F1) and the reference simulation (P_{ref}).

| Sim | Setup | | RMSE | | | | | |
| | τ | $\Delta x, z$ | WD_C | WD_{F1} | $WD_{P_{\text{ref}}}$ | WS_C | WS_{FINO1} | $WS_{P_{\text{ref}}}$ |
	[h]	[m]	[°]	[°]	[°]	[ms^{-1}]	[ms^{-1}]	[ms^{-1}]
P_{ref}	4	20/10	5.8	6.6	–	0.79	1.08	–
P_{τ_1}	1.5	20/10	4.0	5.1	2.5	0.73	0.99	0.16
P_{τ_2}	48	20/10	7.5	8.3	2.8	0.70	1.10	0.36
$P_{\partial_t u = 0}$	4	20/10	8.5	9.4	6.2	1.53	1.76	1.02
$P_{\partial_t \Theta = 0}$	4	20/10	6.9	7.6	1.8	0.77	1.08	0.14
P_{hi}	4	5/5	5.7	6.5	1.4	0.46	0.91	0.42

in the first simulation hours.

All simulations had a domain size of 3200 m × 3200 m × 1700 m and were run with cyclic boundary conditions. The roughness length of momentum was taken from the COSMO-DE model ($z_0 = 1.23 \cdot 10^{-4}$ m); the roughness lengths of temperature and humidity were $z_0^{\Theta,q} = 0.1 \, z_0$.
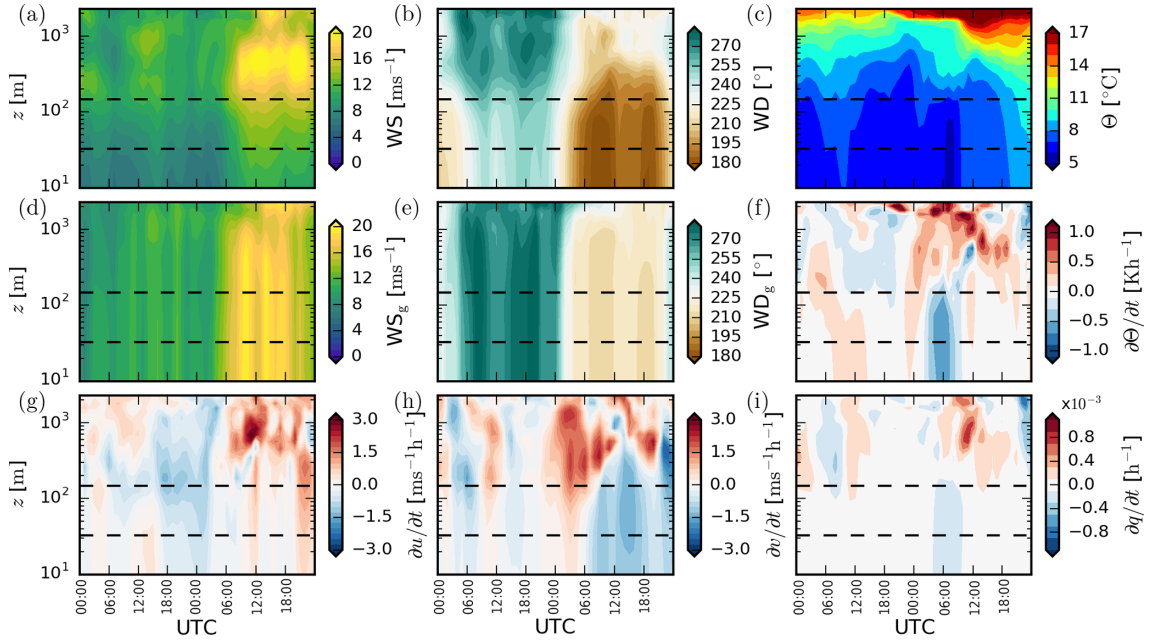
Figure 3.5: Time development of the vertical input profiles for the LES run. **(a)** Wind speed, **(b)** wind direction, **(c)** potential temperature, **(d)** geostrophic wind speed, **(e)** geostrophic wind direction, **(f)** advection of potential temperature, **(g)** advection of zonal wind speed, **(h)** advection of meridional wind speed and **(i)** advection of humidity. Dashed horizontal lines represent the lower and upper rotor tip heights.

Five different simulations with a rather coarse grid were run with different configurations (Table 3.1). One of the setups was then run with a finer resolution as basis for the turbine simulations. The chosen setup is regarded as the reference simulation P_{ref} and the simulation with higher spatial resolution is called P_{hi}. Two alternative relaxation time constants were set in P_{τ_1} and P_{τ_2} and advection of either momentum or potential temperature was switched off in $P_{\partial_t u = 0}$ and $P_{\partial_t \Theta = 0}$.

For evaluation we selected the 10 min mean wind speed and direction at 70 m, as they are close to the hub height and also available from the COSMO-DE model. For better comparison the raw 10 min values from the anemometers and wind vanes were smoothed by means of a 1 h running mean. The RMSE between each simulation time series and the references is compared in Table 3.1.

The evaluation shows that switching off momentum advection appears to have the largest influence on the wind speed and wind direction deviation from the input data. Figure 3.6a reveals that the impact of momentum advection is largest between 12:00 and 18:00 UTC of the second day, after the increase of the mean wind speed during the morning hours. In this period the mean wind speed remains too high when momentum advection is turned off. As illustrated in Neggers et al. (2012), the flow in the LES contains inertia, which delays the reaction to changing boundary conditions. The nudging term is one option to dampen the inertial fluctuations. Here we find that momentum advection is a complementary option.
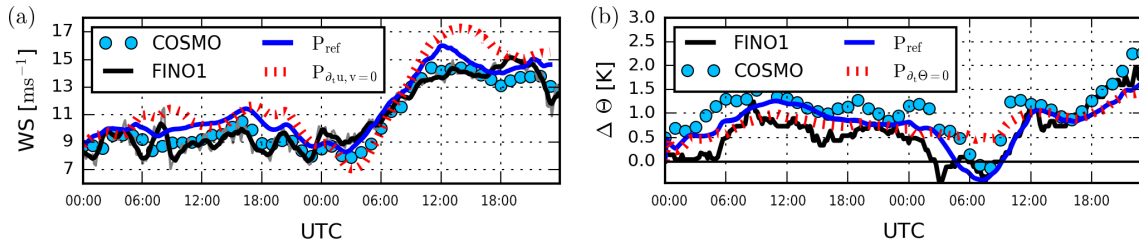
Figure 3.6: **(a)** Wind speed at 70 m with and without momentum advection. **(b)** Potential temperature difference between 35 m and the surface with and without temperature advection.

The advection of potential temperature does not have a large effect on the time series of the wind speed at 70 m. However, Fig. 3.6b shows the importance of the temperature advection for the thermal stability as the sign change of the temperature gradient can indeed be closely related to advection.

The more highly resolved simulation run, which was used as the basis for the turbine simulations, was computed with a relaxation time constant of $\tau = 4$ h, even though the result with a smaller relaxation time provides a slightly lower deviation from the measurements at hub height. We chose the larger relaxation constant to reduce the influence of the unphysical domain-wide relaxation on the wake simulations. Heinze et al. (2017) and Schalkwijk et al. (2015) found that the overall boundary layer properties are quite independent from the relaxation constant, if the constant is in the magnitude of hours.

The time series of the domain-averaged results of P_{hi} are compared to the measurements and the large-scale forcing data in Fig. 3.7. The 10 min turbulence intensity (TI) and the standard deviation of the wind direction are calculated and averaged over multiple virtual met masts evenly distributed over the model domain. The power-law coefficient is calculated for the FINO1 measurements and the LES from a fit to the data between 33 and 90 m, and for COSMO-DE by using the model levels at 35 and 73 m.

LES wind speed and wind direction follow the general trend of the input and measurement data. The averaged magnitude of the turbulent fluctuations on the 10 min scale is also reproduced. The largest discrepancy between simulation and measurements exists in the shear of the vertical wind profile which is almost constantly lower in the LES.

The destabilization of the boundary layer is observable as a decrease of the vertical shear of the LES and the measurements (Fig. 3.7e) on the second day between 00:00 and 06:00 UTC. The event appears to occur earlier in reality than in the simulations, which is likely related to the earlier change of sign of the temperature gradient (Fig. 3.6). The restratification also starts later in the LES and the vertical shear remains constantly lower during the rest of the day.

The comparison of modeled and measured time series shows that the measurements contain additional fluctuations that are not replicated by the model chain of mesoscale and microscale models. Figure 3.8 compares the power spectra of the two time series at hub height. The LES data show the typically stronger drop in the highest frequencies related to
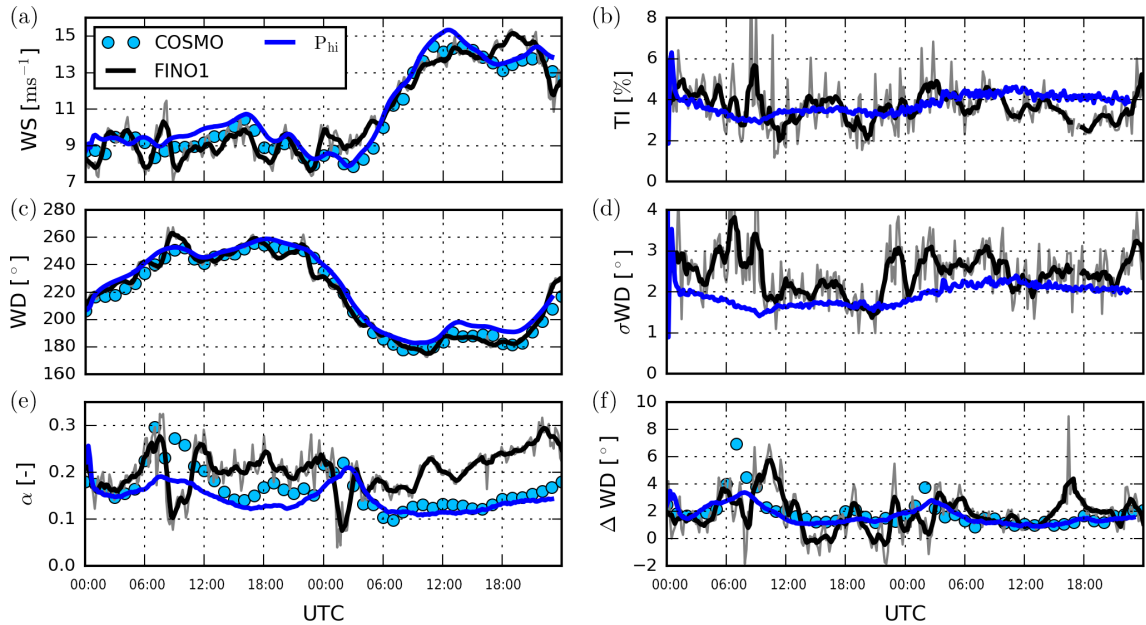
Figure 3.7: Comparison of P_{hi} to COSMO-DE and 1 h running means (black) and 10 min averages (grey) of FINO1 measurements. All time series are at 70 m, if not otherwise specified. **(a)** Wind speed, **(b)** turbulence intensity, **(c)** wind direction, **(d)** 10 min standard deviation of the wind direction, **(e)** vertical power-law coefficient and **(f)** change of the wind direction between 33 and 70 m.

the cutoff by the implicit SGS filtering. At longer periods of about 0.5 to 12 h, the gradient of the measured energy cascade is maintained, while the simulation contains less energy in this range. The model chain thus enables the replication of the synoptic-scale motions and the boundary layer turbulence but fails to reproduce the impact of mesoscale motions. The horizontal averaging of the mesoscale model output to derive smooth boundary conditions might factor into the result. Vincent et al. (2013), however, show that even current highly resolved mesoscale model output is not able to capture mesoscale fluctuations. As this paper only considers a small time period, we refer to Schalkwijk et al. (2015) for a more complete discussion of this topic.
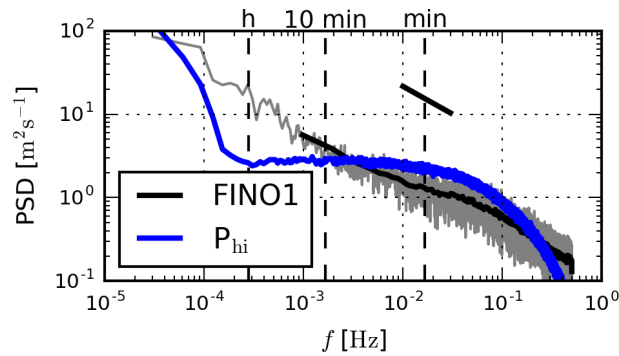
Figure 3.8: Power spectral density derived from the 1 Hz measurements at 90 m height and the simulation time series at 90 m. Grey and black lines represent different window sizes for the Fourier transformation. The short black lines denote the slope of the Kolmogorov cascade.

3.4 Wind turbine wake simulations

3.4.1 Model setup

The wind turbine wake simulations are run with the same domain and setup as the high-resolution simulation P_{hi}, just with the added body forces from the wind turbine, placed in the center of the domain. Due to the cyclic horizontal boundary conditions, the wind turbine wake reenters the domain through the southern boundary after having left it through the northern boundary. However, as the wind direction in the simulations is never directly from the south, the turbine is not subject to its own wake. The turbulence of the wake still modifies the state of the atmospheric boundary layer after some time. Thus, we simulated only intervals of 30 min with the wind turbine, preceded by a 3 min precursor phase for the development of the wake. Wind fields from P_{hi} were used as the initial fields of these simulations.

An enhanced actuator disc model with rotation (ADM-R) is used to calculate the forces of the wind turbine on the flow (Witha et al., 2014a). The model divides the rotor surface into annulus segments, and the local velocities at the segments and tabulated lift and drag coefficients are used to calculate lift and drag forces. The tower and nacelle of the turbine are parameterized by constant drag coefficients. The parameterized wind turbine AV10 is an Adwen AD 5-116 with a rotor diameter (D) of 116 m and a rated power of 5 MW. The hub height of the turbine is at 90 m. Adaptation to the current wind conditions is ensured by a baseline generator torque and pitch controller as described in Jonkman et al. (2009) and a simple yaw controller. Simulations of the generator torque and pitch controller in idealized conditions were performed to ensure that the reference thrust and power curves are replicated. The yaw controller is implemented as described in Storey et al. (2013), with a temporal averaging window of the wind direction of 30 s and a tolerated maximum
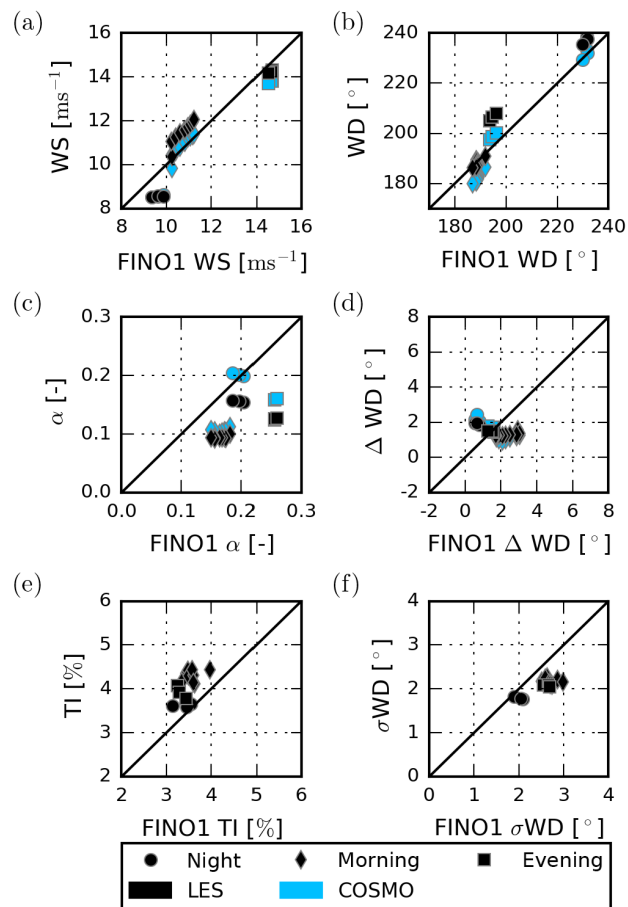
Figure 3.9: Comparison of the simulated state of the boundary layer with the measured state during the 15 10 min time periods of the lidar measurements. The night period is between 01:00 and 01:40 UTC, the morning period between 05:40 and 07:30 UTC, and the evening period between 21:40 and 22:10 UTC.

misalignment of 5°.

3.4.2 Comparison with lidar measurements

Figure 3.9 compares parameters that indicate the state of the atmospheric boundary layer measured at FINO1 with the simulated state during the selected 15 10 min time periods of the lidar measurements at Alpha ventus. As discussed earlier, the biggest disagreement is found in the vertical shear, which is constantly lower in the simulations. The TI is slightly higher in the simulations. Changes of atmospheric stability are small between the different times of measurements with the night and evening periods in slightly stable conditions and the morning period in neutral conditions according to the classification in Peña et al. (2010),
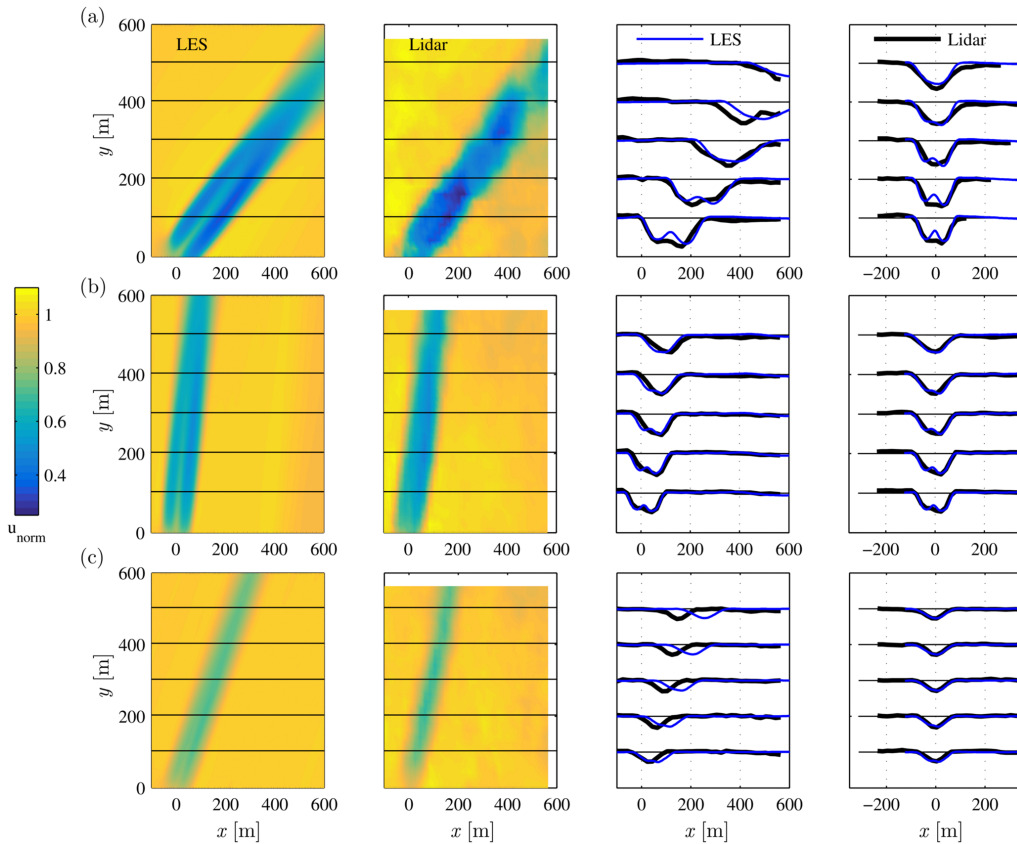
Figure 3.10: Normalized wind fields from LES and lidar measurements. The third column shows horizontal cross sections along the lines at constant y, as depicted in the first two columns. The fourth column shows cross sections at the same distances with the zero coordinate coinciding with the center line of the wake. The full vertical distance between the horizontal lines in the cross section panels equals a normalized velocity of one. The rows represent individual 10 min time periods starting at **(a)** 01:30, **(b)** 06:50 and **(c)** 21:40 UTC.

with the Monin–Obukhov length derived from the model fluxes.

For the wind turbine the three periods represent different operating conditions. With a rated wind speed of the turbine of $12.5\,\mathrm{ms}^{-1}$, the wind speed range lies below rated wind speed during the night period. Below rated wind speed the turbine's power and thrust coefficient are nearly constant. During the evening period the wind speed is clearly above rated conditions; thus, the rotor speed is controlled by collective pitch movement of the blades, and the thrust coefficient decreases with increasing wind speed. The morning period represents conditions that are around rated wind speed at which the thrust coefficient should be lower and pitch control is occasionally applied.

Figure 3.10 shows 10 min averages of the normalized hub-height wind speed during selected time intervals from simulation and measurements. For better comparison, the LES
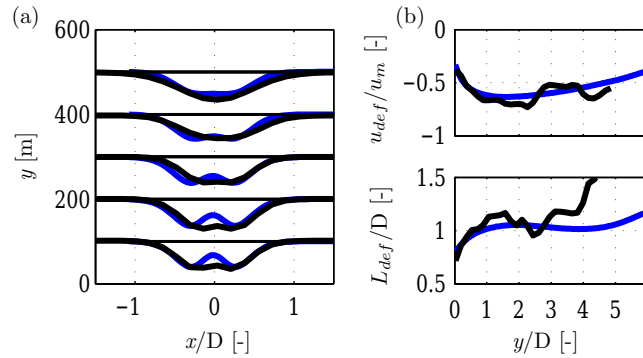
Figure 3.11: Fitted functions to the wake at 01:30 UTC. **(a)** Profiles in different distances. **(b)** Development of normalized deficit and wake width. LES (blue) and lidar (black).
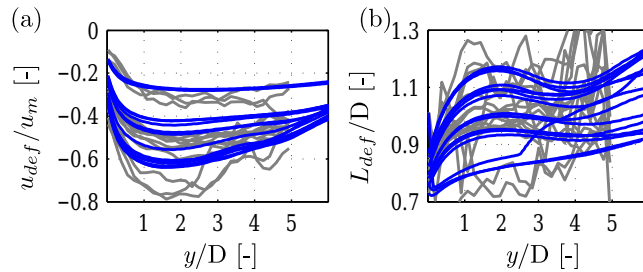

Figure 3.12: **(a)** Wake deficit and **(b)** wake width development from LES (blue) and lidar (grey).

results were averaged on cubes with a side length of 20 m centered at hub height, similar to the postprocessing of the lidar data as explained in Sect. 3.2.1. The slight disagreement of the inflow wind speed was approached by normalizing the velocities of both flow fields. Lidar and LES wind speeds are normalized with the 90 m wind speed measured in the non-wake measurements or simulation data, respectively. To further remove the disagreement caused by the difference in wind direction, the flow fields were rotated in Fig. 3.10 (rightmost panels), so that the wake propagates along the y axis.

The 10 min averaging does not apparently filter all turbulent structures of the measured wake field. This is most probably due to the much lower sampling rate of the lidar measurements. Approximately 8000 single values contribute to the average on the 20 m grid in the LES, considering a time step of about 2 Hz and the original grid resolution of 5 m. In contrast, the sample velocities contributing to the lidar average vary from 100 to 350 individual line-of-sight wind speed values and are not evenly distributed in space and time.

The results show that the unrotated wakes (Fig. 3.10, third column) match very well during the morning period where the wind direction appears to be nearly identical. In this period an asymmetry in the horizontal profile of the wake is also clearly visible, a phenomena related to the interaction of vertical wind shear with the rotation of the wake, as shown for example
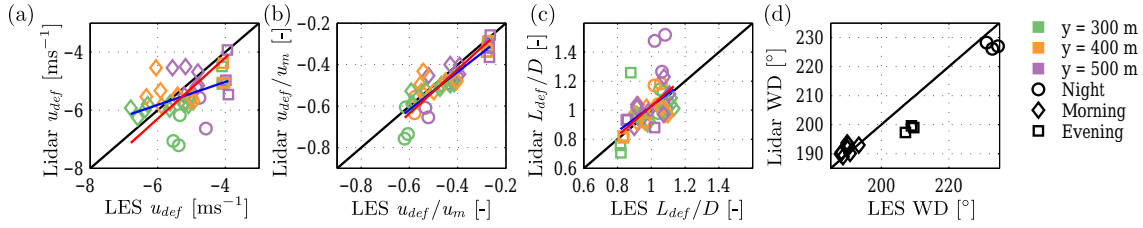
Figure 3.13: Scatter plots of the properties derived from the Gaussian-like fit to the wake profiles of **(a)** the wake deficits, **(b)** the normalized deficits, **(c)** the wake widths and **(d)** the wind direction derived from the propagation direction of the wakes. The three different time intervals are marked with different markers as in Fig. 3.9. Colors represent the downstream distance from the turbine. Lines show simple linear regression (blue) and regression through the origin (red).

in Vollmer et al. (2015). The amplitude of the wake deficit appears to be best simulated in the evening period when the turbine operates above rated power. The lower thrust leads to a wake that shows no signs of double minimums in the near wake as visible in the other measurements and simulations.

In the following an attempt is made to make a quantitative comparison between the measured and simulated wakes. To derive statistics of the wakes, the profiles of all 15 time intervals were fitted to a curve consisting of two Gaussian-like functions:

$$u_w(x) = b \exp\left(-\left(\frac{x-c}{d}\right)^2\right) - e\,b \exp\left(-\left(\frac{x-c}{f\,d}\right)^2\right). \tag{3.5}$$

Within this function, the central region of lower deficit in the near wake is represented by the second exponential function, with $e, f \in [0, 1]$. The wake width (90th percentile) was defined as $L_{\text{def}} = \sqrt{2} \cdot 1.64 \cdot d$, as deficit u_{def} the minimum value of u_w was chosen. Figure 3.11 shows an example of the fits to the data and Fig. 3.12 shows the fitted deficit and wake width for all time periods. Minimums of the deficits can be identified in both data sets at a distance of between 1 and $2\,D$ downstream for the high-thrust situations and at a distance of about $3\,D$ for the low-thrust situations. In general the trajectories from the measurements exhibit much more noise, which makes a comparison especially of the wake widths difficult.

A direct comparison of the wake properties at selected downstream distances is presented in Fig. 3.13. Regression through the origin shows quite a good agreement between lidar and LES wake deficit, though the LES shows a tendency to simulate a higher wake deficit during the morning period and lower deficits otherwise. As no time series of thrust measurements of the turbine were available, we can only speculate if the difference is related to a different thrust of the turbine than in the constructors' specification or if either model or measurement data are inaccurate. The spread decreases by normalizing the deficits and the slope of regression between simulated and measured normalized deficits is 1.05. The simulated wakes are slightly wider on average, except when the turbine is being operated in below-rated conditions (night period), in which the measured wakes are both wider and have a higher deficit.

3.5 Discussion

As demonstrated in this paper, the forcing of LES with mesoscale-model profiles allows for time-dependent LESs that change according to the synoptic meteorological conditions. Thus, a transient state of the atmospheric boundary layer can be used for the analysis of wind farm model performance. This allows, for example, for a direct validation of wake simulations with measured data, which represents a different approach from the classical statistically derived validation data for wind farm models.

The comparison of the ambient flow created by the model chain with met mast data indicates that the synoptic trend of wind speed and direction is maintained and that the average properties of the simulated wind profile during the 2-day period are close to the properties of the measured wind profile. Time series and power spectra, however, reveal a gap of energy contained in the mesoscale fluctuation range. These fluctuations might be partly resolved with a much larger LES domain, if they originate from thermal effects (Schalkwijk et al., 2015). An inclusion of measurement data as a relaxation data set (Rodrigo et al., 2016) might also lead to a closer tracking of the measurements but requires measurements at higher heights than available in this case.

As this paper only looks at a very short time period, we refrain from drawing general conclusions about the model chain's ability to replicate the evolving state of the atmospheric boundary layer and refer to Schalkwijk et al. (2015) and Heinze et al. (2017), who analyze longer time periods. For wind energy purposes we think that the mesoscale model remains the crucial part of the presented model chain to improve the spectral and vertical representation of the wind field. However, at least for the spectral part, current combinations of models and reanalysis data do not appear to be sufficient (Vincent et al., 2013).

The comparison of the wake simulations with the measured wakes represents one of the suggested applications of the model chain. Instead of averaging over similar wind profile states, a direct time series comparison is performed. The visual comparison of simulated with measured wakes shows a good match, indicating that wind direction and wake profile are well replicated. Derived wake statistics of the downstream development, however, reveal that the available measurement data still require a more statistical treatment to be able to draw a conclusion about the goodness of the wake representation in the simulations.

Alternatives to the presented approach for LES of wind turbines in the atmospheric boundary layer are idealized quasi-stationary setups or nested LESs inside a mesoscale model. Both of these approaches have advantages and disadvantages compared to the method in this paper. An idealized setup enables the study of an identified quasi-stationary state of the atmospheric boundary layer in detail, as in Vollmer et al. (2016) and Mirocha et al. (2015), for example, or the replication of an idealized transient state (Abkar et al., 2016). For the simulation of observed transient states, however, information from a larger-scale model becomes necessary. Boundary conditions of quasi-stationary states can also be derived from a mesoscale model with the method presented in this paper, if no sufficient measurement information is available.

The approach of a nested LES domain inside of a mesoscale-model domain might enable

the inclusion of frequencies of the flow in the range of mesoscale fluctuations or the advection of a different level of turbulence created by upstream obstacles. However, it needs a large LES domain for the development of microscale turbulence (Muñoz-Esparza et al., 2014) or a good solution to initialize the turbulence at the inflow boundary. It also requires running a mesoscale model in parallel, which is not necessary for the offline coupling approach, which can be started from external data sources by the use of the COSMO-DE data, as shown in this paper.

3.6 Conclusions

In this paper we introduce and test a method to simulate a wind turbine wake in the offshore atmospheric boundary layer with LESs driven by forcing derived from a mesoscale simulation. The methodology enables the simulation of a transient state of the atmospheric boundary layer for the evaluation of wind farm performance or the validation of wake simulations. The comparison with met mast data shows that the model chain is able to reproduce the synoptic trends and the boundary layer turbulence of the marine wind field during the 2 days analyzed. Most of the mesoscale fluctuations found in the measurements are not replicated, which is most likely related to the deficiencies of the mesoscale model. The wake simulations are compared to lidar measurements downstream of an Alpha ventus turbine. In certain periods the modeled and measured wakes are very similar, as especially the wind direction matches well. A direct comparison of measures to describe the downstream wake development proves to be difficult with a high scatter of the measured wakes. Thus, the limited data set of the lidar measurements and the still-prevailing turbulent structures in the 10 min averages of the data make it difficult to validate the performance of the whole model chain. We think that the methodology might be especially valuable for transient non-neutral states of the atmospheric boundary layer, in which the boundary conditions to set up LESs are difficult to derive. In these cases, the method presented might not only be valuable for the comparison of simulations with measurement data but could also be applied to study wind turbine or wind farm control in changing wind conditions.

Acknowledgements

Chapter 4

A wind turbine wake in changing atmospheric conditions: LES and lidar measurements [1]

Abstract   This work aims to reproduce the measured atmospheric conditions during one day of the CWEX-11 campaign, with a transient LES. The selected period includes several interesting atmospheric conditions for wind power generation such as a nocturnal low-level jet, a highly turbulent convective daytime boundary layer, as well as a distinct evening transition between daytime and nocturnal boundary layers. To include synoptic conditions, large-scale forcing profiles for the LES were derived from a mesoscale simulation with the WRF model. A comparison with lidar measurements shows that the trend of the wind conditions and the diurnal cycle is well replicated by the model chain. Selected periods of the day are simulated with the NREL 5MW turbine model, followed by a qualitative comparison of measured and simulated wakes. We find a strong dependency of the meandering and the shape of the wake on wind profile and turbulence, while a categorization by Obukhov length is less representative for the different conditions. As the veer in the wind profile increases, the deviation of the wind direction at hub height from the direction of the largest wake impact also increases.

4.1 Introduction

The use of ground-based or nacelle-based lidars has rapidly increased knowledge about wind turbine wakes in recent years (Trujillo et al., 2011; Rhodes and Lundquist, 2013; Machefaux et al., 2015b). Lidars are mostly cheaper and are more mobile than meteorological masts, can be easier deployed in complex terrain and the remote technique allows measurements of the wake at a range of heights and distances. Still a single lidar cannot completely probe the three-dimensional structure of the wake as it evolves in time, leading to uncertainties in our understanding of wake evolution.

One method to complement lidar measurements of wind turbine wakes are numerical experiments (Mirocha et al., 2015; Machefaux et al., 2015a; Lundquist et al., 2015). Numerical experiments can deliver a temporally-resolved three-dimensional wind field to study the flow regions that were not observed. The possible benefit of the complementary simulations depends on the ability to reproduce, in the numerical environment, the aerodynamic behaviour of the turbine as well as the state of the atmospheric boundary layer.

Mesoscale models, with typical horizontal grid sizes in the order of 1-10 kilometers, can simulate the mesoscale and synoptic development of the atmospheric boundary layer. These models enable studies of the changing wind conditions at a wind farm site but are not highly resolved enough to model the aerodynamics of turbines and the interaction of turbines by means of their wakes. An approach for further downscaling towards smaller scales has been presented in Vollmer et al. (2015, 2017) using a Large Eddy Simulation model (LES), driven by the data of a mesoscale model. The study showed that it is possible to replicate observed offshore wind conditions with a transient LES and that the simulated wakes show similar behaviour to the measured wakes.

In this paper we use the approach to simulate a case that is more interesting regarding the influence of atmospheric stability on wakes, as it represents an onshore day characterized by a strong diurnal cycle and a well-pronounced evening transition. The case study selected is one day (9 July) of the CWEX-11 measurement campaign in 2011 in Iowa, USA. From the selected day, lidar measurements from two vertical profiling lidars, placed upstream and downstream of a 1.5 MW turbine, and measurements from an upwind flux station are used. A part of the chosen day has been studied by means of quasi-stationary LES in Mirocha et al. (2015). Here we use the transient approach to simulate almost the whole day. During selected time periods, that represent different atmospheric stability conditions, wind turbine wake simulations with the NREL 5MW model turbine (Jonkman et al., 2009) are performed. Due to the different dimensions of the turbines in measurement and simulation, we performed a qualitative comparison in this study, and focused on the potential surplus of information that can be extracted from the accompanying simulations.
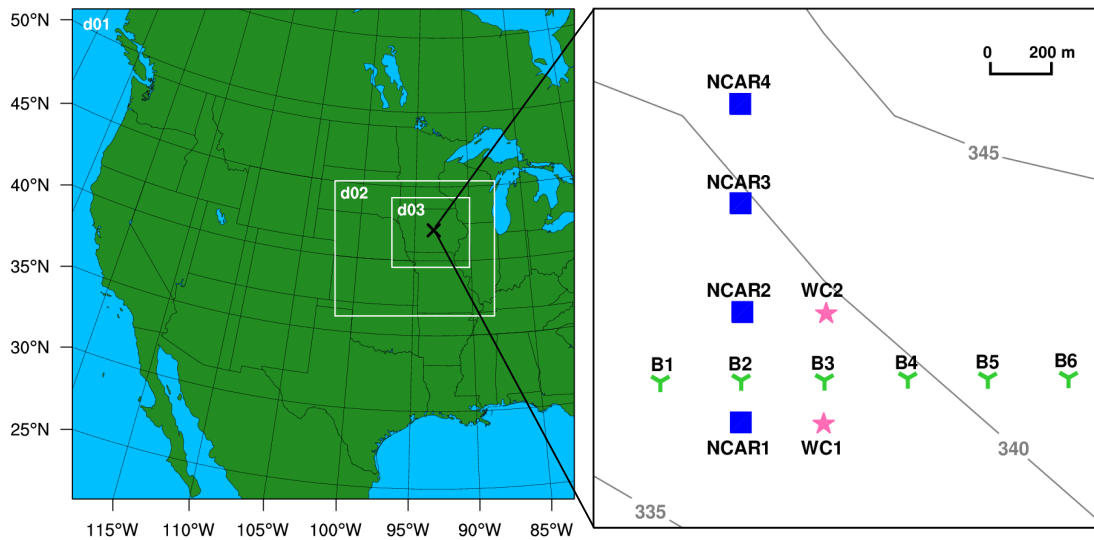
Figure 4.1: WRF model domain with the wind farm marked as cross in the innermost domain and topographic map showing the setup of the CWEX-11 campaign. Wind turbines (B1-B6), lidars (WC1-2) and surface flux stations (NCAR1-4).

4.2 Methods

4.2.1 Observations

The Crop/Wind Energy EXperiment 2011 (CWEX-11) took observations along a row of wind turbines of a 200-turbine wind farm in Iowa, USA, from June to August 2011 (Rajewski et al., 2013; Rhodes and Lundquist, 2013). The turbines are 1.5 MW turbines from General Electric with a rotor diameter (D) of 77 m and a hub height of 80 m. The wind farm is situated in a flat region characterized by extensive agriculture (corn).

Two WindCube v1 lidars (WC1-2) measured the vertical wind profile at altitudes from 40 m to 220 m AGL. The lidars were placed 2.1 D south and 3.2 D north of one turbine of the southernmost row of the wind farm to capture free flow as well as wake flow for the prevailing southerly wind. Surface flux stations were also sampled upwind and downwind in similar fashion but for the next turbine to the west (Fig. 4.1). The original measured wind components from the lidars at 0.25 Hz were averaged every 2 minutes. In this paper we do not further analyse the uncertainty of the wind profile measurements that come from the velocity azimuth display (VAD) technique. For the effect of the individual beams and the volume averaging on the flow reconstruction by the lidar, especially inside wind turbine wakes, the reader is referred to Lundquist et al. (2015).

Five-minute averages of the 20-Hz measurements from the sonic anemometers and gas analysers were made available from the National Center of Atmospheric Research (NCAR). The instruments were operating at 4.5 m above ground level (AGL). The Obukhov length was calculated as

$$L = -\frac{u_*^3 \, T_v}{k \, g \, \overline{w'T'_v}}$$
(4.1)

using the friction velocity u_*, derived from the vertical fluxes of momentum in the streamwise and spanwise directions, the vertical kinematic heat flux $\overline{w'T'_v}$ and the virtual temperature T_v measured by the sonic anemometer. The factors k and g are the von-Kármán constant and the gravitational acceleration, respectively. The bulk Richardson number (Ri) was calculated as an alternative measure for atmospheric stability following Stull (1988).

$$Ri = \frac{g \, \Delta\Theta_v \, \Delta z}{\Theta_v \, [(\Delta u)^2 + (\Delta v)^2]}$$
(4.2)

with $\Delta\Theta_v$, Δu and Δv the difference between the virtual potential temperature Θ_v, the streamwise velocity u and the cross-stream velocity v at two different measurement heights separated by Δz. As temperature measurements were not available above 10 m, Ri could only be calculated from the model results. The bulk Richardson number was calculated between the surface and the hub of the simulated turbine (Ri_0^{90}) and between the lower and upper rotor tip (Ri_{30}^{150})

4.2.2 Models

The model chain for the simulation of the case consisted of two models. The Weather Research and Forecasting (WRF) model (Skamarock et al., 2008) was used to simulate the changing wind conditions at the site during the day, required as large-scale forcing input (Vollmer et al., 2017) for the PArallelized Large Eddy Simulation Model (PALM) (Maronga et al., 2015).

Model version 3.6.1 of WRF was used for a 30 h simulation starting at 00 UTC (five hours ahead of local standard time LST) on 9 July (Lee and Lundquist, 2017). Initial and boundary conditions for the one-way-nested domains were derived from the Global Forecast System (GFS) reanalysis, using the standard procedures as defined in Skamarock et al. (2008). The smallest domain covered the entire state of Iowa with 990 m horizontal resolution and a dimension of 571 x 511 grid points. Vertical levels were stretched towards the top with 70 levels in total and a vertical spacing of about 22 m in the lower 300 m AGL. The MYNN Level 2.5 scheme (Nakanishi and Niino, 2006) was used for the TKE closure in the planetary boundary layer. A more detailed description and analysis of the WRF simulation is presented in Lee and Lundquist (2017).

To create the large-scale forcing profiles for the LES, the hourly model results from WRF were horizontally averaged on a domain of 80 km x 80 km to average out pressure perturbations on smaller scales (See Vollmer et al. (2017) for a discussion on the necessary size of the

averaging domain). The domain was centered around the turbine, where the lidar measurements were made. The mean geostrophic wind vector at this location was calculated from the large-scale pressure gradients over the domain. The vertical profiles of the horizontal advection of temperature, humidity and horizontal momentum as well as the geostrophic wind speed components were used for the large-scale forcing of PALM. To prevent the LES from drifting from the WRF results, a nudging scheme was used with a relaxation time constant of $\tau = 4$ h. Nudging was applied to the domain averaged vertical profiles of potential temperature, humidity and the horizontal wind components. More details about the preparation and application of the large-scale forcing can be found in Vollmer et al. (2017).

Revision 1928 of PALM (Maronga et al., 2015) was used with the same numerical schemes as in Vollmer et al. (2016). Simulations were run on a 640 x 640 x 160 grid with 5 m resolution. Above 600 m, vertical stretching of the grid was applied. The highest grid point is centered at 1715 m. Monin-Obukhov similarity theory is used at the bottom boundary with a surface roughness length of momentum of $z_0 = 0.14$ m, which represents the average roughness length inside of the WRF averaging domain. Roughness lengths of scalars were a factor of ten times smaller.

Sufficient information to implement the GE turbine was not available. However, to allow for a qualitative comparison of the wake behaviour, an ADM-R (Witha et al., 2014b) representation of the NREL 5MW (Jonkman et al., 2009) research turbine model was used for wake simulations. The turbine has a rated power of 5 MW, a rotor diameter of 126 m and its hub is located at 90 m.

Adaptation of the rotor speed of the NREL 5MW turbine to the changing wind is ensured by a generator torque controller below rated wind speed (11.4 ms^{-1}) and a collective pitch controller above rated wind speed. The turbine orientation is controlled by a yaw controller based on a 30-second running average of the wind direction at the turbine hub. The yaw actuator is activated for a misalignment of more than 5 degrees. As the turbine influences the turbulence and fluxes inside the cyclic LES domain, the maximum length of individual turbine simulations was 35 minutes, of which the first 5 minutes were discarded as the wake was still developing. From the total 30 h of simulation, the first eight hours were discarded as they are used for the spin-up of both the WRF model and the LES.

4.3 Results

In the following we will discuss the performance of the model chain to simulate the state and development of the atmospheric boundary layer, followed by an analysis of the wake simulations. Figure 4.2 compares the results of the simulation of the ambient flow with the large scale forcing input data, the lidar measurements and the flux measurements. The wind speed and wind direction follow the trend of the input data, but deviations from the measurements can reach more than 2 ms^{-1} and 20° for wind speed and wind direction, respectively. The measured surface kinematic heat flux (Fig. 4.2g) is well replicated by the WRF simulation with a negative heat flux during nighttime and a positive one during
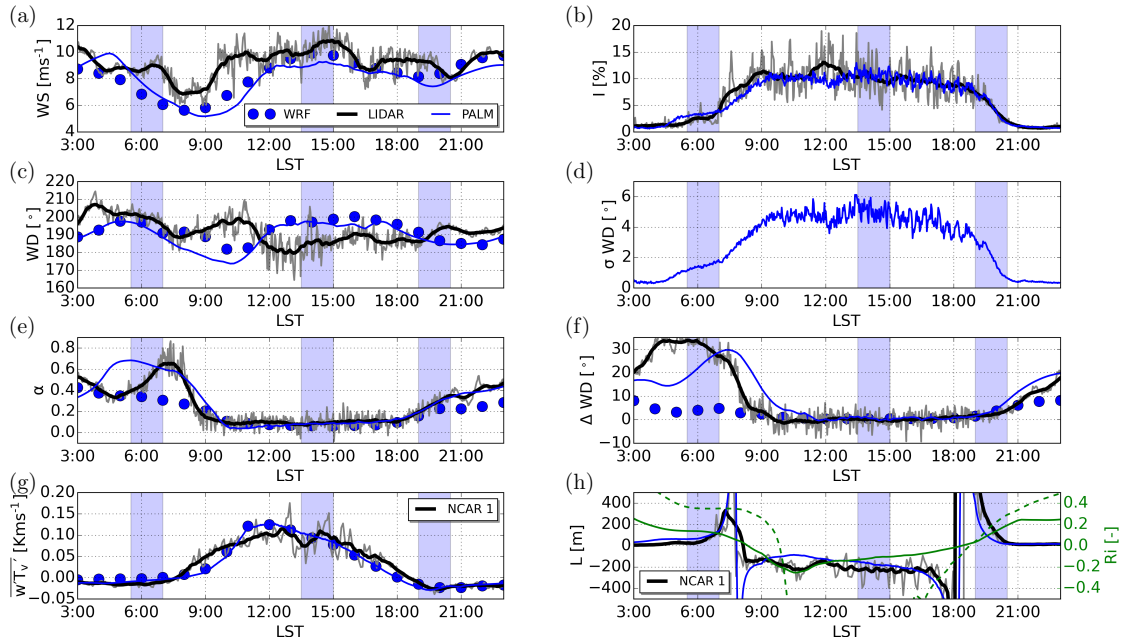
Figure 4.2: Comparison between one-hour running means (black bold), short-term averages (grey) of measurements, the large-scale forcing input from WRF (dots) and the domain averaged LES results (blue thin). (a) Two-minute hub-height wind speed, (b) hub height turbulence intensity, (c) hub-height wind direction and (d) hub-height standard deviation of the wind direction. (e) Two-minute vertical power law coefficient and (f) change of wind direction, both between 40 m and 140 m. (g) Five-minute surface kinematic heat flux, (h) Obukhov length and bulk Richardson number between surface and hub height (solid) and between lower (30 m) and upper (150 m) rotor tip (dashed). Shaded areas mark the selected periods for the turbine simulation. From left to right: SBL, CBL and NNBL.

daytime between 08:00 LST and 18:00 LST. The LES kinematic heat flux almost equals that of WRF. The diurnal cycle of the 2-min turbulence intensity (I) is well reproduced in magnitude, and the moment of restratification, quantified by the sign change of L, during the evening transition matches very well. The largest deviation of the LES from the WRF input is found in the measures for the vertical wind profile (Fig. 4.2e,f). The LES does a better job to simulate the veer of the wind profile of the nocturnal boundary layer than the mesoscale model, which appears to be limited to a maximum veer of $\Delta WD = 10°$ between the two selected heights. The shear of the wind profile on the other hand is well replicated by WRF with the exception of a period at the end of the night where the measured wind shear increases in the measurements. A low-level jet occurs in the simulation between 03:00 LST and 07:00 LST with a core height between 200 m and 300 m (not shown), thus clearly above the maximum rotor height. The core height is consistent with the lidar measurements, as no local maximum of the wind speed can be found in the measured profiles below 220 m.

Based on the results of the simulation of the ambient flow, three periods of 1.5 hours, marked by the shaded areas in Fig. 4.2, were selected in which a simulation with a turbine was conducted. The periods (Tab. 4.1) were selected to represent different meteorological conditions. During the first period, the turbine operates in a strongly sheared and veered wind profile with low turbulence that is created by the strong nocturnal stable stratification (SBL). The second period during the day is characterized by a convective boundary layer (CBL) with nearly no vertical shear but vigorous short scale fluctuations of wind speed and direction (Fig. 4.2b,d). The evening transition from the daytime to the nighttime layer with a near neutral stratification (NNBL) is selected as the third period. While the measures of the wind profile differ considerably between SBL and NNBL, the mean Obukhov length is almost equal and the negative heat flux is even lower during the NNBL period (Fig. 4.2g,h, Tab. 4.1). The long build-up of the strong shear of the nocturnal boundary layer can thus not be captured with the instantaneous measure of Obukhov length and heat flux at the surface. Using the bulk Richardson number as an alternative measure for the classification of the stability conditions during the periods allows to differentiate between the SBL and NNBL period only when using measurements at the heights of the rotor tips.

The wakes in the three situations exhibit very different characteristics, that appear in both, the measurements and the simulations. Fig. 4.3 shows the two-minute averaged

Table 4.1: Average quantities from the PALM simulations during the three periods for which wake simulations were run. Mean and turbulent quantities are at hub height. Vertical temperature flux and Obukhov length are calculated at the vertical center of the lowest grid cell at z = 2.5 m.

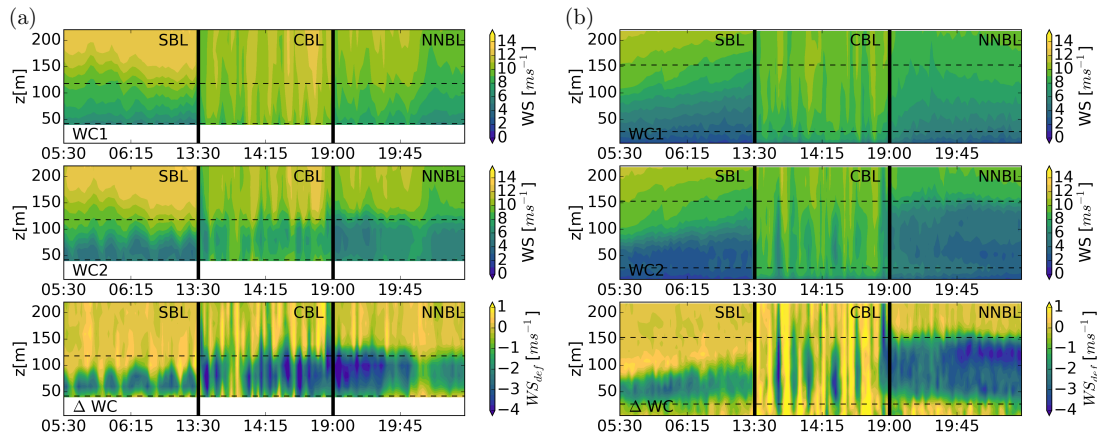| | Start | End | $\overline{WS}$ | $\overline{WD}$ | $\overline{I}$ | $\overline{\sigma WD}$ | $\overline{\Delta WD}$ | $\overline{\alpha}$ | $\overline{w'T'}$ | $\overline{L}$ | $\overline{Ri}_0^{90}$ | $\overline{Ri}_{30}^{150}$ |
	[LST]	[LST]	[ms⁻¹]	[°]	[%]	[°]	[°]	[-]	[K ms⁻¹]	[m]	[-]	[-]
SBL	05:30	07:00	7.5	194	3.4	1.5	22.8	0.65	-0.006	87	0.13	0.35
CBL	13:30	15:00	9.0	197	10.7	5.0	0.5	0.08	0.095	-172	-0.12	-0.75
NNBL	19:00	20:30	7.6	186	4.9	2.0	3.3	0.26	-0.025	93	0.11	0.16

Figure 4.3: Temporal development of the horizontal velocity profile at the position of WC1 (top row) and WC2 (middle row) and difference between the two profiles (bottom row), (a) from the lidar measurements and (b) from the LES. The dashed lines mark the vertical boundaries of the respective rotor.

profiles from the lidar measurements and from the simulations at the upwind and downwind lidar position. Even though the wind turbines in reality and in the LES model are different, and the ambient flow fields are not exactly equal, either, the defining wake characteristics are identical. During the SBL period the wake is weaker and at a lower height than during the NNBL period, while the wake during the CBL period is just intermittently discernible. However, the vertical profiles of course only visualise a fraction of the full wake. Especially in the strong fluctuating wind conditions of the convective boundary layer it is impossible to localise the position inside the wake where it is sliced by the scan.

To gain further insight into the wake characteristics and behaviour, vertical cross-sections of the wake derived from the simulations were used. For this purpose the wind field was averaged along a half-circle downstream of the wind turbine with the radius of 3.22 D, corresponding to the distance of the downstream lidar from the turbine (Fig. 4.3b). This procedure was chosen to retrieve sections of the wake at the same distance for every wind direction. Example cross-sections for the three time intervals are shown in Fig. 4.4. The strong veer of the nocturnal boundary layer leads to a strong cross-stream stretching of the wake. Thus, the vertical profile at the lidar position only captures the lower left corner of the wake. The example wakes during the CBL and NNBL both have a more circular shape.

A direct comparison of the wakes based on the wind speed is difficult as the wakes can not be easily fitted to any geometric structure, e.g. a Gaussian-like shape, due to their asymmetry. To simplify the wake representation, the wind speeds downstream of the turbines were converted to rotor equivalent wind speeds (REWS) (Wagner et al., 2014) as a function of the cross-stream coordinate x as in Vollmer et al. (2016). For this purpose the cube of the wind speed is averaged on virtual rotor surfaces of the diameter D of the NREL 5MW
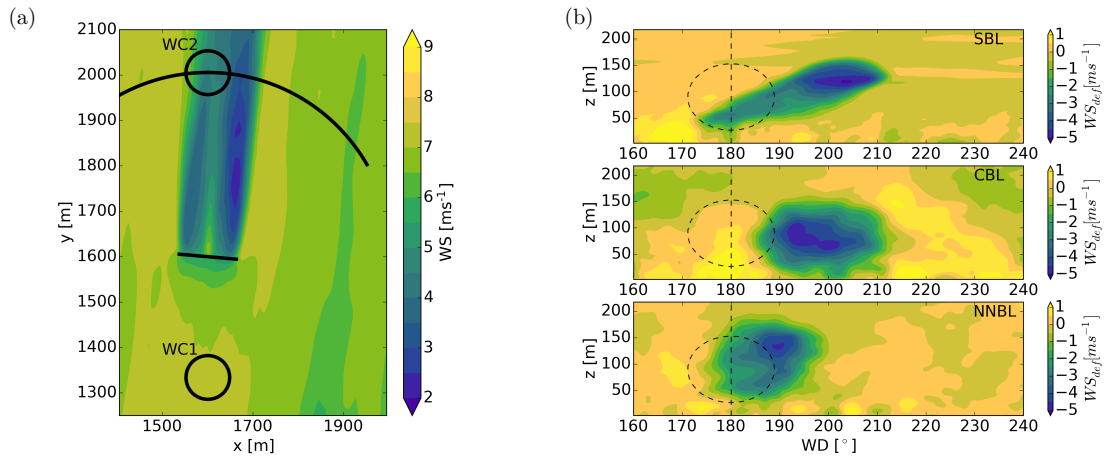
Figure 4.4: (a) LES wind speed average at hub height at 19:45 LST during the SBL period with the positions of the lidars marked as circles. Marked as black line is the line of constant distance to the turbine along which the velocities are analysed in Fig. 4.4 (b) Examples of the 2-min averaged wind speed along a constant distance (3.22 D) downstream of the turbine during the three simulation intervals. The vertical line denotes the position of WC2. The circle denotes the surface used for the calculation of the REWS at WD = 180°.

turbine and converted back to a wind speed.

$$\text{REWS}(x) = \left(\tfrac{1}{A} \int_{x1}^{x2} \int_{z1}^{z2} u^3(x',z') \cos(\beta(x',z')) dz' dx' \right)^{1/3} , \quad (x'-x)^2 + (z'-z_h)^2 \le (D/2)^2$$

(4.3)

The wind veer β over the rotor area A is defined as the difference between the wind direction at hub height and at the specific coordinate (Rodrigo et al., 2016). Here we use the assumption that the virtual rotor is aligned with the wind direction at hub height. By calculating the REWS the wakes are reduced to two-dimensional structures and can be compared easier.

The REWS for all individual 2-minute averages is shown in Fig. 4.5a. Figure 4.5b shows a time series of the deficit position defined as the minimum of the REWS and the 2-minute average of the LES wind direction at the rotor center of the turbine. The analysis shows that the REWS shows a strong asymmetry in the SBL, with a sharp gradient on the right side of the wake and a flat slope on the left side. As the simulated wind veer increases during the SBL period (Fig. 4.2f), the difference between the wind direction of the REWS minimum and the hub height wind direction also increases. This difference reaches a value of 10 degrees by the end of the stable simulation. Though the effect is regarded to depend on both shear interacting with the wake rotation and the veer of the wind profile (Vollmer et al., 2016), it is mainly dependent on wind veer in the analysed case as shown in Fig. 4.5c.

The wake during the NNBL period appears to be more symmetric. While the wake shapes of NNBL and CBL appear similar in Fig. 4.4a, the main difference between the two periods is the strong fluctuation of the wind direction during the CBL period which leads to a perma-
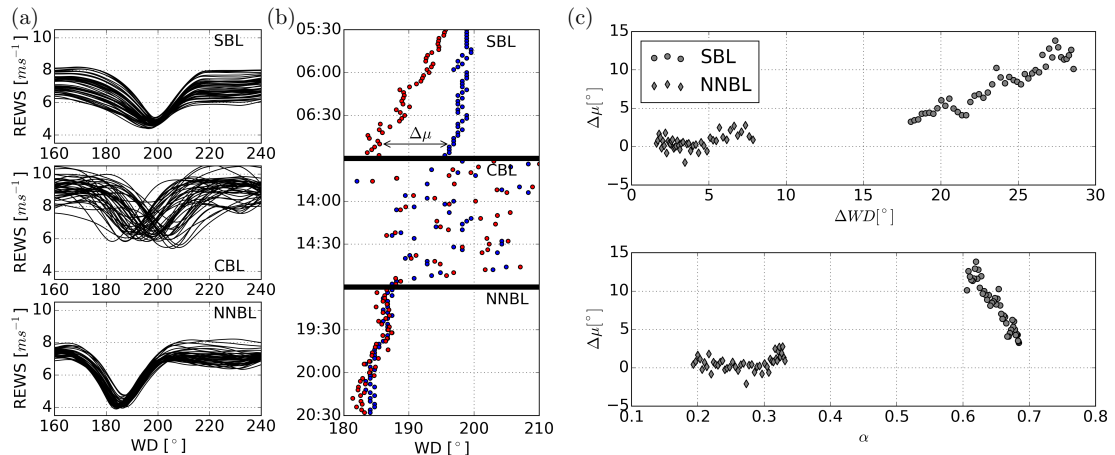
Figure 4.5: (a) REWS as function of wind direction of each 2-min timeframe. (b) Position of the minimum of the REWS (blue) and LES wind direction at the rotor center (red). (c) Difference between wake position and hub height wind direction $\Delta\mu$ plotted over the wind veer and the wind shear coefficient.

nent cross-stream meandering of the wake. During the NNBL period the REWS minimum generally coincides with the measured wind direction at hub height.

4.4 Discussion

Mesoscale to microscale flow modeling is regarded as one of the main research topics for the next generation of wind condition assessment and wind farm design tools (Sanz Rodrigo et al., 2017). The methodology to use a background state derived from mesoscale simulations for cyclic LES, presents an alternative to the so-called nesting of LES in mesoscale simulations. The advantage of the method is that only a limited amount and only low resolved mesoscale data is necessary for the setup of the LES boundary conditions. Thus, the simulations can be run from a database of temporally resolved mesoscale model data like planned e.g. in the New European Wind Atlas (NEWA) project. The disadvantage of the method is that the spatially resolved advection of turbulent structures, for example from orography or from upstream wind farms can not be included in the simulation. Here, nesting presents an advantage, even though the best practices of turbulence instigation and mesh refinement from the meso- to the microscale regime are still under discussion (Muñoz-Esparza et al., 2014).

The results of this paper indicate that the model chain of WRF and PALM is generally able to replicate the state of the atmospheric boundary layer during the selected day. As also concluded in Vollmer et al. (2017), the more important model for a good replication of wind speed and wind direction is the mesoscale model. However, in the given case with a strong diurnal cycle, we find the LES model capable of improving the vertical wind speed and

wind direction profile of a strongly-stratified nocturnal boundary layer. The reason may be primarily related to the lower vertical resolution of the mesoscale model and the consequential parametrization of the boundary layer fluxes. To improve the match between measurements and simulations it might be worth incorporating the measurements into the large-scale forcing and nudging data as in Rodrigo et al. (2016).

The wake simulations performed in the transient flow conditions present a method to enhance the understanding of the measured wake flow. This procedure can be regarded as an alternative or a supplement to long-term measurements that are typically classified in classes of wind speed, wind direction and stability (Mirocha et al., 2015; Hansen et al., 2012; Dörenkämper et al., 2014). While we were not able to replicate the wake in this study due to the lack of sufficient details about the wind turbine, we were still able to show the fundamental differences in wake behaviour and shape in the three periods of different atmospheric stability.

The differences can be related to the vertical profile of wind speed and direction and to the fluctuations of these parameters. The wind veer reaches values of up to 35° over the rotor surface during stable stratification, which leads to a wide stretching of the wake. During the daytime convective period the fluctuation of wake position and intensity is dominating the wind field. The bulk Richardson number, calculated from the vertical wind shear and the temperature difference over the rotor surface allows a categorization of the three periods of different wake behaviour. Atmospheric stability measured in the constant flux layer close to the surface, i.e. characterized by the Obukhov length, on the other hand, appears to be insufficient to differentiate between the periods as it is not able to capture the time history of the evolving flow. Thus, for a classification of wake measurements or performance measurements of wind turbines in stability classes the Richardson number is more suitable.

Abkar et al. (2016) have shown in a simulation of an idealized diurnal cycle in LES how the wind farm power varies with the wind conditions influenced by atmospheric stability. For more sophisticated wind farm control like curtailment or wake steering, a precise knowledge about the wake deficit position is also crucial. Our results show that wind veer needs to be considered as it can indeed influence the wake deficit position.

Acknowledgements

Chapter 5

Wind farm control applied in different atmospheric stabilities

The objective of this chapter is to verify the power increase of a wind farm by wake steering in the experimental environment of an LES. The simulations of the three stability regimes of the ABL as introduced in Ch. 2 are compared to show how the different wake characteristics that were discovered in the previous chapters influence the success of applied wind farm control. Specific situations in which a simple open-loop model-based controller runs into problems are selected to propose and test a more robust solution for the yaw control of the turbines.

The chapter starts with a description of the concept of model-based control and the conditions that are needed to validate the approach. The derivation of an open-loop model-based yaw controller from the LES data of Ch. 2 is explained in Sect. 5.2. The model is used to search for optimal yaw angles for an upwind turbine of a simple wind farm consisting of two turbines. The goal is to attain a maximum energy yield of the wind farm for every wind direction. In Section 5.3, the model-based yaw controller is used in LES to improve the energy yield of the wind farm. The results are compared to reference simulations with a baseline yaw controller. Two critical scenarios for the open-loop model-based control approach are identified and analysed in Sect. 5.4. These results lead to a formulation of modified control set points in Sect. 5.5, a so-called passive wake steering control, that is tested for the same scenarios. The chapter concludes with a summary and discussion of the results.

5.1 Validating wind farm control

In model-based control, a model is consulted to define a new configuration of control parameters for a system. Usually these models represent a simplification of the complete state of the system. In principle, a differentiation can be made between models that calculate the new configuration online on real time and those that create databases beforehand to cover the possibly occurring system states. A real-time model has to find a solution in a short period, so that the system has not already evolved to a different state. Thus, these kind of models usually are more simplified than models that can be used to create a database. On the other hand, real-time models allow for a modification of the model on the fly, depending on the
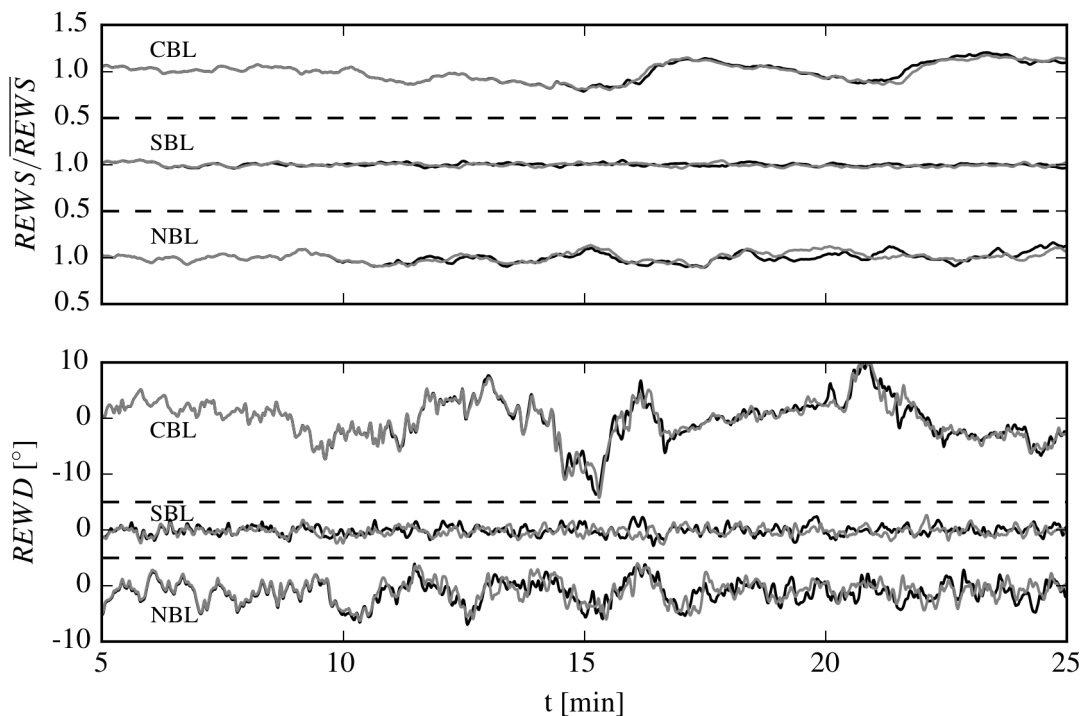
Figure 5.1: Comparison of the timeseries of rotor equivalent wind speed (REWS) and direction (REWD) 2.5 D upstream of the wind turbine from two randomly selected simulations with different yaw angle in each ABL scenario. The REWD is the average wind direction over the rotor surface.

response of the system. This procedure is called closed-loop model-based control (e.g. Vali et al., 2016). In contrast, an open-loop controller does not allow the system response to change the underlying model.

A critical part of model-based control is how well the real system state is represented by the simplification. This aspect is a critical reason for the difficulty of model-based control of wind farms. A simplified model for wind farm control has to be able to replicate the flow inside the farm and the response of the turbines to the flow without having access to many measurements. Challenges for the model include i.a. the inhomogeneity and the different scales of turbulence of the flow and the temporal delay between a change on the turbine configuration and the change of the flow at the turbine.

An alternative to model-based control can be a machine-learning algorithm. Such an algorithm is not replicating the system state but just focuses on how the objective function behaves on changes to the control parameters. A model-free approach can for instance be established by machine-learning techniques. This approach requires a training period during which the reaction of the objective function to perturbations of the system is analysed. The identification of optimal or better control parameters requires an iterative process in real

time. Thus, machine-learning approaches are susceptible to changes of the system state during the optimization process.

The validation of both, model-free and model-based control approaches relies heavily on the available measurements and how well they are able to characterise the flow inside the wind farm. The main difficulty is how to prove that a certain control algorithm leads to an improvement of the performance of the wind farm without being able to reproduce identical wind conditions. One approach is to classify the measured system states and to compare two equivalent states that were run with different controllers. However, as shown in the previous chapters, the standard of measuring hub-height wind speed and wind direction or using the wind turbines' energy yield is usually not sufficient to describe the flow field. The change of the vertical profile and the turbulent characteristics of the flow by atmospheric stability leads to different boundary conditions for wind farm control. Without even considering the issue that these properties need to be measured, the further classification reduces the comparable amount of system states during a measurement period.

A test environment for the validation of the benefit of wind farm control needs to be able to either verify the occurrence of equivalent wind conditions or to reproduce equivalent or identical wind conditions. While the former is part of recent measurement campaigns (Bromm et al., 2018; Fleming et al., 2017b), the latter is possible for example with wind tunnels or numerical experiments. The previous chapters have shown that LES with the model PALM and the ADM-R wind turbine model compare well to measurements of the ABL and real-size wind turbine wakes. Furthermore, when LES are initialized with the same wind fields and the same inflow conditions, the simulations are not only statistical equal but also nearly identical. Figure 5.1 demonstrates that the simulations of Ch. 2 contain the same large scale turbulent structures that pass the wind farm. This allows for collecting information about different control modes in only short simulations even in a CBL, in which a statistical convergence would require rather long simulation times. Thus, the simulation setups from Ch. 2 appear to be capable test environments for wind farm control.

5.2 Construction of the wake model

To simplify the open-loop model-based control approach in this study, the model that is used in this analysis is also derived from the LES of Ch. 2, thus from the same environment in which the wind farm control simulations are conducted. The model represents a database that covers the mean system states that can occur during the simulations. This largely excludes the error source of an incorrect flow model for the construction of the control set points and permits to focus on other aspects of the controller. As a consequence the focus lies on the testing of the maximum power benefit of the control strategy of wake steering and the analysis of situations that prevent the controller from achieving the maximum benefit.

The wake model is constructed from the LES results by reducing the mean wind field to a two-dimensional field of REWS as introduced in Ch. 4, Eq. 4.3. Figure 5.2 shows examples of the REWS for different simulations with different yaw angles of the upwind turbine T_{up}.
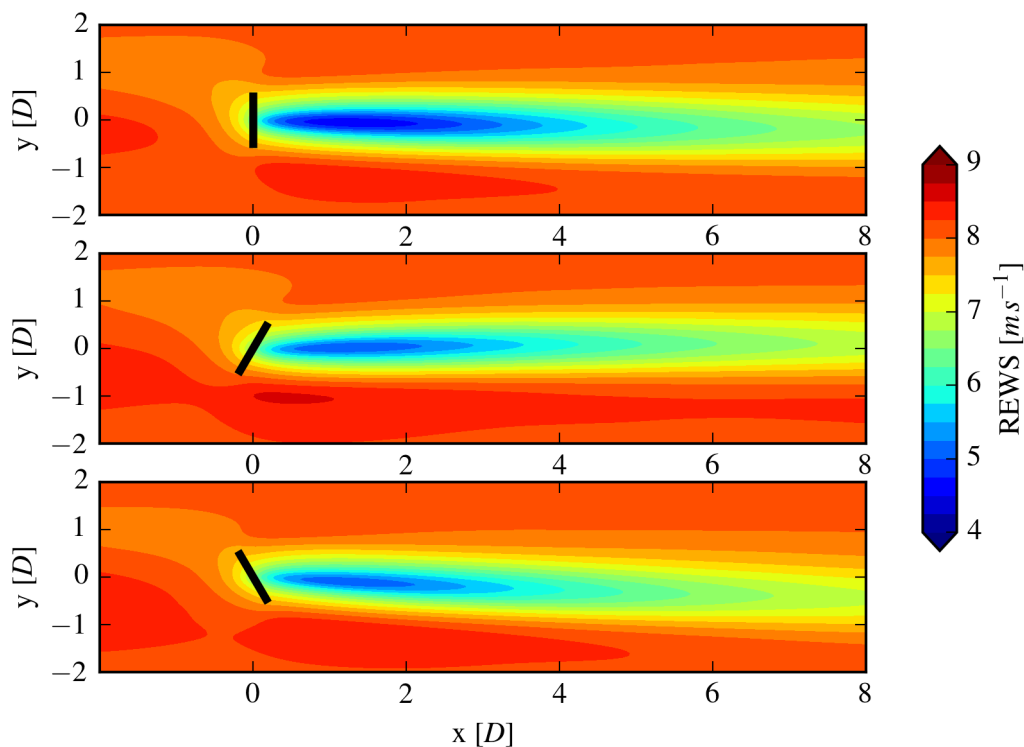
Figure 5.2: REWS calculated from the NBL mean wind fields with turbines yawed by **(a)** $0°$ **(b)** $20°$ and **(c)** $-20°$.

Each grid point represents the REWS for a full turbine centered at this position with the rotor perpendicular to the flow facing upstream. The expected power of the wind turbine can thus be calculated by multiplying the value at the grid point with the power coefficient of the turbine for this wind speed.

The wake model is in the following used to search for the optimal yaw angles of T_{up} that maximize the energy yield of a two-turbine wind farm. Figure 5.3 displays the derivation of the optimal control point for the situation, that T_{down} is placed downstream from T_{up} at $\Delta x = 4D$ and $\Delta y = -0.5D$ as shown in Fig. 5.4, which will be the reference layout NBL_{stag} of a staggered wind farm in the following. The wind field is identical to the NBL wind field in Ch. 2, thus the mean wind speed is $8\,\text{ms}^{-1}$. The same applies for the simulations in the SBL and CBL wind field conducted in this chapter. The wind turbines are the also the same ADM-R representations of the NREL 5MW research turbine (Jonkman et al., 2009). For every yaw angle γ of T_{up}, the energy yield of the wind farm is the sum of the power of T_{down}, derived from the REWS field, and the power of T_{up} from the simulations. As only simulations for seven discrete yaw angles were made in Ch. 2, the total energy yield for the other yaw angles is approximated with a third-order polynomial fit (Fig. 5.3). For wind along the x-axis, the optimal power gain is 8.6 % and can be achieved with a yaw angle of T_{up} of
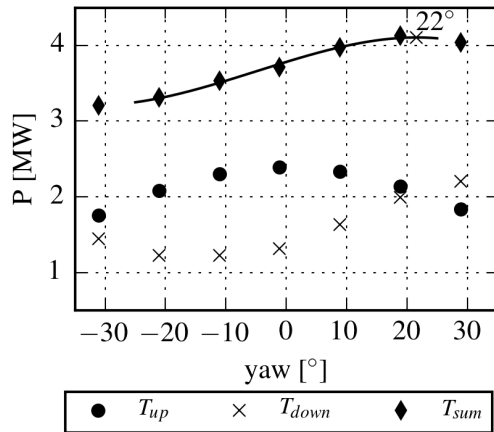
Figure 5.3: Estimated power of NBL_{stag} with the wind along the x-axis and for different yaw angles of T_{up}. The line shows the polynomial fit to the discrete T_{sum} values, with the maximum marked at 22°.
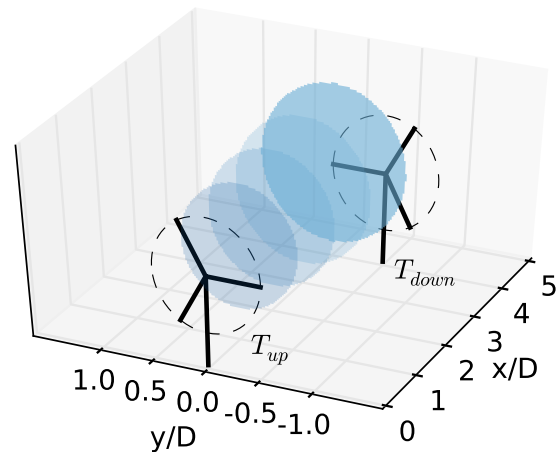
Figure 5.4: Layout of the wind farm NBL_{stag} used for the tests of the model-based control concept.

22° (Fig. 5.3).

An optimization for all wind directions can be made by a relative movement of T_{down} in the REWS field on a circular path. The resulting control points and the calculated benefits are shown in Fig. 5.5(a). Here, the maximum relative yaw angle was limited to 25°, a simple load constraint to prevent potentially high loads on the turbine at high yaw angles. Figure 5.5(a) reveals the possible benefit for different wake situations. Apparently, the maximum gain can not be reached for full wake situations (for this case around 7° wind direction), but for partial wake situation. This is plausible, as the steering of the wake does not achieve a complete movement of the wake out of the rotor area of a downwind turbine (as visible in Fig. 5.2). Thus, the increase of REWS at a turbine that is already partially in the wake is potentially larger. Figure 5.5(a) also shows that wake steering requires a larger activity of the yaw actuator than baseline control, as the gradient of the orientation is larger in the relevant wind direction region. Especially in the region around the full wake situation a large correction of orientation is necessary when the wind direction changes. This control point will be called the *turning point* in the following, and its relevance for successful wake steering will be further analysed in Sect. 5.4.

Figure 5.5(b) shows the same analysis as in Fig. 5.5(a) but for the same wind farm in the SBL (SBL_{stag}). As shown in Ch. 2, the NBL and SBL wind field exhibit nearly the same wind speed and wind direction at hub height, but differ in the turbulence characteristics and the vertical wind profile. The higher possible benefit of yaw control in the stable situation can be related to the slower wake recovery due to the lower turbulence level. Figure 5.5
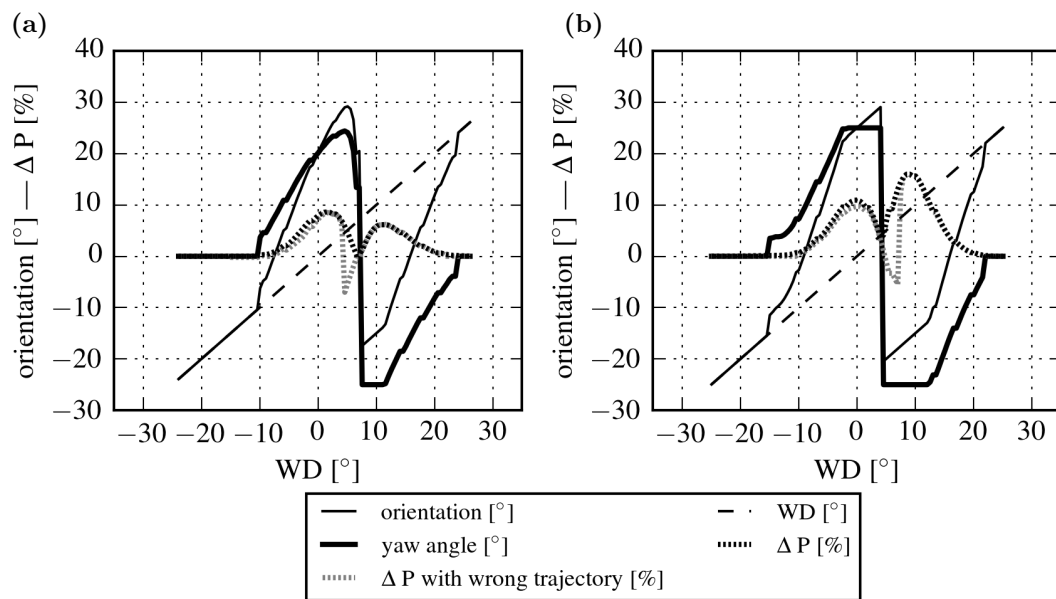
Figure 5.5: Turbine orientation and optimal yaw angles of T_{up} for the wind directions in which T_{down} is effected by the wake, the calculated power benefit Δ P of the wind farm and the benefit when the "wrong" optimal yaw angles of SBL_{stag} are used in NBL_{stag} and vice versa. **(a)** For NBL_{stag}. **(b)** For SBL_{stag}.

also reveals that the optimal yaw angles of the two models differ. This difference becomes apparent for example in the position of the *turning point*, which is shifted by 4° in SBL_{stag}. As found in Ch. 2 and 4, the center of the wake is displaced to the right in veered flow on the northern hemisphere. The difference in the *turning point* position is a direct consequence of this wake displacement. When the trajectory of NBL_{stag} is used for the controller in SBL_{yaw} or vice versa, the biggest error is made in the vicinity of the *turning point*. The errors for the other wind directions remain small.

The maximum benefit and the average benefit over the wind sector of $-30°$ to $30°$ and a hub height wind speed of $8\,\mathrm{ms^{-1}}$ for different positions of T_{down} are shown in Fig. 5.6. The maximum benefit in the NBL can be reached for a turbine placed at roughly 3 D downstream and -0.5 D cross-stream. For a uniform distribution of the wind direction in the considered sector, a wind farm with T_{down} placed much closer downwind at roughly 2 D would experience the maximum average increase in power of 2.2 % in the NBL. For the SBL conditions benefits are much higher, with the maximum benefit peaking at a distance of about 5.5 D at 17 % and the maximum average benefit reaching values of 4 % at a distance of 2.5 D. The benefit in the SBL could be even higher, when allowing yaw angles larger than 25°, as the optimal yaw angle is at the allowed maximum for all distances (Fig. 5.6(b)).
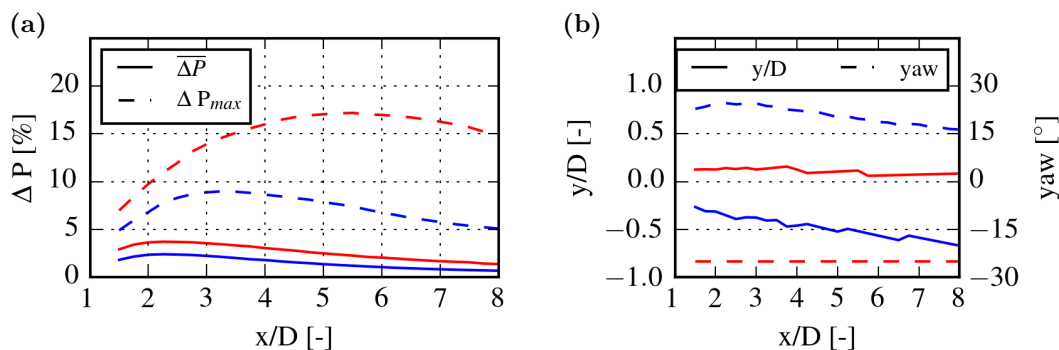
Figure 5.6: **(a)** Maximum potential benefit ΔP_{max} for different distances between the turbines and integrated benefit $\overline{\Delta P}$ over $WD \in [-30°, 30°]$ with the upstream turbine following the optimal yaw trajectory. **(b)** y-Position of T_{down} for the maximum benefit and the corresponding yaw angle of T_{up}. (blue) NBL. (red) SBL.

5.3 Evaluation of open-loop model-based wind farm control

For an application of the previously presented open-loop model-based wind farm control, the measured input variables to the model have to be defined. Considering the optimal yaw trajectory in Fig. 5.5(a), the only input to the model is the mean wind direction at hub height. However, in a turbulent environment the definition of the mean wind direction is not trivial. As discussed in Ch. 2 the temporal averaging window influences the uncertainty of the estimation. On the one hand a longer window leads to a more converged mean, while on the other hand a shorter window is able to react quicker on changes in the wind field. Another aspect is the location of the wind measurement. While in Ch. 2 the wind was measured along a cross-stream horizontal line at hub height upstream of the turbine, the more realistic, as regularly available, measure is a point measurement of wind direction and speed at the turbine's nacelle just downstream of the hub.

The evaluation of the perfect combination of temporal averaging interval and measurement location as controller input would require a multi-dimensional analysis including different turbulence conditions and relative turbine positioning. This analysis is not feasible yet with the current computational resources and the applicability on real wind farm sites might be restricted as the wind conditions are usually site-dependent. What is done in this evaluation is a qualitative analysis of open-loop model-based wake steering with the nacelle measurements in well-known wind fields.

The yaw controller was implemented in the turbine model of PALM following Storey et al. (2013) with a short averaging window of 30 s of the wind direction measured at the hub, which allows for quick reactions on the changing wind field. The condition for the yaw actuation was a deviation of the turbine orientation from the 30-s average measurement of

the wind direction of more than $5°$. If this condition was fulfilled the actuation was started and a new averaging window of $2\,$s was initialized. The actuation was stopped when either the deviation between the new orientation and the short average wind direction was below $0.5°$ or when the turbine already yawed beyond the short-term average of the measured wind direction. The speed of the yaw actuator was set to $0.3°s^{-1}$.

Two different modes of operation were implemented:

1. When operated in **baseline control**, the turbine orientation is controlled as described in the previous paragraph. Thus the orientation is trying to match the filtered wind direction measurement.

2. In **wake steering** mode, the turbine is yawed towards the optimal yaw control points defined in the look-up table for the wind farm configuration (i.e. given in Fig. 5.5). The yaw angle is updated during the simulation according to the optimal angle for the current filtered wind direction.

Two simulations in each, the NBL and the SBL windfield were run for 25 min with the previously introduced two-turbine setup and the initial orientation of the rotors perpendicular to the flow. While T_{down} was run in baseline control in both cases, T_{up} was once run in baseline control and once in wake steering mode. Figure 5.7 compares the results of the energy yield and the turbine orientations during the NBL_{stag} simulations. For the last 20 minutes of the simulation the wind farm's power increase by using wake steering was 9.4%, thus even slightly higher than the predicted benefit from the wake model (see Fig. 5.3(a)), which assumes a fixed optimal yaw angle during the whole averaging period. In SBL_{stag} (not shown) the power improvement by wake steering was 12.0%, which is also close to the model prediction. The results are compared in Tab. 5.1 at the end of the chapter.

The numerical experiment thus shows that the modified yaw control of T_{up} can increase the total energy yield of the wind farm and that the result can be well predicted by calculating the REWS in the wake. Meanwhile, for the selected sensitivity of the yaw actuator the correction of the wind turbine orientation is very frequent, which is related to the steeper yaw trajectory when wake steering is applied.

5.4 Evaluation of critical scenarios

Two scenarios were selected as critical scenarios for wake steering in a wind farm. Both of these scenarios inherit that they only occur in a turbulent environment, thus can not be observed or evaluated with static wind farm models. As first scenario, the behavior of the controller in the vicinity of the *turning point* is selected. Figure 5.7 visualizes one aspect that is difficult to consider with static wind farm models: due to the finite speed of the yaw actuator, the state of optimal orientation of the turbine occurs with a delay, proportional to the difference to the previous orientation. At the *turning point*, when both turbines are
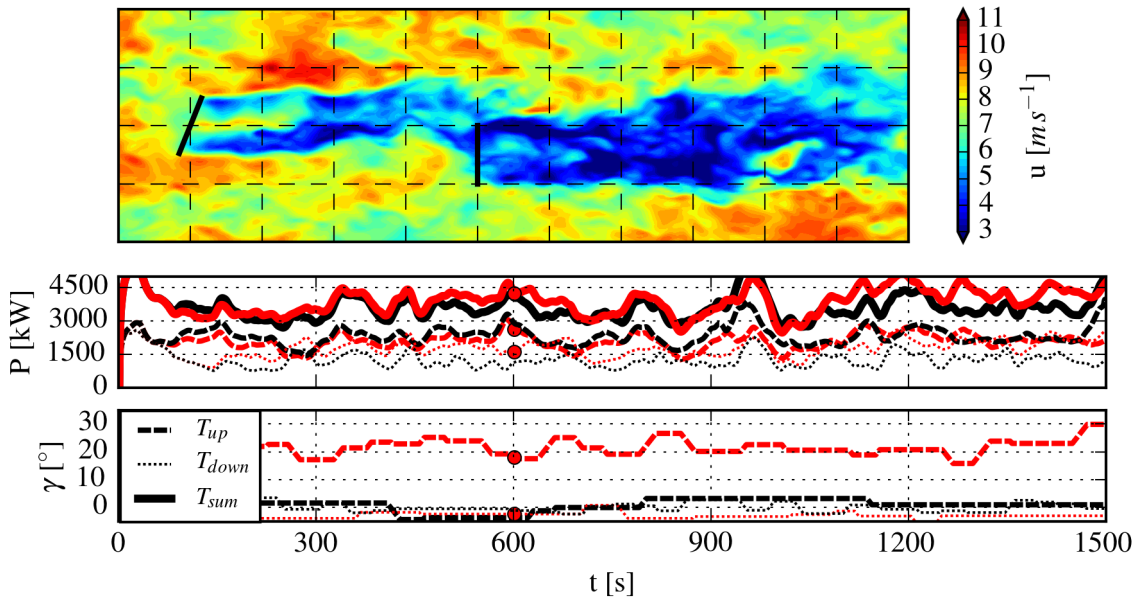
Figure 5.7: Comparison of baseline control and wake steering for the case NBL_{stag}. Snapshot of the hub-height wind speed at $t = 600\,s$ with T_{up} in wake steering mode. Power P of each turbine, summed power of the wind farm and yaw angle γ of each turbine. Simulation with T_{up} in (black) baseline mode and (red) wake steering mode.
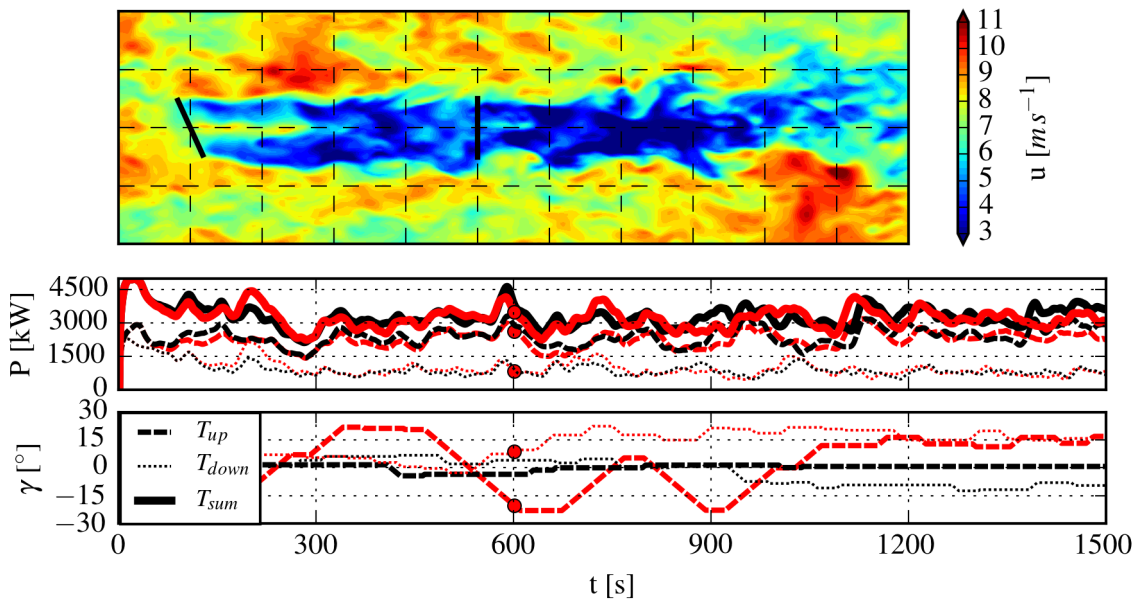
Figure 5.8: Same illustration as in Fig. 5.7 but for the wind farm configuration NBL_{line} in which the turbines are positioned directly along the wind direction.

Figure 5.9: Comparison of the timeseries of the power benefit Δ P, yaw angle and the controller input wind direction average of T_{up} for baseline control and wake steering in the four rows of CBL_{stag}.

aligned to the wind direction, the gradient between the optimal turbine orientations is largest.

Figure 5.8 shows the timeseries of the power and yaw angle for a setup NBL_{line}, in which T_{down} is placed at x = 4 D and y = 0 D. The mean energy yield with wake steering is 3.1 % lower than the respective baseline case. The REWS model 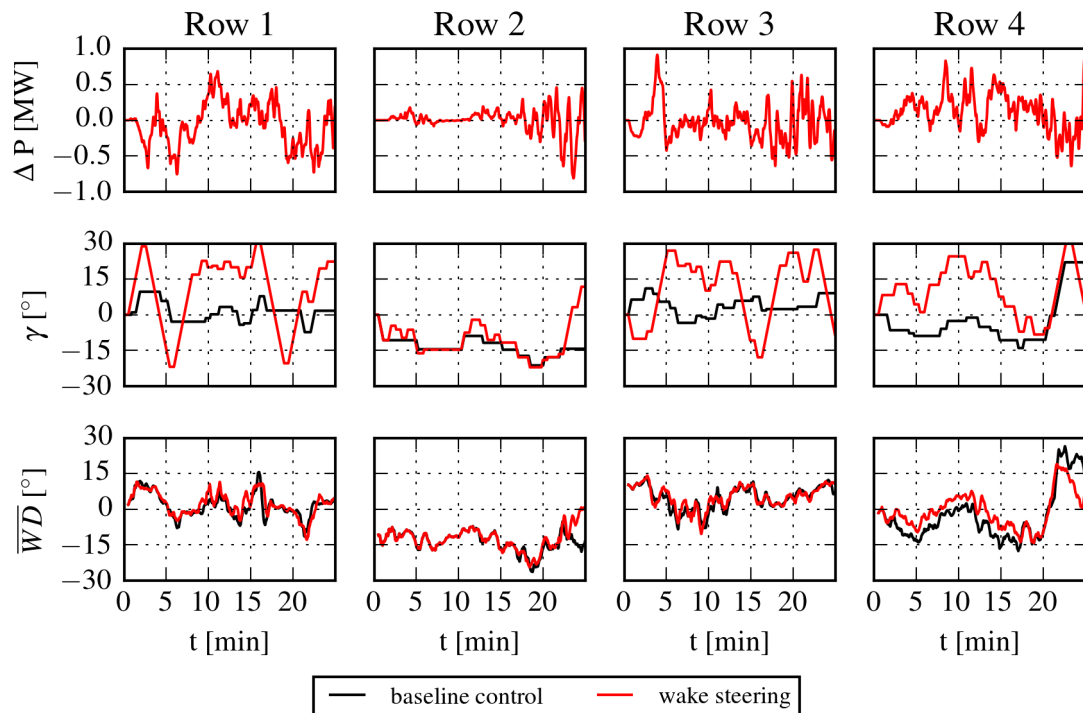can not explain this behaviour, as the theoretical calculation provide a surplus of +2.5 %. In addition, the yaw actuator is used during 50% of the time steps. Thus, wake steering is not only disadvantageous regarding the energy yield but also regarding the loading of the yaw actuator. The reason for this is that the wind direction fluctuates around the mean during the simulation. At the *turning point*, this can lead to the problem that a previously advantageous yaw angle, that leads to a wake steering away from T_{down}, can be disadvantageous only few seconds later as the wake is actually steered into T_{down}.

As shown in Ch. 2, the wind direction fluctuates most in a CBL. Thus, the performance of wake steering in the very turbulent environment of the CBL is selected as second scenario. As model for the control set points, the model for NBL_{stag} (Fig. 5.5)(a) was selected, as the CBL results from Ch. 2 could not be used as model, due to an unclear relationship between yaw and wake position. The assumption is, that the CBL wind field is similar to the NBL, just with a higher turbulence level (see Fig. 2.3). In this case the wake model used for the optimal

yaw control is expected to be less accurate, but it represent the best available approximation.

The setup for the CBL simulations is similar to the NBL_{stag} situation. The wind farm consists of eight turbines in four rows, where in each row the turbines are aligned as in the NBL_{stag} simulation with a staggering of T_{down} to create a half-wake situation. The cross-stream distance between the turbines was chosen large enough to prevent a mutual interaction of the rows. Simulations with baseline yaw control and wake steering applied at the four upwind turbines were run for 25 minutes each.

The time series of the turbine states during the simulations are shown in Fig. 5.9. The energy yield differs between the four rows, which can be related to the locally different wind conditions. The results of row two and row four are not further considered in the following, due to following reasons: In row two the local wind conditions do rarely cause a wake influence on the downwind turbine for most of the simulation, thus the controller only applies wake steering during a short period. In row four the wind conditions, visualized in Fig. 5.9 by the 30s-average of the wind direction, diverge already at the start of the simulation, which prevents a reasonable direct comparison.

In total, wake steering in rows one (-1.9%) and three (-1.1%) produces less energy than baseline control. In addition, the yaw actuator of T_{up} is on average used 67 % of the time with wake steering, compared to 20 % in baseline control.

To evaluate the influence of the controller sensitivity on the results in both critical scenarios, the simulations were repeated with a significantly less sensitive yaw actuator, which uses an averaging window of 180 seconds instead of 30 seconds. For the NBL_{line} case (c.f. Fig. 5.8) this change actually increases the energy yield, with a benefit of 0.9% compared to the baseline case without wake steering. In the two rows of the CBL case, the energy yield slightly increases for one row and further decreases for the other. This demonstrates that a less sensitive controller is apparently not the solution for the difficulties of the controller around the turning point. The results of all simulation cases are compared in Tab. 5.1. The conclusion of the selected study cases in this section is, that a modified control strategy is necessary for some scenarios even in case of a perfect wake model.

5.5 Passive wake steering

A modified control strategy could for example consider more measurement signals to decide if a controller on the wind farm level should replace the baseline controller. A measurement of the turbulence intensity of the flow could be such a parameter. The disadvantage of this approach is that the controller gets more and more dependent on the quality of the available measurements. In this section a control approach is investigated that should reduce the dependency on the measurements. The so-called **passive wake steering** approach is based on the work of Rott et al. (2018).

The idea of the control is to present a solution for wake-steering-based wind farm control, while considering the uncertainties coming from the measurements. Measurement uncertainties can principally have statistical and systematic sources (Sanz Rodrigo et al., 2017). While
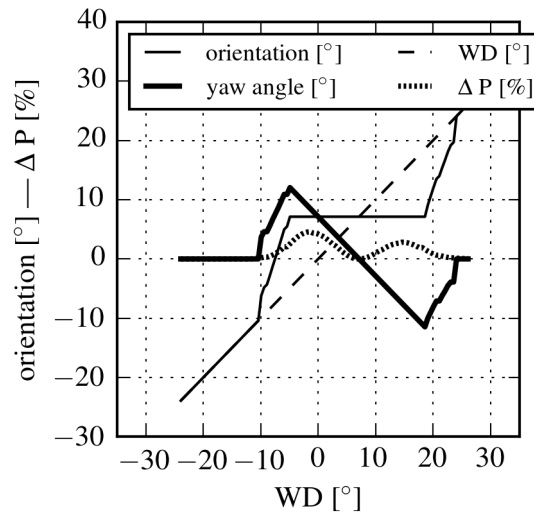
Figure 5.10: Yaw angles for passive wake steering of T_{up} and the calculated surplus of power of the wind farm. The difference to Fig. 5.5(a) is that the turbine orientation remains constant between a wind direction of $-5°$ and $18°$.

the systematic source can be reduced by the right choice and the quality of the measurement, the statistical source of uncertainty is related to the stochastic nature of the wind. Thus, a control concept in a turbulent and inhomogeneous environment like the atmospheric boundary layer needs to consider at least statistical uncertainties. In the passive wake steering approach uncertainties are considered by acknowledging that a derivation of a representative wind direction information as precise as considered for the look-up tables in the previous section is impossible.

The yaw angles for the passive wake steering approach are shown in Fig. 5.10. The concept of the control is, that the orientation of the controlled turbine does not change inside of a selected wind direction sector. The borders of the sector are defined as the range of wind directions in which an influence of the wake on T_{down} is beginning to appear. In the present case this range can be identified by the REWS wake model constructed from the LES. To decrease the gradient at the corners of the sector, transition regions were included at both sides (Fig. 5.10).

The orientation of the turbine in the constant orientation region is fixed to be aligned with T_{down} in the full wake situation, i.e. when the wind flows directly along the line of turbines. For this situation no difference exists between baseline control and passive wake steering. The consequence of the constant orientation of the turbine is that a deviation of the wind direction from the full wake case results in a yaw misalignment of the turbine to the wind (Fig. 5.10). This yaw angle stays rather small compared to the model-based wake steering approach in Fig. 5.5(a) and the maximum power benefit does not exceed 5 %, but the concept eliminates the problem of the *turning point* discussed in the previous section and
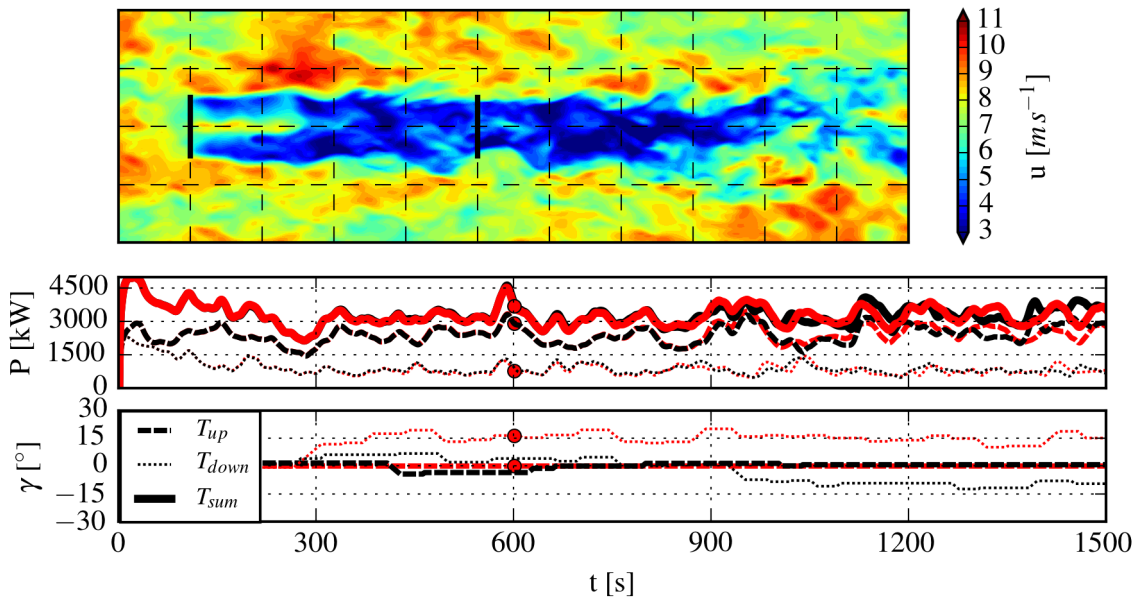
Figure 5.11: Same simulation as in Fig. 5.8 for the case NBL_{line} but with the yaw controller of T_{up} run in passive wake steering mode (red).

thus should be more robust towards fluctuations and measurement uncertainties.

A test run of passive wake steering is done for the scenarios NBL_{line}, NBL_{stag} and CBL_{stag} as described in the previous section. As shown in Fig. 5.11 the time series of the baseline control mode and passive wake steering nearly match each other for the NBL_{line} scenario, in which the turbine orientations are aligned with the wind direction. The wind farm power in the simulation with the passive wake steering is slightly (-1.0%) smaller than with the baseline yaw controller, which still represents an improvement upon the loss with wake steering based on optimal yaw angles (optimal wake steering) with the quickly reacting yaw controller. In addition, the yaw actuator is not used during the time period. For NBL_{stag} the benefit of passive wake steering is 5.6%, in contrast to 9.4% with optimal wake steering. As an advantage, the orientation of T_{up} remains constant during the simulation with a yaw angle of $\gamma \approx 10°$.

In the CBL_{stag} wind farm setup, passive wake steering leads to a power increase by 0.9% in row one and no change in row three (Fig. 5.12, Tab. 5.1). Both represent an improvement compared to optimal wake steering. The use of the yaw actuator is largely decreased with passive wake steering. The approach thus allows to handle the large fluctuations better than the optimal wake steering approach and even leads to less yawing than baseline control.
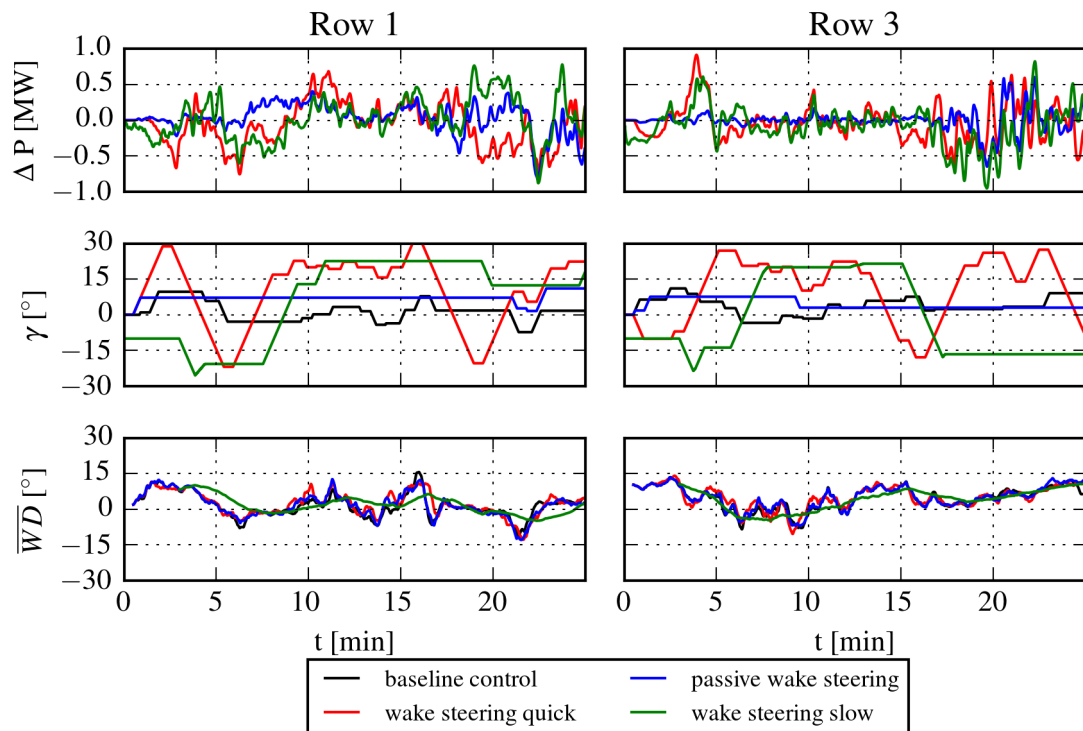
Figure 5.12: Comparison of the timeseries of power benefit Δ P, yaw angle and controller input wind direction average of T_{up} of rows one and two of CBL_{stag} for four different control modes.

5.6 Summary

In this chapter a modified yaw controller is used to illustrate the influence of atmospheric stability on the concept of wind farm control by means of wake steering. It is shown that LES of the ABL can be a good test environment for this controller as the wind conditions can be closely replicated for a period of about 20 to 25 minutes in most cases. The main findings of the chapter are summarized in the following.

An energy yield benefit is possible with open-loop model-based wake steering, when the underlying wake model is able to deliver a good representation of the wind conditions. Thus, the surplus of power at a downwind turbine is larger than the sacrifice at the upwind turbine for the wind sector with wake influence. Furthermore, the first part of the chapter underlines certain observations that were made in the earlier chapters. For the SBL, the optimal yaw angles are different from the optimal yaw angles in the NBL, which can be mostly related to a horizontal displacement of the wake, caused by ambient wind shear and veer. This finding is especially relevant as the potential benefit appears to be much larger due to the slower wake recovery in an SBL. For the example cases of this study, the effect of using the yaw

angles derived from a wind field of different stability (e.g. yaw angles derived from the NBL field applied in the SBL field) on the benefit of wake steering is quite small. In a CBL, the presumption from the previous chapters was confirmed, as the strong fluctuations of wind direction and wake lead to an increase of power only in one of four setups and to losses otherwise.

The different test cases illustrate the potential benefit of a modified open-loop model-based wake steering approach. The so-called passive wake steering concept of a constant orientation of the upwind turbine in a certain range of wind directions helps to reduce yaw actuation and thus loads on this turbine component, while still taking advantage of the wake steering concept for overall wind farm power increase. For application, the passive wake steering concept is interesting as it requires less model and measurement detail about the wind direction and can be otherwise constructed from quite simple wake models.

To assess the results of this chapter, it needs to be considered that only a single hub height wind speed was analysed for which good wake models existed. Furthermore, the yaw controller is quite simple and the comparison of the different averaging windows for the input wind direction reveals the sensitivity of the results on this parameter. Longer averaging or more sophisticated yaw controllers with e.g. hysteresis functions could further improve or even worsen the performance of the controller. These studies could be feasible in the presented LES, but probably the experiments need to rely on a statistical similarity of the wind conditions, rather than identical wind fields, as used in this chapter, to be able to conduct longer simulations.

From the simulations in this chapter it can be concluded that it is only useful to employ wake steering in non-convective conditions. Furthermore the optimal yaw angles change in presence of strong wind veer and shear in a SBL, which means that these quantities need to be assessed to maintain optimal control.

	NBL_{stag} $\overline{WD}=1°$		NBL_{line} $\overline{WD}=1°$		SBL_{stag} $\overline{WD}=0°$		CBL_{stag}^{row1} $\overline{WD}=2°$		CBL_{stag}^{row3} $\overline{WD}=5°$	
	ΔP [%]	t_γ [%]	ΔP [%]	t_γ [%]	ΔP [%]	t_γ [%]	ΔP [%]	t_γ [%]	ΔP [%]	t_γ [%]
baseline	-	4	-	4	-	0	-	20	-	19
optimal wake steering										
- REWS model	8.6	-	2.5	-	10.9	-	8.5	-	4.6	-
- quick control	9.4	25	-3.1	50	12.0	6	-1.9	70	-1.1	65
- slow control	n/a	n/a	0.9	13	n/a	n/a	0.6	41	-2.6	39
passive wake steering										
- REWS model	3.6	-	0.0	-	2.6	-	2.9	-	0.6	-
- quick control	5.6	2	-1.0	0	n/a	n/a	0.9	18	0.0	11

Table 5.1: Performance of the different controllers in the different wind fields and wind farm configurations. The power difference ΔP is always related to the respective baseline case. The columns t_γ denote the percentage of time during which the yaw actuator was changing the turbine orientation. In quick control mode the averaging of the wind direction as input to the yaw actuator is done for 30 s, in slow control mode for 180 s. The table also compares the theoretical values calculated with the REWS wake model for the mean wind directions $\overline{WD}$ of each scenario with the results of the simulations.

Chapter 6

Conclusion and Outlook

6.1 Conclusion

This thesis is a contribution to the ongoing research on wind farm control. It focuses on the influence of atmospheric stability on the behavior of wind turbine wakes and the impact on the concept of wake steering. An important result of the thesis is that wake steering is a method that is capable of increasing the power output of a simple two-turbine wind farm in Large-Eddy-Simulations of the atmospheric boundary layer, if the inflow conditions are properly known. However, it has also been shown that the concept of wake steering is not successful in a strongly turbulent environment like a convective ABL. A proper characterization of the inflow conditions is thus a key condition to ensure successful wind farm control. LES can be an appropriate experimental environment to test which measurements are necessary to characterize the inflow. The analyzed offline coupling of LES to a mesoscale model allows to study multiple inflow situations inside one single simulation, which represents an advantage to the alternative method of creating multiple quasi-steady state simulations with respect to computational costs. In the following, the new and important results of the thesis are summarized with a focus on the three main research questions that were posed in the introduction.

a) For the further development of wind farm control, the following relevant influences of atmospheric stability on the application of wake steering were identified:

- The wake recovery depends on atmospheric stability. This aspect has not been a focal point of this work as there has been already enough evidence that the wake recovery depends on the ambient turbulence intensity, which, at most sites, directly depends on atmospheric stability. The largest difference for a wake in a CBL compared to more stable ABLs is not the higher streamwise variance of the wind but the higher energy in the low-frequent fluctuations of the wind direction at the time scale of minutes, as shown in Ch. 2. As these fluctuation occur on the time-scale of several minutes, the magnitude of the mean deficit and the wake position can vary significantly if the averaging interval is in the same order. For longer averaging intervals the wake then appears weaker and wider.

- The wake is horizontally displaced with increasing shear and veer of the wind profile, caused by a stable stratification of the ABL. The wake center, identified as the area with lowest available mean kinetic energy for a wind turbine, is shifted to the right when looking downstream. It is shown that the main driver for this effect is the wind veer, which leads to a different advection of the initial shear-related asymmetry of the wake with height[1].

- The wake exhibits a strong asymmetry for strong veer and also for large yaw angles. The first effect can be related to the previously mentioned different advection direction with height in a veered wind profile. The wake asymmetry for large yaw angles, which was termed "crescent shape", is not related to atmospheric stability but to two counter-rotating vortices created by the induction of cross-stream momentum by the rotor. It can be pronounced by the veer-related deformation. The shape of the wake in these conditions makes a parametrization of the wake trajectory with a simplified axi-symmetric description challenging. The calculation of the minimum of the rotor-equivalent wind speed, that is determined by averaging the wind over virtual rotor surfaces, appears to be the best option for the wake center identification.

- The strong fluctuations of the wind direction in CBLs make a successful active control of the wake position unlikely. Especially the slow fluctuations are difficult to handle for a controller as they might not be easily differentiated from trends related to mesoscale or synoptic changes of the wind and interfere with the usual averaging intervals of yaw controllers.

- For the identification of atmospheric stability conditions that influence the turbines' wake, the bulk Richardson number over the height of the rotor proved to be a superior indicator to flux measurements close to the ground. Direct measurements of shear and veer over the rotor height, and turbulence, however, appear to be the best option as they directly capture the influencing factors for the wake development.

b) A numerical experiment was made to calculate the power benefit of wake steering in a small wind farm of two turbines with different setups of yaw controllers with the following results:

- The power benefit of an open-loop model-based optimal yaw control was verified. As expected from the wake analysis, the benefit is higher in stable stratification. The highest benefit is achievable in a staggered wind farm, in which the downwind turbine is normally only partially in the wake of the upstream turbine. REWS proved to be a good estimator for the wind farm's power production.

- The optimal yaw angles in stably stratified and neutral conditions differ, which is not only caused by the different wake recovery but also by the different displacement of the wake due to the wind veer in the inflow. In the example case of stable stratification

---

[1]Note that the sign of the stability-related wind veer is reversed in the Southern Hemisphere.

the wind farm power still increases, when the yaw model is used that was derived from the neutral wind field. It is however likely, albeit not shown here, that this might not be the case for more stable situations with stronger shear and veer.

- The open-loop controller based on the optimal yaw setting for each wind direction faces problems when the two turbines are directly in line with the wind direction. For this situation, both, a large negative and a large positive yaw represent an improvement to the wind farms energy yield. Thus, due to fluctuations of the wind direction, the turbine tends to alternate between these two states which results in frequent yaw actuation. In the test cases, the energy yield could not be increased in that situation.

- The energy yield could not be increased by wake steering in three of four test cases in the CBL. The issues in the CBL for wake steering are twofold: The strong fluctuations of the wind direction in a CBL represent a challenge to the controller, as they enforce frequent yaw actuation. Thus, even in baseline control, which aims to align the turbine axis with the wind direction, this alignment is rarely accomplished. As demonstrated on a single wake, these fluctuations also dominate the downwind position of the wake. So, most of the time in the CBL simulations, the upwind turbine was not operating with the desired yaw angle to the wind, and, in addition, the wake was not following a well-described trajectory but was strongly meandering.

- A modified passive wake steering controller, based on the work of Rott et al. (2018), which relies on a constant orientation of the upwind turbine, was tested as a more pragmatic alternative to the optimal yaw controller. While the improvement was small for the aforementioned problematic scenarios, the approach reduced the yaw actuation significantly, even compared to baseline control. A further advantage of the passive wake steering approach is, that it requires less input from a wake model and is more robust against high uncertainties of the measured input signals, while still improving the overall energy yield of the test wind farm. A disadvantage of the approach is, that the theoretical maximum benefit is smaller than with the above-mentioned controller.

c) The methodology to drive LES with data from numerical weather models to study wind farm flow was analyzed in two test cases. The main take-aways of these studies are summarized in the following:

- By using the transient LES approach, synoptic frequencies can be included in an LES with wave lengths that extend the horizontal extensions of the simulation domain. This allows to simulate slowly changing wind conditions, e.g. caused by the daily cycle of atmospheric stability on a clear-sky day. The analysis showed that the methodology is not able to replicate mesoscale fluctuations that might interact with the boundary layer turbulence. If the main purpose of the numerical experiment is to include mesoscale fluctuations, the method offers little advantage to quasi-steady situations with constant forcing. For studying the behavior of a wind farm in changing atmospheric conditions, however, the transient method is advantageous because it contains multiple states of

the ABL in only one longer simulation.

- The transient LES approach can be useful to replicate the wind conditions during a specific measurement period. Combined with a turbine model, LES can be a valuable tool to interpret the data from lidar measurement campaigns of wakes. The simulation of the *alpha ventus* case in Ch. 3 allowed to understand the asymmetry in the measured horizontal wake profiles. In Chapter 4 the simulation of the case could explain the different vertical positions of the wake observed by the VAD lidar.

- In contrast to online coupling approaches the method can be run independently from a mesoscale simulation with preprocessed data. In the future the method could for example be used to downscale the results of wind atlases created by mesoscale model data.

6.2 Outlook

Since the start of the work on this thesis in 2013, wind farm control has developed from a small topic in the wind energy research community to one of the larger contributors to yearly publications in the field. The topic should even gain further importance with the increasing share of renewable energy sources in the energy market. As grid managers have to deal with the fluctuating nature of the resource wind, wind farms will eventually be forced to provide backup power or to follow an enforced power trajectory to stabilize the electricity grid. Due to the complex feedbacks inside of a wind farm due to wakes, controllers have to be specifically designed to be able to fulfill these needs (Pao, 2015). For these reasons, institutions and companies are starting to work on the topic worldwide with a variety of methods.

The previously published content of this thesis has already influenced the topics of the current research and the choice of methods. Gebraad et al. (2016a), for example, have worked on modifying the simplified wind farm control model Floris to include the effects of wind veer on wake propagation. Schottler et al. (2017) analyzed the lateral displacement of the wake in a sheared wind profile in the wind tunnel and found a reversal of the sign of displacement when the shear is reversed. Several publications have addressed the origins of the *crescent shape* (or termed *kidney shape* by Churchfield et al. (2016)) and the consequences for simplified models and measurement campaigns (Fleming et al., 2017b). The discussion about the best method to define the wake center has influenced the post-processing of recent measurement campaigns that measured wake deflection in the field. Bromm et al. (2018) have found that the use of the minimum REWS as an estimator produced more robust results for wake tracking compared to other methods.

LES has become an established tool for experiments with wind farm control. It is for example used in Gebraad et al. (2016b) to improve the simple flow model Floris, or in Vali et al. (2018) for developing model-predictive wind farm control. Goit and Meyers (2015) are using a different approach by applying adjoint techniques to find the optimal control of a

wind farm. While this approach is unrealistic for real application, it delivers quite interesting results regarding the processes that influence wake recovery and the correlation of the control of individual turbines.

While many studies on wind farm control focus on the improvement of power production, the study of fatigue loads might be even more challenging. Full studies of turbine loads in wake conditions usually require higher temporal and spatial resolutions than the simulations conducted for this thesis. Fleming et al. (2015) and Bromm et al. (2017) both use aeroelastic codes coupled with LES to analyze wake induced loads, a much more computational heavy method than the ADM-R method. Bastine et al. (2015) propose a dynamic wake model based on proper orthogonal decomposition of the downstream wind field for fatigue analysis in wakes, as a full LES analysis requires much longer time series than currently feasible. The general engineering assumption in assessing fatigue loads for wind turbines in wakes is that the loads are proportional to the variance of the wind speed (Frandsen and Thøgersen, 1999). Lower wake deficits, a consequence of both wind farm control strategies, induction and wake steering, should lead to a lower variance, as the gradient between wake and ambient wind becomes smaller. Thus, both controls should be beneficial for the fatigue loads on downstream turbines, an assumption that is already used for wind sector management in wind farms by commercial programs. At the upwind turbine, Zalkind and Pao (2016) found that the increased load of a frequent yaw misalignment is low and that damage-equivalent loads even decrease when the turbine blades retreat from the crosswind at the top of the turbine.

An important aspect for the application of wind farm control that was not directly addressed in the thesis are measurement uncertainties. In the simulations, the wind direction was determined by a accuracy of less than $1°$ to prove that the wake is deflected. Modern wind vanes or ultrasonic anemometers have an accuracy of the wind direction of up to 2 to $3°$. This deficiency needs to be considered by the controller. In addition to the uncertainties, most devices have a bias of several degrees as the calibration of the total orientation is rarely done correctly. A measurement setup for wind farm control probably requires a test period, after which the devices are recalibrated. Mittelmeier et al. (2017) have shown that proper calibrated standard sensors on a wind turbine can already provide a lot of information about the wind farm performance in different atmospheric conditions. The passive wake steering approach from Ch. 5 is based on work by Rott et al. (2018), that actually considers the measurement uncertainties for the derivation of the controller trajectory.

Several new techniques have been developed in recent years to measure the wind field around the turbine. Bottasso and Riboldi (2014) have proposed to use load sensors on the blades to estimate the inhomogeneity of the wind over the rotor surface. They have been quite successful in measuring wind shear and even in identifying the presence of a wake at downstream turbines (Cacciola et al., 2016). A different approach is the use of nacelle-mounted upstream-looking lidars as proposed for individual turbine control by e.g. Schlipf et al. (2013). A lidar can deliver a more complete picture of the wind field and allows a controller to respond to changing conditions before they actually enter the wind farm. With falling prices for lidars and steadily increasing turbine dimensions, the benefit of this instrumentation could eventually outweigh the costs. The latest development in regards of remote

sensing is the application of Doppler radars that have a much larger range than lidars and are thus able to scan the wind field inside and around large wind farms with only few devices (Hirth et al., 2015). While remote sensing devices are very interesting for research, a reliable operational use is still challenging as the availability depends on the weather conditions.

The goal of the different measurement techniques is to get more information about the wind field in the farm. This thesis supports this aspiration as it has shown that wind farm control might fail, when the wind conditions are only vaguely known. A differentiation may be made between wind conditions in large and small wind farms. In large wind farms the wind conditions at the inlet and inside of the farm differ considerably as the wind field inside the farm is dominated by the wake-induced turbulence (Dörenkämper, 2015). As a consequence, the turbulence level inside wind farms is much higher than even the turbulence level of a CBL. Following the results of this thesis, the control by means of wake steering should be challenging in these situations. For turbines inside large wind farms the more robust passive wake steering control approach might thus be a reasonable solution, while at the inlet or in small wind farms the optimal wake steering approach could be more successful. At onshore wind farms, turbulence and wind shear are of course not only stability-dependent but can also be related to inhomogeneities in terrain, forest and land-use. As a consequence a control that is constructed to approach optimal wake steering requires not only permanent observations, but also a profound sector-wise site assessment of wind speed and turbulence intensity.

All considered, the application of wind farm control will require more measurement calibration and more data analysis. First tests of a wake steering-based wind farm control were recently executed in a Chinese wind farm by Fleming et al. (2017a). These tests produce a slight surplus in power production, but with a high uncertainty. Further studies on the effects of characteristics or uncertainties of the inflow are necessary to eventually convince wind farm operators or turbine manufacturers to allow for well-equipped measurement campaigns in their wind farms. The progress made in this thesis can be a valuable part of this process.

Bibliography

Abkar, M. and F. Porté-Agel, 2013: The effect of free-atmosphere stratification on boundary-layer flow and power output from very large wind farms. *Energies*, **6 (5)**, 2338–2361, doi:10.3390/en6052338.

Abkar, M., A. Sharifi, and F. Porté-Agel, 2016: Wake flow in a wind farm during a diurnal cycle. *Journal of Turbulence*, **17 (4)**, 420–441, doi:10.1080/14685248.2015.1127379.

Ainslie, J. F., 1988: Calculating the Flowfield in the Wake of Wind Turbines. *J. Wind Eng. Ind. Aerodyn.*, **27**, 213–224, doi:10.1016/0167-6105(88)90037-2.

Annoni, J., P. M. O. Gebraad, A. K. Scholbrock, P. A. Fleming, and J.-W. v. Wingerden, 2016: Analysis of axial-induction-based wind plant control using an engineering and a high-order wind plant model. *Wind Energy*, **19 (6)**, 1135–1150, doi:10.1002/we.1891.

Archer, C. L., B. A. Colle, D. L. Veron, F. Veron, and M. J. Sienkiewicz, 2016: On the predominance of unstable atmospheric conditions in the marine boundary layer offshore of the u.s. northeastern coast. *Journal of Geophysical Research: Atmospheres*, **121 (15)**, 8869–8885, doi:10.1002/2016JD024896.

Aubrun, S., S. Loyer, P. E. Hancock, and P. Hayden, 2013: Wind turbine wake properties: Comparison between a non-rotating simplified wind turbine model and a rotating model. *J. Wind Eng. Ind. Aerodyn.*, **120**, 1–8, doi:10.1016/j.jweia.2013.06.007.

Baldauf, M., J. Förstner, S. Klink, T. Reinhardt, C. Schraff, A. Seifert, and K. Stephan, 2009: Kurze Beschreibung des Lokal-Modells Kürzestfrist COSMO-DE (LMK) und seiner Datenbanken auf dem Datenserver des DWD. *Deutscher Wetterdienst, Geschäftsbereich Forschung und Entwicklung, Offenbach, Germany*.

Barthelmie, R. J., K. S. Hansen, and S. C. Pryor, 2013: Meteorological controls on wind turbine wakes. *Proceedings of the IEEE*, Vol. 101, 1010–1019, doi:10.1109/JPROC.2012.2204029.

Barthelmie, R. J. and L. E. Jensen, 2010: Evaluation of wind farm efficiency and wind turbine wakes at the Nysted offshore wind farm. *Wind Energy*, **13 (6)**, 573–586, doi:10.1002/we.408.

Bastine, D., B. Witha, M. Wächter, and J. Peinke, 2015: Towards a simplified dynamic wake model using pod analysis. *Energies*, **8 (2)**, 895–920, doi:10.3390/en8020895.

Beare, R. J. and M. K. Macvean, 2004: Resolution sensitivity and scaling of large-eddy simulations of the stable boundary layer. *Boundary-Lay. Meteorol.*, **112 (2)**, 257–281, doi:10.1023/B:BOUN.0000027910.57913.4d.

Boersma, S., B. Doekemeijer, M. Vali, J. Meyers, and J.-W. van Wingerden, 2018: A control-oriented dynamic wind farm model: Wfsim. *Wind Energy Science*, **3 (1)**, 75–95, doi:10.5194/wes-3-75-2018.

Bottasso, C. and C. Riboldi, 2014: Estimation of wind misalignment and vertical shear from blade loads. *Renewable Energy*, **62**, 293 – 302, doi:10.1016/j.renene.2013.07.021.

Bottasso, C. L., F. Campagnolo, and V. Petrović, 2014: Wind tunnel testing of scaled wind turbine models: Beyond aerodynamics. *J. Wind Eng. Ind. Aerodyn.*, **127**, 11 – 28, doi:10.1016/j.jweia.2014.01.009.

Bromm, M., A. Rott, H. Beck, L. Vollmer, G. Steinfeld, and M. Kühn, 2018: Field investigation on the influence of yaw misalignment on the propagation of wind turbine wakes. *Wind Energy*, **21 (11)**, 1011–1028, doi:10.1002/we.2210.

Bromm, M., L. Vollmer, and M. Kühn, 2017: Numerical investigation of wind turbine wake development in directionally sheared inflow. *Wind Energy*, **20 (3)**, 381–395, doi:10.1002/we.2010.

Cacciola, S., M. Bertelè, J. Schreiber, and C. Bottasso, 2016: Wake center position tracking using downstream wind turbine hub loads. *J. Phys. Conf. Ser.*, **753 (3)**, 032 036, doi:10.1088/1742-6596/753/3/032036.

Churchfield, M., Q. Wang, A. Scholbrock, T. Herges, T. Mikkelsen, and M. Sjöholm, 2016: Using high-fidelity computational fluid dynamics to help design a wind turbine wake measurement experiment. *J. Phys. Conf. Ser.*, **753 (3)**, 032 009, doi:10.1088/1742-6596/753/3/032009.

Churchfield, M. J., S. Lee, J. Michalakes, and P. J. Moriarty, 2012: A numerical study of the effects of atmospheric and wake turbulence on wind turbine aerodynamics. *J. Turbulence*, **13 (14)**, 1–32, doi:10.1080/14685248.2012.668191.

Churchfield, M. J., P. J. Moriarty, G. Vijayakumar, and J. G. Brasseur, 2010: Wind Energy-Related Atmospheric Boundary Layer Large-Eddy Simulation Using OpenFOAM. *19th Symposium on Boundary Layers and Turbulence, Keystone, Colorado, August 2-6, 2010*.

Corten, G. P. and P. Schaak, 2003: Heat and Flux - Increase of Wind Farm Production by Reduction of the Axial Induction. *EWEC 2003, 16-19 June, Madrid, Spain*.

Deardorff, J., 1980: Stratocumulus-capped mixed layers derived from a three-dimensional model. *Boundary-Lay. Meteorol.*, **18**, 495–527, doi:10.1007/BF00119502.

Dörenkämper, M., 2015: *An investigation of the atmospheric influence on spatial and temporal power fluctuations in offshore wind farms*. 1st ed., Verlag Dr. Hut, ISBN: 978-3843923736.

Dörenkämper, M., M. Optis, A. Monahan, and G. Steinfeld, 2015a: On the Offshore Advection of Boundary-Layer Structures and the Influence on Offshore Wind Conditions. *Boundary-Lay. Meteorol.*, **155**, 459–482, doi:10.1007/s10546-015-0008-x.

Dörenkämper, M., J. Tambke, G. Steinfeld, D. Heinemann, and M. Kühn, 2014: Atmospheric Impacts on Power Curves of Multi-Megawatt Offshore Wind Turbines. *J. Phys. Conf. Ser.*, **555**, 012 029, doi:10.1088/1742-6596/555/1/012029.

Dörenkämper, M., B. Witha, G. Steinfeld, D. Heinemann, and M. Kühn, 2015b: The impact of stable atmospheric boundary layers on wind-turbine wakes within offshore wind farms. *J. Wind Eng. Ind. Aerodyn.*, **144**, 146–153, doi:10.1016/j.jweia.2014.12.011.

Emeis, S., 2010: A simple analytical wind park model considering atmospheric stability. *Wind Energy*, **13 (5)**, 459–469, doi:10.1002/we.367.

Emeis, S., 2014: Wind speed and shear associated with low-level jets over Northern Germany. *Meteorol. Z.*, **23 (3)**, doi:10.1127/0941-2948/2014/0551.

España, G., S. Aubrun, S. Loyer, and P. Devinant, 2011: Spatial study of the wake meandering using modelled wind turbines in a wind tunnel. *Wind Energy*, **14 (7)**, 923–937, doi:10.1002/we.515.

Etling, D. and R. A. Brown, 1993: Roll vortices in the planetary boundary layer: A review. *Boundary-Lay. Meteorol.*, **65**, 215–248, doi:10.1007/BF00705527.

Fleming, P., P. M. Gebraad, S. Lee, J.-W. Wingerden, K. Johnson, M. Churchfield, J. Michalakes, P. Spalart, and P. Moriarty, 2015: Simulation comparison of wake mitigation control strategies for a two-turbine case. *Wind Energy*, **18 (12)**, 2135–2143, doi:10.1002/we.1810.

Fleming, P., J. Annoni, J. J. Shah, L. Wang, S. Ananthan, Z. Zhang, K. Hutchings, P. Wang, W. Chen, and L. Chen, 2017a: Field test of wake steering at an offshore wind farm. *Wind Energy Science*, **2 (1)**, 229–239, doi:10.5194/wes-2-229-2017.

Fleming, P., J. Annoni, A. Scholbrock, E. Quon, S. Dana, S. Schreck, S. Raach, F. Haizmann, and D. Schlipf, 2017b: Full-scale field test of wake steering. *J. Phys. Conf. Ser.*, **854 (1)**, 012 013, doi:10.1088/1742-6596/854/1/012013.

Fleming, P. A., A. Ning, P. M. O. Gebraad, and K. Dykes, 2016: Wind plant system engineering through optimization of layout and yaw control. *Wind Energy*, **19 (2)**, 329–344, doi:10.1002/we.1836.

Fleming, P. A., P. M. Gebraad, S. Lee, J.-W. van Wingerden, K. Johnson, M. Churchfield, J. Michalakes, P. Spalart, and P. Moriarty, 2014: Evaluating techniques for redirecting turbine wakes using sowfa. *Ren. Energ.*, **70**, 211–218, doi:10.1016/j.renene.2014.02.015.

Frandsen, S., R. Barthelmie, P. S, O. Rathmann, S. Larsen, J. Hojstrup, and M. Thogersen, 2006: Analytical Modelling of Wind Speed Deficit in Large Offshore Wind Farms. *Wind Energy*, **9 (1–2)**, 39–53, doi:10.1002/we.189.

Frandsen, S. and M. L. Thøgersen, 1999: Integrated fatigue loading for wind turbines in wind farms by combining ambient turbulence and wakes. *Wind Engineering*, **23 (6)**, 327–339, URL `http://www.jstor.org/stable/43749903`.

Gebraad, P., J. J. Thomas, A. Ning, P. Fleming, and K. Dykes, 2017: Maximization of the annual energy production of wind power plants by optimization of layout and yaw based wake control. *Wind Energy*, **20 (1)**, 97–107, doi:10.1002/we.1993.

Gebraad, P. M. O., M. J. Churchfield, and P. A. Fleming, 2016a: Incorporating atmospheric stability effects into the floris engineering model of wakes in wind farms. *J. Phys. Conf. Ser.*, **753 (5)**, 052 004, doi:10.1088/1742-6596/753/5/052004.

Gebraad, P. M. O., F. W. Teeuwisse, J. W. van Wingerden, P. A. Fleming, S. D. Ruben, J. R. Marden, and L. Y. Pao, 2016b: Wind plant power optimization through yaw control using a parametric model for wake effects—a cfd simulation study. *Wind Energy*, **19 (1)**, 95–114, doi:10.1002/we.1822.

Global Wind Energy Council, 2018: Global wind statistics 2017. URL `http://gwec.net/global-figures/graphs/`, online; Accessed: 2018-04-04.

Goit, J. P. and J. Meyers, 2015: Optimal control of energy extraction in wind-farm boundary layers. *Journal of Fluid Mechanics*, **768**, 5–50, doi:10.1017/jfm.2015.70.

Gryning, S.-E., E. Batchvarova, B. Brümmer, H. Jorgensen, and S. Larsen, 2007: On the Extension of the Wind Profile over Homogeneous Terrain Beyond the Surface Boundary Layer. *Boundary-Layer Meteorol.*, **124**, 251–268, doi:10.1002/qj.714.

Gryschka, M., B. Witha, and D. Etling, 2008: Scale analysis of convective clouds. *Meteorol. Z.*, **17 (6)**, 785–791, doi:10.1127/0941-2948/2008/0345.

Hancock, P. E. and S. Zhang, 2015: A Wind-Tunnel Simulation of the Wake of a Large Wind Turbine in a Weakly Unstable Boundary Layer. *Boundary-Layer Meteorol.*, **156 (3)**, 395–413, doi:10.1007/s10546-015-0037-5.

Hansen, K. S., R. J. Barthelmie, L. E. Jensen, and A. Sommer, 2012: The impact of turbulence intensity and atmospheric stability on power deficits due to wind turbine wakes at Horns Rev wind farm. *Wind Energy*, **15 (1)**, 183–196, doi:10.1002/we.512.

Heinze, R., C. Moseley, L. N. Böske, S. K. Muppa, V. Maurer, S. Raasch, and B. Stevens, 2017: Evaluation of large-eddy simulations forced with mesoscale model output for a multi-week period during a measurement campaign. *Atmospheric Chemistry and Physics*, **17 (11)**, 7083–7109, doi:10.5194/acp-17-7083-2017.

Hirth, B. D., J. L. Schroeder, W. S. Gunter, and J. G. Guynes, 2015: Coupling doppler radar-derived wind maps with operational turbine data to document wind farm complex flows. *Wind Energy*, **18 (3)**, 529–540, doi:10.1002/we.1701.

IEC-61400-12-1, 2005: Part 12-1: Power performance measurements of electricity producing wind turbines; iec tc/sc 88. Tech. rep., IEC 61400-12-1.

Jensen, N. O., 1983: A Note on Wind Generator Interaction. Tech. Rep. Riso-M-2411, Riso National Laboratory.

Jimenez, A., A. Crespo, and E. Migoya, 2010: Application of a LES technique to characterize the wake deflection of a wind turbine in yaw. *Wind Energy*, **13 (6)**, 559–572, doi:10.1002/we.380.

Jonkman, J. M., S. Butterfield, W. Musial, and G. Scott, 2009: Definition of a 5-MW reference wind turbine for offshore system development. Technical Report NREL/TP-500-38060, National Renewable Energy Laboratory, 1617 Cole Boulevard, Golden, Colorado 80401-3393. doi:10.2172/947422.

Keck, R.-E., M. de Maré, M. J. Churchfield, S. Lee, G. Larsen, and H. A. Madsen, 2014: On atmospheric stability in the dynamic wake meandering model. *Wind Energy*, **17 (11)**, 1689–1710, doi:10.1002/we.1662.

Kost, C., S. Shammugan, V. Jülch, H.-T. Nguyen, and T. Schlegl, 2018: Stromgestehungskosten Erneuerbare Energien. Tech. rep., Fraunhofer ISE. URL `https://www.ise.fraunhofer.de/de/veroeffentlichungen/studien/studie-stromgestehungskosten-erneuerbare-energien.html`.

Larsen, G., E. Machefaux, and A. Chougule, 2015: Wake meandering under non-neutral atmospheric stability conditions-theory and facts. *J. Phys. Conf. Ser.*, **625 (1)**, 012 036, doi:10.1088/1742-6596/625/1/012036.

Larsen, G. C., 1988: *A simple wake calculation procedure*. Risø National Laboratory Risø-M-2760.

Larsen, G. C., H. A. Madsen, K. Thomsen, and T. J. Larsen, 2008: Wake meandering: a pragmatic approach. *Wind Energy*, **11 (4)**, 377–395, doi:10.1002/we.267.

Lee, J. C. and J. K. Lundquist, 2017: Observing and simulating wind-turbine wakes during the evening transition. *Boundary-Layer Meteorol.*, **164 (3)**, 449–474, doi:10.1007/s10546-017-0257-y.

Lorius, C., J. Jouzel, D. Raynaud, J. Hansen, and H. L. Treut, 1990: The ice-core record: climate sensitivity and future greenhouse warming. *Nature*, **347**, 139–145, doi:doi:10.1038/347139a0.

Lu, H. and F. Porté-Agel, 2011: Large-eddy simulation of a very large wind farm in a stable atmospheric boundary layer. *Phys. Fluids*, **23**, 065 101, doi:10.1063/1.3589857.

Lundquist, J. K., M. J. Churchfield, S. Lee, and A. Clifton, 2015: Quantifying error of lidar and sodar doppler beam swinging measurements of wind turbine wakes using computational fluid dynamics. *Atmos. Meas. Tech.*, **8 (2)**, 907–920, doi:10.5194/amt-8-907-2015.

Machefaux, E., G. C. Larsen, T. Koblitz, N. Troldborg, M. C. Kelly, A. Chougule, K. S. Hansen, and J. S. Rodrigo, 2015a: An experimental and numerical study of the atmospheric stability impact on wind turbine wakes. *Wind Energy*, **19 (10)**, 1785–1805, doi:10.1002/we.1950.

Machefaux, E., G. C. Larsen, N. Troldborg, M. Gaunaa, and A. Rettenmeier, 2015b: Empirical modeling of single-wake advection and expansion using full-scale pulsed lidar-based measurements. *Wind Energy*, **18 (12)**, 2085–2103, doi:10.1002/we.1805.

Maronga, B., M. Gryschka, R. Heinze, F. Hoffmann, F. Kanani-Sühring, M. Keck, K. Ketelsen, M. O. Letzel, M. Sühring, and S. Raasch, 2015: The Parallelized Large-Eddy Simulation Model (PALM) version 4.0 for atmospheric and oceanic flows: model formulation, recent developments, and future perspectives. *Geosci. Model Dev.*, **8 (8)**, 2515–2551, doi:10.5194/gmd-8-2515-2015.

Medici, D. and J. Dahlberg, 2003: Potential improvement of wind turbine array efficiency by active wake control (AWC). *Proceedings of European Wind Energy Conference, Madrid, Spain, 2003*, 65–84.

Meyers, J. and C. Meneveau, 2010: Large Eddy Simulations of large wind-turbine arrays in the atmospheric boundary layer. *48th AIAA Aerospace Sciences Meeting Including the New Horizons Forum and Aerospace Exposition, 4 - 7 January 2010, Orlando, Florida*.

Mikkelsen, R., 2003: Actuator disc methods applied to wind turbines. Ph.D. thesis, Technical University of Denmark.

Mirocha, J. D., D. A. Rajewski, N. Marjanovic, J. K. Lundquist, B. Kosović, C. Draxl, and M. J. Churchfield, 2015: Investigating wind turbine impacts on near-wake flow using profiling lidar data and large-eddy simulations with an actuator disk model. *J. Renew. Sust. Energ.*, **7 (4)**, 043143, doi:10.1063/1.4928873.

Mittelmeier, N., J. Allin, T. Blodau, D. Trabucchi, G. Steinfeld, A. Rott, and M. Kühn, 2017: An analysis of offshore wind farm scada measurements to identify key parameters influencing the magnitude of wake effects. *Wind Energy Science*, **2 (2)**, 477–490, doi:10.5194/wes-2-477-2017.

Moriarty, P., J. S. Rodrigo, P. Gancarski, M. Chuchfield, J. W. Naughton, K. S. Hansen, E. Machefaux, E. Maguire, F. Castellani, L. Terzi, S.-P. Breton, and Y. Ueda, 2014: Iea-task 31 wakebench: Towards a protocol for wind farm flow model evaluation. part 2: Wind farm wake models. *J. Phys. Conf. Ser.*, **524 (1)**, 012 185, doi:10.1088/1742-6596/524/1/012185.

Motta, M., R. J. Barthelmie, and P. Vølund, 2005: The influence of non-logarithmic wind speed profiles on potential power output at danish offshore sites. *Wind Energy*, **8 (2)**, 219–236, doi:10.1002/we.146.

Muñoz-Esparza, D., B. Kosovic, J. Mirocha, and J. van Beeck, 2014: Bridging the Transition from Mesoscale to Microscale Turbulence in Numerical Weather Prediction Models. *Boundary-Layer Meteorol.*, **153**, 409–440, doi:10.1007/s10546-014-9956-9.

Nakanishi, M. and H. Niino, 2006: An Improved Mellor–Yamada Level-3 Model: Its Numerical Stability and Application to a Regional Prediction of Advection Fog. *Boundary-Layer Meteorol.*, **119**, 397–407, doi:10.1007/s10546-005-9030-8.

Neggers, R. A. J., A. P. Siebesma, and T. Heus, 2012: Continuous single-column model evaluation at a permanent meteorological supersite. *Bulletin of the American Meteorological Society*, **93 (9)**, 1389–1400, doi:10.1175/BAMS-D-11-00162.1.

Pao, L. Y., 2015: *Active Power Control of Wind Power Plants for Grid Integration*, 1–5. Springer London, London, doi:10.1007/978-1-4471-5058-9_272.

Peña, A., S.-E. Gryning, and J. Mann, 2010: On the length-scale of the wind profile. *Quarterly Journal of the Royal Meteorological Society*, **136 (653)**, 2119–2131, doi:10.1002/qj.714.

Porté-Agel, F., Y.-T. Wu, H. Lu, and R. J. Conzemius, 2011: Large-eddy simulation of atmospheric boundary layer flow through wind turbines and wind farms. *J. Wind Eng. Ind. Aerod.*, **99**, 154–168, doi:10.1016/j.jweia.2011.01.011.

Rajewski, D. A., E. S. Takle, J. K. Lundquist, S. Oncley, J. H. Prueger, T. W. Horst, M. E. Rhodes, R. Pfeiffer, J. L. Hatfield, K. K. Spoth, and R. K. Doorenbos, 2013: Crop wind energy experiment (CWEX): Observations of surface-layer, boundary layer, and mesoscale interactions with a wind farm. *Bull. Amer. Meteor. Soc.*, **94 (5)**, 655–672, doi:10.1175/BAMS-D-11-00240.1.

Rhodes, M. E. and J. K. Lundquist, 2013: The Effect of Wind-Turbine Wakes on Summertime US Midwest Atmospheric Wind Profiles as Observed with Ground-Based Doppler Lidar. *Boundary-Layer Meteorol.*, **149 (1)**, 85–103, doi:10.1007/s10546-013-9834-x.

Rijsberman, F. R. and R. J. Swart, 1990: *Targets and indicators of climatic change*, Vol. 1666. Stockholm Environment Institute Stockholm.

Rodrigo, J. S., M. Churchfield, and B. Kosovic, 2016: A wind energy benchmark for ABL modelling of a diurnal cycle with a nocturnal low-level jet: GABLS3 revisited. *J. Phys. Conf. Ser.*, **753 (3)**, 032 024, doi:10.1088/1742-6596/753/3/032024.

Rott, A., B. Doekemeijer, J. K. Seifert, J.-W. van Wingerden, and M. Kühn, 2018: Robust active wake control in consideration of wind direction variability and uncertainty. *Wind Energy Science*, **3 (2)**, 869–882, doi:10.5194/wes-3-869-2018.

Réthoré, P., 2009: Wind turbine wake in atmospheric turbulence. Ph.D. thesis, Aalborg University.

Sanderse, B., S. van der Pijl, and B. Koren, 2011: Review of computational fluid dynamics for wind turbine wake aerodynamics. *Wind Energy*, **14 (7)**, 799–819, doi:10.1002/we.458.

Sanz Rodrigo, J., R. A. Chávez Arroyo, P. Moriarty, M. Churchfield, B. Kosović, P.-E. Réthoré, K. S. Hansen, A. Hahmann, J. D. Mirocha, and D. Rife, 2017: Mesoscale to microscale wind farm flow modeling and evaluation. *Wiley Interdisciplinary Reviews: Energy and Environment*, **6 (2)**, e214, doi:10.1002/wene.214, e214.

Schalkwijk, J., H. J. J. Jonker, A. P. Siebesma, and F. C. Bosveld, 2015: A year-long large-eddy simulation of the weather over cabauw: An overview. *Monthly Weather Review*, **143 (3)**, 828–844, doi:10.1175/MWR-D-14-00293.1.

Schlipf, D., D. J. Schlipf, and M. Kühn, 2013: Nonlinear model predictive control of wind turbines using lidar. *Wind Energy*, **16 (7)**, 1107–1129, doi:10.1002/we.1533.

Schottler, J., A. Hölling, J. Peinke, and M. Hölling, 2017: Brief communication: On the influence of vertical wind shear on the combined power output of two model wind turbines in yaw. *Wind Energy Science*, **2 (2)**, 439–442, doi:10.5194/wes-2-439-2017.

Skamarock, W., J. Klemp, J. Dudhia, D. Gill, D. Barker, M. Duda, X. Huang, W. Wang, and J. Powers, 2008: A description of the advanced research WRF version 3. Tech. Rep. NCAR/TN–475+STR, NCAR - National Center for Atmospheric Research, Boulder, Colorado, USA.

Smedman, A.-S., U. Högström, and H. Bergström, 1996: Low level jets: A decisive factor for off-shore wind energy siting in the Baltic Sea. *Wind Engineering*, **20**, 137–147, URL http://www.jstor.org/stable/43749611.

Steinfeld, G., J. Tambke, J. Peinke, and D. Heinemann, 2010: Application of a large-eddy simulation model to the analysis of flow conditions in offshore wind farms. *Proceedings of DEWEK 2010, November 17th-18th, 2010, Bremen, Germany*.

Storey, R., S. Norris, and J. Cater, 2013: Large Eddy Simulation of Wind Events Propagating through an Array of Wind Turbines. *Proceedings of the World Congress on Engineering 2013 Vol III, WCE 2013, July 3 - 5, 2013, London, U.K.*

Stull, R. B., 1988: *An Introduction to Boundary Layer Meteorology*. 1st ed., Kluwer Academic Publishers.

Sørensen, J. N. and W. Z. Shen, 2002: Numerical Modeling of Wind Turbine Wakes. *Journal of Fluids Engineering*, **124**, 393–399, doi:10.1115/1.1471361.

Troldborg, N., J. N. Sørensen, R. Mikkelsen, and N. N. Sørensen, 2014: A simple atmospheric boundary layer model applied to large eddy simulations of wind turbine wakes. *Wind Energy*, **17 (4)**, 657–669, doi:10.1002/we.1608.

Trujillo, J.-J., F. Bingöl, G. C. Larsen, J. Mann, and M. Kühn, 2011: Light detection and ranging measurements of wake dynamics. Part II: two-dimensional scanning. *Wind Energy*, **14 (1)**, 61–75, doi:10.1002/we.402.

Türk, M., 2008: Ermittlung designrelevanter Belastungsparameter für Offshore-Windkraftanlagen. Ph.D. thesis, Universität zu Köln.

Vali, M., V. Petrovic, G. Steinfeld, L. Y. Pao, and M. Kühn, 2018: Large-eddy simulation study of wind farm active power control with a coordinated load distribution. *J. Phys. Conf. Ser.*, **1037 (3)**, 032 018, doi:10.1088/1742-6596/1037/3/032018.

Vali, M., J.-W. van Wingerden, S. Boersma, V. Petrović, and M. Kühn, 2016: A predictive control framework for optimal energy extraction of wind farms. *J. Phys. Conf. Ser.*, **753 (5)**, 052 013, doi:10.1088/1742-6596/753/5/052013.

van der Laan, M. P., K. S. Hansen, N. N. Sørensen, and P.-E. Réthoré, 2015: Predicting wind farm wake interaction with rans: an investigation of the coriolis force. *J. Phys. Conf. Ser.*, **625 (1)**, 012 026, doi:10.1088/1742-6596/625/1/012026.

van Dooren, M. F., D. Trabucchi, and M. Kühn, 2016: A methodology for the reconstruction of 2d horizontal wind fields of wind turbine wakes based on dual-doppler lidar measurements. *Remote Sensing*, **8 (10)**, 809, doi:10.3390/rs8100809.

Vanderwende, B. J. and J. K. Lundquist, 2012: The modification of wind turbine performance by statistically distinct atmospheric regimes. *Environmental Research Letters*, **7 (3)**, 034 035, doi:10.1088/1748-9326/7/3/034035.

Vincent, C., X. Larsén, S. Larsen, and P. Sørensen, 2013: Cross-spectra over the sea from observations and mesoscale modelling. *Boundary-Layer Meteorol.*, **2 (146)**, 297–318, doi:10.1002/joc.2175.

Vollmer, L., G. Steinfeld, D. Heinemann, and M. Kühn, 2016: Estimating the wake deflection downstream of a wind turbine in different atmospheric stabilities: an LES study. *Wind Energy Science*, **1 (2)**, 129–141, doi:10.5194/wes-1-129-2016.

Vollmer, L., G. Steinfeld, and M. Kühn, 2017: Transient LES of an offshore wind turbine. *Wind Energy Science*, **2 (2)**, 603, doi:10.5194/wes-2-603-2017.

Vollmer, L., M. van Dooren, D. Trabucchi, J. Schneemann, G. Steinfeld, B. Witha, J. Trujillo, and M. Kühn, 2015: First comparison of LES of an offshore wind turbine wake with dual-Doppler lidar measurements in a German offshore wind farm. *J. Phys. Conf. Ser.*, **625 (1)**, 012 001, doi:10.1088/1742-6596/625/1/012001.

Wagner, R., B. Canadillas, A. Clifton, S. Feeney, N. Nygaard, M. Poodt, C. S. Martin, E. Tüxen, and J. W. Wagenaar, 2014: Rotor equivalent wind speed for power curve measurement – comparative exercise for iea wind annex 32. *J. Phys. Conf. Ser.*, **524 (1)**, 012 108, doi:10.1088/1742-6596/524/1/012108.

Walker, K., et al., 2016: An evaluation of the predictive accuracy of wake effects models for offshore wind farms. *Wind Energy*, **19 (5)**, 979–996, doi:10.1002/we.1871.

Weitemeyer, S., N. Reinke, J. Peinke, and M. Hölling, 2013: Multi-scale generation of turbulence with fractal grids and an active grid. *Fluid Dynamics Research*, **45 (6)**, 061 407, doi:10.1088/0169-5983/45/6/061407.

Wharton, S. and J. K. Lundquist, 2012: Assessing atmospheric stability and its impacts on rotor-disk wind characteristics at an onshore wind farm. *Wind Energy*, **15 (4)**, 525–546, doi:10.1002/we.483.

Wind Europe, 2017: The European offshore wind industry, key trends and statistics 2016. URL `http://windeurope.org/about-wind/statistics/offshore/european-offshore-wind-industry-key-trends-and-statistics-2016/`, online; Accessed: 2018-04-04.

Wiser, R., K. Jenni, J. Seel, E. Baker, M. Hand, E. Lantz, and A. Smith, 2016: Expert elicitation survey on future wind energy costs. *Nature Energy*, **1**, 16 135, doi:10.1038/nenergy.2016.135.

Witha, B., G. Steinfeld, M. Dörenkämper, and D. Heinemann, 2014a: Large-eddy simulation of multiple wakes in offshore wind farms. *J. Phys. Conf. Ser.*, **555**, 012 108, doi:10.1088/1742-6596/555/1/012108.

Witha, B., G. Steinfeld, and D. Heinemann, 2014b: High-Resolution Offshore Wake Simulations with the LES Model PALM. *Wind Energy - Impact of Turbulence*, M. Hölling, J. Peinke, and S. Ivanell, Eds., Springer Berlin Heidelberg, Research Topics in Wind Energy 2, 175–181, doi:10.1007/978-3-642-54696-9_26, ISBN: 978-3-642-54696-9.

Wu, Y.-T. and F. Porté-Agel, 2011: Large-Eddy Simulation of Wind-Turbine Wakes: Evaluation of Turbine Parametrisations. *Boundary-Layer Meteorol.*, **138**, 345–366, doi:10.1007/s10546-010-9569-x.

Zalkind, D. S. and L. Y. Pao, 2016: The fatigue loading effects of yaw control for wind plants. *2016 American Control Conference (ACC)*, 537–542, doi:10.1109/ACC.2016.7524969.

Publication list

List of publications on which this thesis is based

Peer-reviewed articles

Vollmer, L., G. Steinfeld, D. Heinemann, and M. Kühn, 2016: Estimating the wake deflection downstream of a wind turbine in different atmospheric stabilities: an LES study. *Wind Energy Science*, **1 (2)**, 129–141, doi:10.5194/wes-1-129-2016.

Authors' contributions:
Gerald Steinfeld had a supervising function and was involved in the design of the study. Detlev Heinemann and Martin Kühn were involved in the design of the study. Lukas Vollmer performed the simulations, analysed the data and wrote the manuscript. All authors reviewed the manuscript.

Vollmer, L., G. Steinfeld, and M. Kühn, 2017: Transient LES of an offshore wind turbine. *Wind Energy Science*, **2**, 603–614, doi:10.5194/wes-2-603-2017.

Authors' contributions:
Gerald Steinfeld had a supervising function and was involved in the design of the study. Martin Kühn was involved in the design of the study and in the measurement campaign. Lukas Vollmer performed the simulations, analysed the measurement and simulation data and wrote the manuscript. All authors reviewed the manuscript.

Peer-reviewed Conference Proceedings

Vollmer, L. J.C. Yi, G. Steinfeld and J.K. Lundquist, 2017: A wind turbine wake in changing atmospheric conditions: LES and lidar measurements. *Journal of Physics Conference Series*, **854(1)**, 012050 , doi:10.1088/1742-6596/854/1/012050.

Authors' contributions:
Julie Kay Lundquist had a supervising function and provided the data from the measurement campaign. Gerald Steinfeld had a supervising function and was involved in the design of the study. Joseph Cheuk Yi did the WRF simulations and provided Fig. 1. Lukas Vollmer performed the LES, analysed the measurement and simulation data and

wrote the manuscript. All authors reviewed the manuscript.

Additional publications

Peer-reviewed articles

Bastine, D., L. Vollmer, M. Wächter and J. Peinke, 2018: Stochastic Wake Modelling Based on POD Analysis. *Energies*, **11(3)**, 612, doi:10.3390/en11030612.

Bromm, M., A. Rott, H. Beck, G. Steinfeld, L. Vollmer, and M. Kühn, 2018: Field investigation on the influence of yaw misalignment on the wake propagation of a wind turbine. *Wind Energy*, **21(11)**, 1011–1028, doi:10.1002/we.2210.

Bromm, M., L. Vollmer, and M. Kühn, 2016: Numerical investigation of wind turbine wake development in directionally sheared inflow. *Wind Energy*, **20(3)**, 281–395, doi:10.1002/we.2010.

Trabucchi, D., L. Vollmer and M. Kühn, 2017: 3-D shear-layer model for the simulation of multiple wind turbine wakes: description and first assessment. *Wind Energy Science*, **2(2)**, 569–586, doi:10.5194/wes-2-569-2017.

Peer-reviewed Conference Proceedings

Vollmer, L., M. van Dooren, D. Trabucchi, J. Schneemann, G. Steinfeld, B. Witha, J. Trujillo, and M. Kühn, 2015: First comparison of LES of an offshore wind turbine wake with dual-Doppler lidar measurements in a German offshore wind farm. *J. Phys. Conf. Ser.*, **625(1)**, 012001, doi:10.1088/1742-6596/625/1/012001.

Acknowlegments

Curriculum vitae

Personal Information

Name: Lukas Hannes Vollmer
Birthday: 30.04.1986
Place of Birth: Dortmund

Education

Oct. 2010 - Mar. 2013   M.Sc. Oceanography
                          Universität Hamburg, Germany

Oct. 2006 - Sept. 2010   B.Sc. Physics
                          Universität Bremen, Germany

June 2005   High School Diploma (Abitur)
                          Reismann Gymnasium Paderborn, Germany

Scientific experience

Apr. 2017 - now   Research Fellow
                          Fraunhofer IWES Oldenburg, Germany

Sept. 2013 - Mar. 2017   Research Assistant
                          Institute of Physics, ForWind - Carl von Ossietzky
                          Universität Oldenburg, Germany

Oct. 2015 - Dec. 2015   Visiting Researcher
                          ATOC, University of Colorado, Boulder, USA

Eidesstattliche Erklärung

Hiermit versichere ich, die vorliegende Arbeit selbstständig verfasst, keine anderen als die angegebenen Quellen und Hilfsmittel verwendet und die Leitlinien guter wissenschaftlicher Praxis der Carl von Ossietzky Universität Oldenburg befolgt zu haben.

Die Arbeit hat weder in ihrer Gesamtheit noch in Teilen einer anderen Hochschule zur Begutachtung in einem Promotionsverfahren vorgelegen und im Zusammenhang mit dem Promotionsvorhaben wurden keine kommerziellen Vermittlungs- oder Beratungsdienste in Anspruch genommen.

Teile der Arbeit sind bereits veröffentlicht.

Oldenburg, den 11.04.2018

_____

Lukas Vollmer